AN ABSTRACT OF THE DISSERTATION OF

Nicholas Cohn for the degree of Doctor of Philosophy in Geology presented on
May 10, 2018.

Title: From the Shoreface to the Foredunes: Coastal Morphodynamics Across the
Land-Sea Interface

Abstract approved: _____

Peter Ruggiero

Coastal flooding and erosion are major concerns for low lying coastal communities
– particularly in light of accelerated sea level rise and climate change. To improve quan-
titative understanding of the physical drivers of both flooding and coastal landscape change,
this dissertation explores coastal morphodynamics bridging the land-sea interface on modally
dissipative beaches throughout the U.S. Pacific Northwest (PNW). Both new and existing
morphologic datasets spanning from the shoreface to the foredunes, at time scales of days
to decades, are utilized to explore morphodynamic processes. Process-based numerical
models are then used to interpret and extrapolate the findings from the field observations.

The timing and processes contributing to seasonal erosion and growth of the beach
and dune are first investigated at a dissipative system in Oysterville, WA, with the primary
goal of relating seasonal scale morphology changes to longer term coastal evolution (years
to decades). It is shown that the largest wind driven growth of the foredune at this site
occurs in winter in response to the largest wind events but out of phase with summertime
beach growth via the welding of intertidal sandbars. The lack of synchronization between
maximum beach sediment supply and dune growth indicates that aeolian sand transport on
dissipative coasts is primarily transport, rather than supply, limited.

Although aeolian processes contribute the majority of sediment for dune growth, it is shown that total water levels exceeding the dune toe may be constructive to lower dune growth, in contrast to the expected erosional dune response from total water levels in the collision regime of Sallenger's (2000) Storm Impact Scaling Model. A new morpho-stratigraphic approach, which combines repeat topographic transect data with time series of oceanographic conditions, is developed to relate seasonal scale deposition across the beach and dune portions of the coastal profile to either a marine or aeolian origin. This method estimates that between 9% and 38% ($\sim$1 to 5 m^3/m/yr) of annual volumetric dune growth at Oysterville, WA results directly from marine processes.

Environmental and morphologic controls on the physical drivers of wave-driven dune response are further explored for additional sites throughout the PNW. Topographic data from South Beach, OR, Netarts, OR and Oysterville, WA collectively support previous observations that found that low sloping beaches are generally less vulnerable to storm-induced dune erosion than nearby steeper beach segments. Morphologic controls, including the effects of variable shelf, nearshore, beach, and dune morphology, on influencing storm-induced dune accretion and erosion are explored using XBeach, a process-based numerical model which simulates nearshore hydrodynamics and morphology change. The model results reveal that wave-driven dune accretion can occur on low sloping beaches when dynamic still water levels (still water level combined with wave setup) are below the dune toe. Although total water levels in the collision regime occur numerous times per year in many parts of the PNW, dynamic still water levels infrequently exceed the dune toe because of the uncommon co-occurrence of large wave energy and high still water levels in the PNW. The XBeach results suggest that at Oysterville, WA the oceanographic conditions promoting wave-driven dune accretion are more common than driving dune erosion. The model outputs indicate that $\sim$15 m^3/m/yr of average annual dune growth could be derived from marine-driven processes at Oysterville, WA. Numerical model simulations also show that the shelf and nearshore bathymetry have an influence on total water levels and resulting dune impacts.

While the nearshore zone is characterized by a wide range of morphologies (e.g., slopes) throughout the region, temporal variability of the nearshore profile at many PNW

locations is dominated by the formation and migration of subtidal sandbars. Process-based numerical models are used to explore how seasonal to interannual variability in nearshore sandbar configuration and beach characteristics each influence wave runup processes. Simulations using XBeach show that interannual variability in sandbar configuration, associated with multi-year cycles of net offshore sandbar migration, has a larger influence on wave runup than does seasonal variability in sandbar morphology. While subtidal sandbars do alter wave setup and swash, the model simulations also suggest that temporal variability in intertidal beach morphology (> -2 m relative to local mean sea level) has a comparatively larger morphologic influence on wave runup.

While marine processes have a large control on evolving the coastal profile, aeolian processes are generally thought to be the primary builder of coastal foredunes. Windsurf, a new process-based numerical modeling framework for simulating the co-evolution of the coastal profile in response to both marine and aeolian forcings, is developed to further explore nearshore-beach-dune interactions. Windsurf is applied to the dissipative Oysterville, WA site in order to investigate the relative roles of marine and aeolian processes on coastal foredune growth. Consistent with field measurements, the model simulates seasonal cycles of beach growth in summer, shoreline recession in winter, and net dune growth annually. The model results support the hypothesis that there are both marine ($\sim$7 m^3/m/yr) and aeolian ($\sim$14 m^3/m/yr) contributions to coastal foredune growth at this site. Consistent with field observations, Windsurf simulates positive marine contributions to the dune growth during fall. Aeolian contributions to dune growth occur intermittently throughout the year, but are lowest in summer and highest in winter. Although cross-shore oriented winds are relatively infrequent at Oysterville, WA, Windsurf simulations suggest that cross-shore winds provide a proportionally larger contribution to upper dune growth than obliquely oriented winds.

Together, this collection of manuscripts explores the influence of coastal morphodynamic processes on flooding and erosion hazards along dissipative beaches. It is confirmed that wave runup on infragravity-dominated dissipative coasts is influenced by both subtidal and intertidal morphology, with intertidal morphology having a larger influence. Field measurements and numerical modeling both suggest that marine contributions to dune growth

can be accretional under certain morphologic configurations and certain environmental conditions. Wave-driven dune accretion appears to be driven largely by infragravity swash processes on low sloping beaches – with these marine processes shown to contribute between ~1 and 15 m^3/m/yr to coastal foredune growth for an end-member dissipative beach. However, these marine accumulations are restricted to the lower portion of the dune and are generally smaller in total magnitude than aeolian contributions to upper dune growth. Therefore, consistent with the conventional process understanding of dune dynamics, aeolian processes are still found to be the primary contributor to overall coastal foredune growth on low gradient, dissipative beaches.

From the Shoreface to the Foredunes: Coastal Morphodynamics Across the
Land-Sea Interface

by

Nicholas Cohn

A DISSERTATION

submitted to

Oregon State University

in partial fulfillment of
the requirements for the
degree of

Doctor of Philosophy

Presented May 10, 2018
Commencement June 2018

Doctor of Philosophy dissertation of Nicholas Cohn presented on May 10, 2018.

APPROVED:

_____

Major Professor, representing Geology

_____

Dean of the College of Earth, Ocean, and Atmospheric Sciences

_____

Dean of the Graduate School

I understand that my dissertation will become part of the permanent collection of Oregon State University libraries. My signature below authorizes release of my dissertation to any reader upon request.

_____

Nicholas Cohn, Author

John Stanley and Jeff Wood have also helped tremendously with technical support of this work. I have particularly come to appreciate John's wisdom and untraditional caring nature over the last few years. Our talks about Nucs, Arduinos, ODroids, and server specs have opened my eyes to the value of knowing someone that understands hardware. Watching John work diligently and efficiently in setting up 50+ instruments during SEDEX[2] was truly inspiring and I hope he knows just how important he is for much of work that happens in the CIL.

I also would particularly like to thank Jim Dickson and Mary Hitch for helping with many crucial travel, purchasing, and logistics tasks that helped make our many field initiatives a success. Thanks also goes to Heather Weiner (Washington State Department of Ecology), Anne Verheijen (Technical University of Delft), and Patricia Chardon-Maldonado (University of Delaware) who also contributed substantially to field data collection efforts at SEDEX[2].

I of course also wish to thank the other members of my committee, Tuba Özkan-Haller, Rob Holman, and Michael Olsen as well. I have been lucky to have many great conversations with all of the committee members over the last few years which has provided direction and encouragement when needed.

Benvy and Yebo are first and foremost the biggest supporters of mine. Benvy has put up with a lot over the last few years and now knows way more about coastal processes than she ever wished she did. Even when going out for a beer with officemates means that we are just going to talk shop, Benvy is always tolerant, patient, and understanding. More than anything Benvy reminds me that there is more to life than work; I would likely not leave the office (or field) if it were not for her. For that I am grateful! I can't guarantee that the work conversations will stop, but I look forward to our amazing adventures around the world and weekends of forgetting about work unfinished. I am very thankful that all the Nearshore Allstars (mostly) tolerated the field puppy even when it slowed everything down!

CONTRIBUTION OF AUTHORS

Dr. Sierd de Vries contributed to Chapter 2 through discussion and review of the manuscript.

Dr. George Kaminsky contributed to Chapter 2 through providing topographic data and review of the manuscript.

Dr. Gabriel García-Medina, Dylan Anderson, Dr. Katherine Serafin, and Dr. Rueben Biel contributed to Chapter 4 through collection of field data, discussion of the research ideas, and review of the manuscript.

Dr. Bas Hoonhout, Dr. Evan Goldstein, Dr. Sierd de Vries, Dr. Laura Moore, Dr. Dano Roelvink, and Dr. Orencio Durán contributed to Chapter 5 through contributions to the development of Windsurf, the coupled numerical modeling framework developed as part of this chapter.

TABLE OF CONTENTS (Continued)

TABLE OF CONTENTS (Continued)

LIST OF FIGURES

LIST OF TABLES

Chapter 1: General Introduction

Sitting at the land-sea interface, the coastal zone is a thin strip of land actively influenced by marine processes. Despite the relatively small global area that the coast encompasses, the shallow ocean promotes commerce and recreation which serves as the economic backbone for many communities and countries (e.g., Luger, 1991; McGranahan et al., 2007). Yet, oceanographic and atmospheric processes can drive rapid flooding and erosion of these low lying regions – putting coastal communities at risk. Major storm events such as Hurricanes Sandy, Harvey, Irma, and Maria have resulted in over $300B in damages since 2012 (corresponding to the approximate start of this dissertation) in the U.S. alone (NOAA NCEI, 2018). Impacts from these episodic events include the loss of economically valuable beaches (e.g., Houston, 1995), destruction of ecologically important coastal foredunes (e.g., Miller et al., 2010) through wave impact and overwashing, and direct damages to infrastructure. While devastating, these extreme events are typically infrequent for any particular stretch of coast. Therefore, there are many intermittent periods when the coast has the opportunity to recover, grow, or otherwise experience changes that are not catastrophic in nature. These calmer periods play a major role in forming the emergent coastal landscape on sandy, outer coast systems.

As the number of people living in flood-prone coastal regions continues to grow contemporaneous with rising sea levels (e.g., Neumann et al., 2015), there is an increasing need to be able to accurately predict coastal landscape change. While there is reasonable predictive capability of coastal profile change in response to individual storm events (e.g., Roelvink et al., 2009; Johnson et al., 2012; Larson & Kraus, 1989), there is a shortage of reliable tools available to predict coastal evolution across the full range of human-relevant time scales (days to centuries). Across this broad range of time scales, properly characterizing sediment exchanges across the land-sea interface is critically important. However, many of the processes that contribute to both erosive and accretive coastal profile change are poorly understood (e.g., Elko et al., 2015). This gap in knowledge is in part due to the

historical compartmentalization of the coastal zone by scientists and engineers into discrete morphologic zones (e.g., shelf, nearshore, beach, and dune), when in fact there are numerous interactions between these compartments (e.g., Gallop et al., 2015; Ruggiero et al., 2016). These interactions include feedbacks of morphology on hydrodynamics and aerodynamics (e.g., coastal morphodynamics) and direct sediment exchanges between different portions of the coastal profiles. Quantifying these cross-compartment interactions requires detailed field measurements which are often challenging to collect. For example, measurements during storm events require a rapid response capability, poses safety concerns during data collection, and may lead to the loss of expensive instrumentation. Conversely, morphologic changes during low energy conditions are often difficult to measure because changes are typically slow and smaller in magnitude. Furthermore, the multitude of marine, aeolian, and ecological processes operating simultaneously within the coastal zone have further encouraged compartmentalization in order to make incremental advances in understanding of dominant physical processes. Unfortunately, these complexities and limitations have resulted in a predictive capability of coastal zone evolution on sandy coasts that still lacks sufficient skill across these human relevant time scales. Improving our understanding of coastal morphodynamics is a critical step toward improving these predictive capabilities.

The aim of this dissertation is to explore targeted questions related to coastal morphodynamics spanning the land-sea interface. The investigations described herein are focused on modally dissipative coastal systems within the U.S. Pacific Northwest (PNW). Much of this thesis is focused on a progradational, dissipative field site in Oysterville, Washington, USA where a rich dataset of morphology change exists, although morphologic and hydrodynamic data from three other PNW field sites (South Beach, OR; Agate Beach, OR; Netarts, OR) are also used to explore morphodynamic processes in parts of this thesis. Although dissipative beaches, which consist of either low-gradient and/or high energy beach systems as defined by the Wright & Short (1984) beach classification model, are an end-member coastal system – rapid and measureable morphological changes in these environments provide unique insight into complex morphodynamic processes. When possible, this work specifically aims to utilize field measurements of in-situ hydrodynamics and morphology

change to improve understanding of morphodynamic processes, with field observations subsequently used to inform, validate, and test process-based numerical models.

In pursuit of exploring interactions across the land-sea interface from the shoreface to the foredunes, morphology and environmental data are first utilized to explore nearshore-beach-dune sediment exchanges at an end-member dissipative beach in Oysterville, WA. Using datasets that span time scales of days to decades, Chapter 2 explicitly tests the hypothesis that dune growth is controlled by the synchronization of intertidal sandbar welding and wind capable of transporting beach sediments. Detailed measurements of coastal profile change show that while summertime beach growth at the field site is driven by the onshore migration and welding of intertidal sandbars, maximum dune growth does not co-occur with maximum beach sediment supply. In addition to seasonal trends in beach and dune behavior being explored in detail over a one year period when frequent ($\sim$ monthly) data exists, a new morpho-stratigraphic approach is developed in order to relate seasonal scale deposition across the beach and dune portions of the coastal profile to either a marine or aeolian origin. A key result of Chapter 2 is the finding that total water levels (TWLs) impacting the dune toe can add constructively to dune growth under some conditions. The morpho-stratigraphic approach suggests that between 9% and 39% ($\sim$1 to 5 m^3/m/yr) of annual dune growth at Oysterville, WA is a result of marine processes. This result contrasts with the traditional conceptual model which relates water levels in the collision regime to erosional impacts (e.g., Sallenger, 2000). The work presented in Chapter 2 has been published in *Geophysical Research Letters*.

As explored in Chapter 2, TWLs are an important driver of morphology change. Wave runup, which is the wave driven contribution to TWLs, is known to be influenced by characteristics of the coastal profile (e.g., Cox et al., 2013; Shand et al., 2006). In Chapter 3, process-based numerical models are utilized to explore the influence of nearshore sandbar morphology on wave runup. A coastal profile model, Unibest-TC (Bosboom et al., 2000), is first utilized to simulate the migration of subtidal sandbars during a one year period at Oysterville, WA. XBeach (Roelvink et al., 2009), a process-based hydrodynamic, sediment transport, and morphology change model, is next used to explore how modelled seasonal variability in nearshore sandbar configuration and measured interannual variabil-

ity in nearshore profiles influence wave runup and TWLs. It is found that while subtidal sandbars do alter inner surf zone hydrodynamics, such as wave setup and swash, temporal variability in morphology that is shallower than -2 m (relative to local mean sea level) has the largest morphologic influence on wave runup at the Oysterville, WA site. The results of this work have been published in *Coastal Engineering*.

The observations of wave driven dune accretion presented in Chapter 2 differ from the expected dune response from TWLs in the collision regime of Sallenger's (2000) Storm Impact Scaling Model, confirming that our conceptual understanding of marine controls on coastal profile change is incomplete. In Chapter 4, new field datasets, combined with numerical modeling, are used to further explore the morphologic and environmental factors which control dune response to high water level events. Data from three PNW fields sites are first used to provide insights into the morphologic controls on marine contributions to dune response. The field observations reveal that coastal segments with low sloping (wide) beaches are generally less vulnerable to dune erosion than nearby steeper (narrow) beaches. Additionally, exploratory numerical simulations using XBeach are completed which (1) alter details of the shelf, nearshore, beach, and dune morphology in order to isolate morphologic controls on dune response and (2) investigate a wide range of oceanographic forcing conditions to determine the physical drivers of wave driven erosion and accretion. On end-member, lowing sloping beaches, the model results suggest that wave driven dune accretion may occur where the dynamic still water level (still water level combined with wave setup) is below the dune toe. Although total water levels are typically in the collision regime numerous times per year in the PNW (e.g., Ruggiero et al., 2001), dynamic still water levels infrequently exceed the dune toe because of the uncommon co-occurrence of large wave energy and high still water levels in the PNW. Consequently, the model results suggest that on average ~15 m^3/m/yr of dune growth is directly from marine-driven processes at Oysterville, WA. The model simulations also suggest that coastal profiles with steeper nearshore, beach, and dune profiles will generally experience dune erosion, rather than accretion, due to morphodynamic feedbacks. The work in Chapter 4 has been prepared for submission to *Geomorphology*.

As discovered in the previous chapters, marine processes are important contributors to the growth of coastal foredunes for some dissipative coastal systems. However, wind driven processes are still generally thought to be the predominant driver of coastal foredune growth. In Chapter 5 the development of a new, coupled numerical modeling framework is presented to simulate the co-evolution of the coastal zone in response to both wind and wave driven forces. Windsurf, the numerical modeling framework, is applied to the Oysterville, WA field site to explore the processes contributing to coastal foredune growth over an annual time scale. Consistent with field measurements, the model simulates seasonal cycles of beach growth in summer, shoreline recession in winter, and net dune growth annually. Windsurf also supports key findings from Chapter 2 and 4, showing that that there are both marine (6.6 m^3/m/yr) and aeolian (14.2 m^3/m/yr) contributions to coastal foredune growth at Oysterville, WA. These aeolian contributions are simulated to occur intermittently throughout the year in response to moderate wind speeds, while the marine driven dune growth occurs primary as a result of high TWLs during the fall. This model application indicates that the newly developed coupled numerical modeling framework can simulate many complex ecomorphodynamic processes relevant to prograding, dissipative coastal systems. More work is underway to continue model development and testing.

Chapter 6 summarizes the findings of the work presented in this disseration and provides some concluding thoughts. Together, these chapters reveal new insights into the time scales of sediment exchanges between the nearshore, beach, and dune and explore the contributing role of antecedant morphology (both subaqueous and subaerial) on controlling the hydrodynamic processes driving coastal change. For example, this work diverges from conventional frameworks that unconditionally relate marine impacts to coastal foredunes as erosional. Both the field-based and numerical methods presented in Chapters 2, 4, and 5 independently support the finding that marine processes may contribute to annual dune growth at Oysterville, WA. Marine driven dune growth was also observed at two other PNW field sites (Chapter 4), further suggesting that this process is not unique to a single site. Although field data are a key component of this research, this work also demonstrates that existing process-based tools do show reasonable skill at simulating complex hydrodynamic and coastal change processes in high energy, dissipative coastal settings. Significant

work remains to reliably simulate coastal landscape change across the full range of human-relevant time scales, however an improved process-understanding and numerical simulation capability of dissipative coastal morphodynamics is an increment step towards this goal.

Chapter 2: New insights on coastal foredune growth: the relative contributions of marine and aeolian processes

Nicholas Cohn, Peter Ruggiero, Sierd de Vries, and George Kaminsky

Abstract

Coastal foredune growth is typically associated with aeolian sediment transport processes while foredune erosion is associated with destructive marine processes. New datasets collected at a high energy, dissipative beach suggest that total water levels in the collision regime can cause dunes to accrete - requiring a paradigm shift away from considering collisional wave impacts as unconditionally erosional. From morphologic change datasets, it is estimated that marine processes explain between 9% and 38% of annual dune growth with aeolian processes accounting for the remaining 62% to 91%. The largest wind-driven dune growth occurs during the winter, in response to high wind velocities, but out of phase with summertime beach growth via intertidal sandbar welding. The lack of synchronization between maximum beach sediment supply and wind-driven dune growth indicates that aeolian transport at this site is primarily transport, rather than supply, limited, likely due to a lack of fetch limitations.

2.1   Introduction

Sandy coastal systems evolve at a range of time and space scales reflecting the complexity of the processes influencing the coastal zone. On sub-hourly scales, cross-shore subaqueous sediment transport gradients result from the competing processes of onshore, off-shore, and longshore directed wave and current forcings (e.g., Roelvink & Stive, 1989). In general, low-energy conditions drive net onshore sediment transport via nonlinear wave processes (e.g., Hoefel, 2003) contributing to beach growth. Conversely, undertow and low-frequency wave motions typically erode the beach during elevated energy conditions (e.g., Russell, 1993). Over longer time scales (>seasonal), longshore sediment transport gradients are often the primary driver of shoreline change (e.g., Harley et al., 2011b).

Foredune growth is believed to be primarily driven by aeolian sediment transport and associated feedbacks with sand trapping vegetation (e.g., Hesp, 1981). While instantaneous dry sand transport is controlled predominantly by wind velocity and local grain size characteristics (Bagnold, 1937), foredune growth on annual to decadal scales is often poorly correlated with wind conditions (de Vries et al., 2012). Even in the presence of wind,

sediment supply limiters such as armoring (Hoonhout & de Vries, 2017b), moisture content (Davidson-Arnott et al., 2005), cementation (Nickling & Ecclestone, 1981), and fetch limitations (e.g., Delgado-Fernandez, 2010) limit or prevent aeolian sediment transport to the dunes. These findings in part promote a hypothesis whereby dune growth is thought to be controlled primarily by the synchronicity of sediment supply from the nearshore to the beach, via the welding of intertidal sandbars (IBW), with the capacity to mobilize this sediment by wind (Houser, 2009). That is, dune growth will not occur, or is volumetrically limited, when IBW does not coincide with wind sufficient to cause saltation. The rarity of observed foredune erosion on some dissipative beaches has been previously credited as evidence for synchronization (Houser, 2009). However, limited quantitative data exists demonstrating that synchronized transport between the nearshore, beach, and dune is a universal factor in controlling dune growth.

Here we explore the time scales and processes driving sediment exchanges between the nearshore, beach, and dune using morphologic and environmental datasets spanning time scales of days to decades at a dissipative field site in Oysterville, Washington, USA. Utilizing these data, we test the hypothesis that dune growth is controlled by the synchronization of IBW and aeolian transport capacity.

2.2 Field Datasets and Methods

2.2.1 Geographic Setting

The town of Oysterville, WA (Figure 2.1a) is located on the Long Beach Peninsula (LBP) within the U.S. Pacific Northwest and is a modally dissipative, mesotidal (2-3 m tidal range) system with low-gradient, fine sand (D50 ~ 0.2 mm) beaches and densely vegetated foredunes (Ruggiero et al., 2005; Hacker et al., 2012). LBP is one of the largest continuous stretches of open coast in the world, with subaqueous sandbars, beaches, and dunes all exhibiting relative alongshore uniformity on scales of multiple kilometers (e.g., Mull & Ruggiero, 2014; Di Leonardo & Ruggiero, 2015; Ruggiero et al., 2016). Oceanographic conditions vary seasonally, with the lowest wave energy and water levels occurring in boreal summer (Figure 2.2; Serafin and Ruggiero, 2014). Winter is more energetic, with the
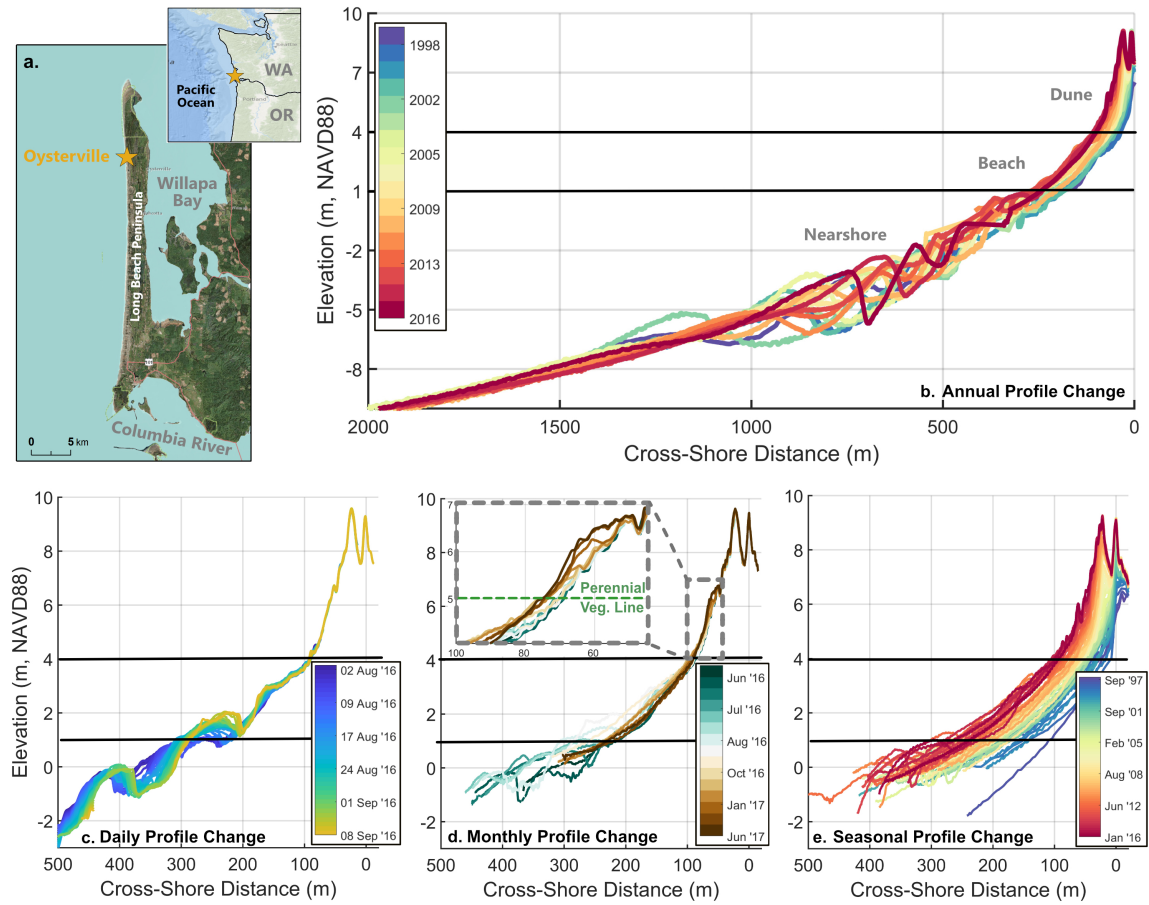
Figure 2.1: (a) Field site location and (b) annual [1998-2016], (c) daily [summer 2016], (d) monthly [June 2016 June 2017], and (e) seasonal [1997-2016] cross-shore profile changes at Oysterville.
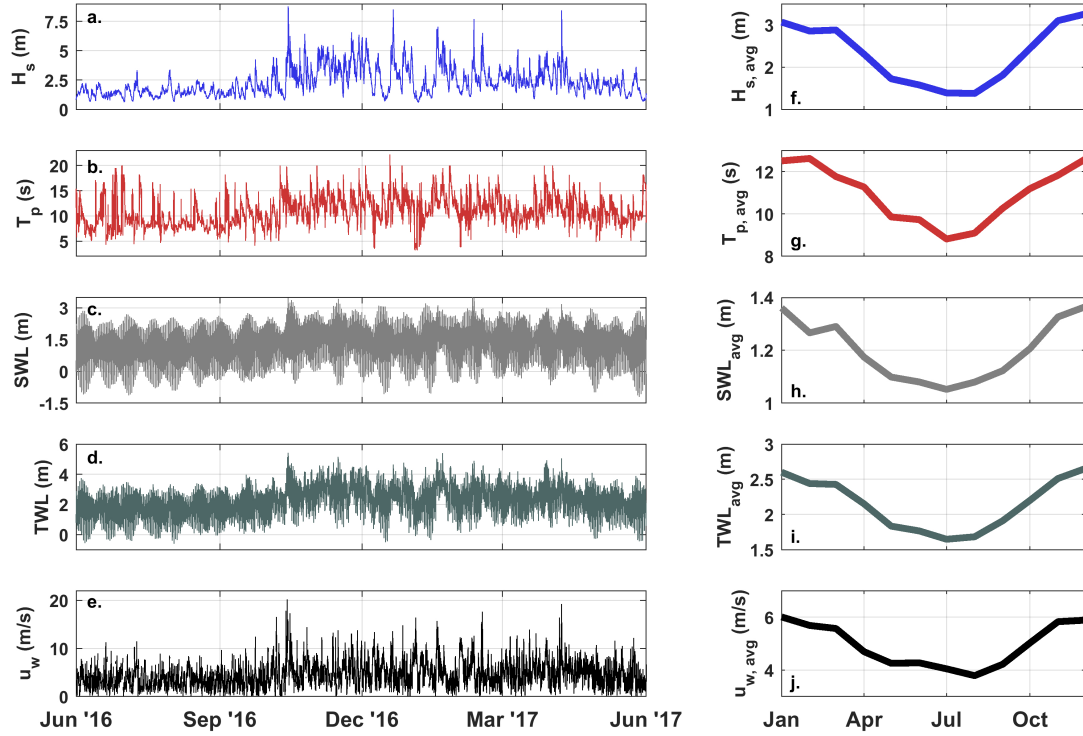
Figure 2.2: Significant wave height (H$_s$), peak wave period (T$_p$), still water level (SWL), total water level (TWL), and wind velocity (u$_w$) time series for June 2016 to May 2017 (a,b,c,d,e) and multi-decadal (1997-2017) monthly averages (f,g,h,i,j).

average annual winter storm having H$_s$ exceeding 10 m. The wind climate is also seasonally variable and in phase with the wave climate (Figure 2.2f,j), with the largest wind speeds typically corresponding to winter storms. The seasonal cycles in forcing drive seasonal cycles of shoreline recession and progradation. However, on longer time scales, sediment inputs from longshore transport gradients and cross-shore shoreface feeding results in average shoreline progradation of about 4 m/yr (Ruggiero et al., 2016). Despite the high energy wave climate, foredune erosion is rarely observed and an entirely new foredune has developed at the study site since the late 1990s (Moore et al., 2016).

2.2.2 Morphology Measurements

A long-term coastal monitoring program has measured bathymetric (annual) and topographic (seasonal) changes since 1997 (Ruggiero et al., 2005; Figure 2.1b,e). The seasonal topographic surveys are typically collected in March (winter), June (spring), September (summer), and December (fall). Additional daily topographic and weekly bathymetric measurements were made during a 38 day period in August and September 2016 as part of the Sandbar Aeolian Dune Exchange Experiment (SEDEX[2]) (Figure 2.1c). Bracketing the main SEDEX[2] period, topographic data was collected nominally monthly between June 2016 and June 2017 (Figure 2.1d). For this study, a single, regionally representative cross-shore transect from these daily to decadal scale field initiatives is utilized. These data are interpolated onto a cross-shore grid (dx = 0.1 m) in order to assess volumetric and contour changes. For these analyses, the nearshore is defined as the region from -12 m (the seaward limit of data) to 1 m, with all vertical references relative to the NAVD88 datum. The 1 m contour (approximately local mean sea level) is used as a proxy for the nearshore-beach boundary. The beach is defined from 1 m to 4 m, where this upper limit is associated with the approximate dune toe elevation and the zone landward of the dune toe is classified as the dune (e.g., Mull & Ruggiero, 2014). There are vertical uncertainties of ~ ±0.07 m for the backpack-based topography (e.g., Ruggiero et al., 2005) and ~ ±0.13 m for the single-beam bathymetry (e.g., Gelfenbaum et al., 2015) surveys. Accordingly, there are uncertainties of approximately 250 m^3/m, 10 m^3/m, and 5 m^3/m in each nearshore, beach, and dune volume calculation, respectively.

2.2.3 Environmental Conditions

The total water level (TWL), a key driver of short-term beach erosion (e.g., Ruggiero et al., 2001), represents the vertical water level excursion on the beach resulting from the combination of tides, non-tidal residuals (e.g., storm surge), and wave runup. For this study, the 2% exceedance value of wave runup maxima ($R_{2\%}$) is calculated using the dissipative form of the Stockdon et al. (2006) empirical runup predictor, defined as:

$$R_{2\%} = 0.046\,\sqrt{H_s L_o} \tag{2.1}$$

where L_o is the deep-water wavelength. An hourly TWL time series is calculated using wave height and period information from the Coastal Data Information Program (CDIP) buoy 036 located 35 km northwest from the study site and still water levels (tides plus non-tidal residuals) measured at the National Oceanic and Atmospheric Administration (NOAA) Toke Point, WA station 9440910 located 20 km northeast from Oysterville in Willapa Bay (Figure 2.2). Wind information is also obtained from the NOAA station.

2.2.4   Morpho-Stratigraphic Analysis

Stratigraphy has been used in a wide range of applications to infer processes driving coastal landscape change (e.g., Clemmensen et al., 2008; Hein et al., 2012; Storms, 2003). To elucidate the timing of net sediment deposition at Oysterville, a morpho-stratigraphic cross-section is developed from the morphology data. From each of the seasonal topographic profiles, the timing of the first instance of deposition that is not subsequently re-eroded is recorded for each cell on a grid that covers the entire beach and dune region ($dx = 0.1$ m, $dz = 0.1$ m).

Based on the environmental conditions which occurred between the recorded deposition date and the preceding survey date, volumetric changes for each grid cell can be attributed to either wind or wave forcing. Since wave-driven transport rates are typically much larger than aeolian transport rates based on the three orders of magnitude difference in the transporting fluid density (e.g., Bagnold, 1937), deposition in areas affected by TWLs likely reflects transport by wave processes. Regions influenced by TWLs more than 2% of the time within a given season (TWL$_{2\%}$, ~44 hrs/season) are assumed to be wave dominated. Above the maximum seasonal TWL (TWL$_{max}$) it is assumed that aeolian and ecological processes (Zarnetske et al., 2012) dominate net geomorphic changes in the dunes. The region between TWL$_{2\%}$ and TWL$_{max}$ is potentially affected by both marine and aeolian processes.

As an example, at a cross-shore distance of 50 m (based on the coordinate system in Figure 2.1e) deposition at 4 m elevation was first recorded on 7 December 2003. The $TWL_{2\%}$ and TWL_{max} were 4.5 m and 5.8 m, respectively, between the two relevant surveys. As both TWL values exceed 4 m, deposition recorded at the 50 m location is attributed solely to wave forcing. Conversely, new deposition in cells higher than 5.8 m were assumed to be driven by aeolian forcing as this region was not influenced by TWLs in fall 2003. Deposition between 4.5 m and 5.8 m in this season may represent wave and/or wind forcing.

The grid-based morpho-stratigraphic results are subsequently averaged within 1 m vertical bins to assess the timing and process controls on deposition across the beach and dune.

2.3 Results

2.3.1 Daily Morphology Change

Cross-shore topographic surveys were completed for 38 consecutive days at low tide during SEDEX[2] (Figure 2.1c). The four sandbars present during SEDEX[2] all migrated onshore under sustained low-energy conditions (Cohn et al., 2017). The single sandbar located entirely within the intertidal zone migrated onshore at an average rate of 1.2 m/day, shallowing in the process and contributing to the growth of a berm above the mean high water contour (MHW, 2.1 m). Although IBW was not completed during the experiment, the seaward-most berm position prograded by about 16 m and 42 m^3/m of sediment was added to the beach (Figure 2.3a). Negligible volume changes were observed in the dune during the experiment.

2.3.2 Monthly Morphology Change

Intertidal sandbars were intermittently present throughout spring and summer 2016 (Figure 2.1d) and, when present, continuously migrated onshore when H_s was below about 2 m. Resulting from this sandbar migration and welding sequence, which was partially captured during SEDEX[2], the most prograded position of the 1 m contour occurred in September
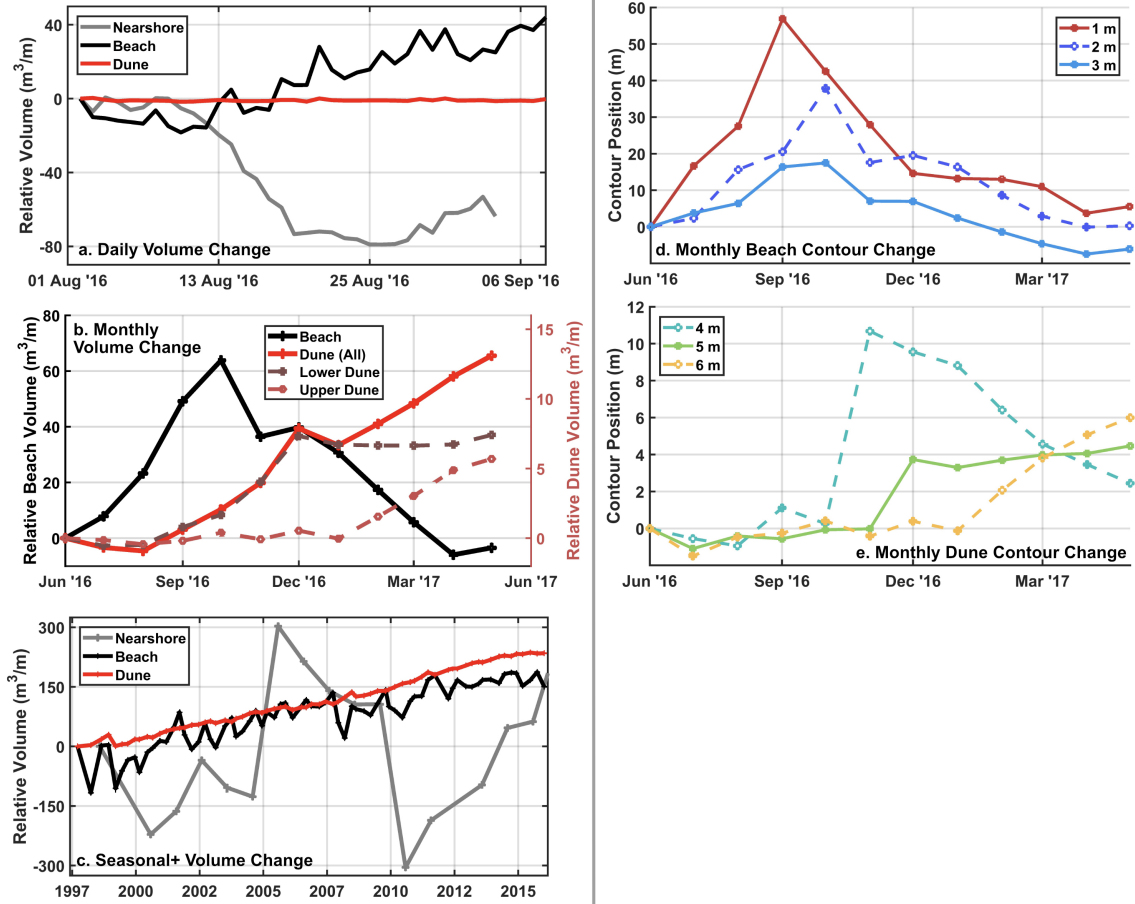
Figure 2.3: Nearshore, beach, and dune volume changes at daily (a), monthly (b), and seasonal to interannual scales (c). Contour changes for the beach (d) and dune (e) are shown at monthly scale. Monthly dune volume changes (b) are grouped into the lower dune (4.0 < z ≤ 5. 4m) and upper dune (z > 5.4 m) based on TWL_{max}.

2016. Elevated water levels later in September (Figure 2.2a) contributed to erosion of the intertidal sandbar and berm morphology and smoothed the beach topography. In response, the 1 m contour eroded between September and October while the 2 m and 3 m contours prograded (Figure 2.3d). Thereafter, the 1, 2, and 3 m beach contours continued to retreat until May 2017. Volume changes to the beach (ΔV_{beach}) behaved similarly (Figure 2.3b), with 64 m^3/m of sediment temporarily added to the beach during summer but with almost no net annual ΔV_{beach}.

Negligible contour and volume changes occurred within the dune (Figure 2.3b,e) between June and September 2016. Energetic conditions during October resulted in four hours when TWLs exceeded 5 m (Figure 2.2d), approximately corresponding to the perennial seaward extent of *Ammophila breviligulata* (American beach grass), with TWL$_{max}$ as high as 5.4 m. Between October and November the 4 m contour prograded by 10 m and the lower dune (4 to 5.4 m) volume increased by about 2 m^3/m (significant relative to measurement uncertainty). A TWL$_{max}$ event of 5.2 m in November coincided with an additional 4 m^3/m of lower dune growth. Visual observations of swash and freshly deposited marine macrophyte wrack found proximal to the perennial vegetation line during field surveys corroborate that TWLs reached above 5 m. Negligible sediment deposition above TWL$_{max}$ in October and November suggests that limited aeolian transport occurred in this early fall period (Figure 2.3b). These combined observations support a potential wave-driven origin of these accumulated lower dune sediments (Figure 2.3b). Throughout the remainder of the monthly survey period, continually high TWLs (253 hours >4 m, 11 hours >5 m between November and May) did not drive lower dune volume losses (Figure 2.3b), though a gradual retreat of the 4 m contour occurred after November (Figure 2.3e).

Sediment deposited above 5.4 m (TWL$_{max}$) in 2016-2017 is assumed to result solely from aeolian processes. The largest rates of upper dune growth (>5.4 m) occurred between February and May 2017 (Figure 2.3b,e) coinciding with a period of relatively high wind energy (Figure 2.2) and the most eroded beach state (Figure 2.3b,d). Over the full year, 13 m^3/m of sediment accumulated in the foredune (ΔV_{dune}).

2.3.3   Seasonal to Decadal Morphology Change

The seasonal topographic data shows sustained dune growth over the past two decades, with an average ΔV_{dune} of 13 m^3/m/yr (Figure 2.3c). The dataset shows negative ΔV_{beach} in winter, positive ΔV_{beach} in summer, and a mean net ΔV_{beach} of 8 m^3/m/yr. Interannual nearshore volume changes show larger variability, exceeding the large measurement uncertainties of bathymetry data ($\sim \pm 250$ m^3/m) and therefore partially reflecting variability in gradients in longshore sediment transport.

The morpho-stratigraphic cross-section shows that the largest volume gains to the beach occur in spring, with spring accounting for 65% of volumetric changes between the 1 to 2 m contours (Figure 2.4a,b). Because intertidal sandbars are transient features, net deposition on the beach is relatively minimal in summer. The lower portion of the dune is dominated by deposition in fall. Some aeolian transport occurs to the dune year-round, but the winter accounts for 31% of total ΔV_{dune} and 56% of the growth above 8 m.

The morpho-stratigraphic analysis also shows that volume changes above 6 m are controlled primarily by aeolian and ecological processes, where the shaded regions in Figure 4 2.4c,d reflect uncertainty in wave and wind contributions to deposition between TWL$_{2\%}$ and TWL$_{max}$. Conversely, deposition below 3 m is driven exclusively by wave processes. Consistent with the detailed 2016 observations, maximum rates of wave-driven lower dune growth are inferred to occur in the fall.

2.4   Discussion

Agreeing with previous studies, IBW is an important sediment delivery mechanism from the nearshore to the beach (e.g., Aagaard et al., 2004; Anthony et al., 2006). However, for this dissipative setting where the wind and wave climates are in-phase (Figure 2.2f,g,h,i,j) and beach growth occurs during low wave energy conditions (Figure 2.3d), there is little opportunity for sandbar-derived sediments to be mobilized by winds prior to a seasonal increase in wave energy. Based on the morphology datasets, maximum ΔV_{dune} is generally about 6 months out of phase with maximum beach sediment supply (Figure 2.4d), where the available sediment supply is approximated with the average seasonal dry beach width
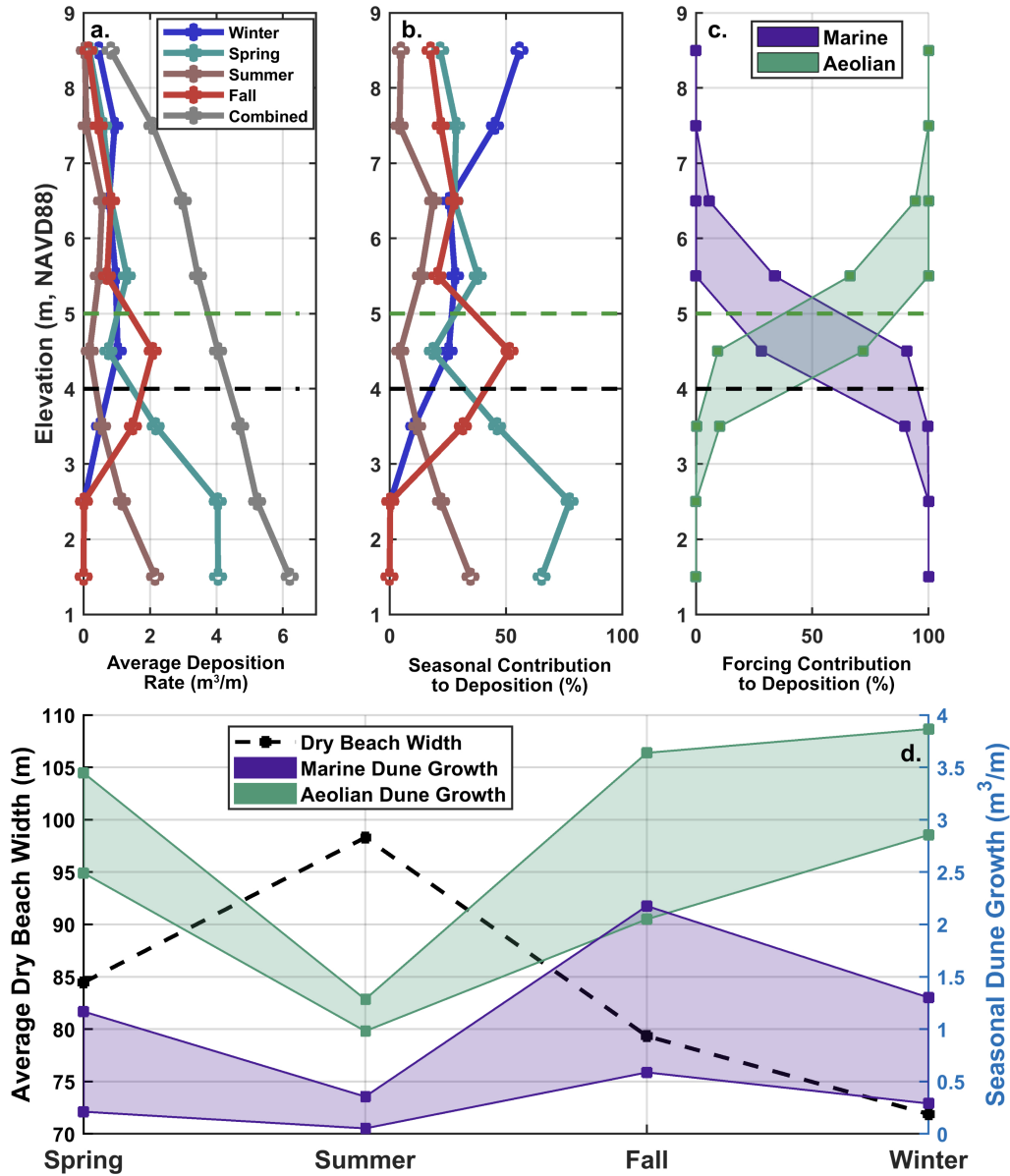
Figure 2.4: (a) Average seasonal deposition rates, (b) relative seasonal contribution to deposition, and (c) inferred dominant depositional transport process based on the morphostratigraphic analysis, and (d) inferred transport process on seasonal dune growth rates compared against average seasonal dry beach width. Shaded regions in c/d reflect uncertainty in process contribution to dune growth rates between $TWL_{2\%}$ and TWL_{max}.

(MHW to 4 m) (e.g., Diez et al., 2018). Maximum ΔV_{dune} instead occurs in phase with high wind velocities in winter despite the co-occurrence of an eroded beach state. Additionally, it is shown that annual ΔV_{dune} is relatively consistent with time despite large temporal variability in nearshore and beach volumes (Figure 2.3c). These observations suggest that transport limitations are more important than supply limitations for governing wind-driven dune growth at Oysterville. This may be a function of the large beach widths, fine grained sand, and oblique winds at the field site, which collectively limit fetch effects on aeolian transport to the dune (e.g., Davidson-Arnott & Law, 1996).

Paleo-dune development at LBP has previously been related to the formation of a series of marine beach ridges (Cooper, 1958), which were only later capped by aeolian deposits following ridge abandonment. Contrasting with the distinct separation between wind and wave processes on coastal landform evolution described within the beach/dune ridge literature (e.g., Taylor & Stone, 1996; Hesp, 2006), the data presented here suggests that both marine and aeolian processes can simultaneously contribute to foredune growth. While dune erosion from direct wave impact and the landward transport of dune sediments via overwash have been widely documented (e.g., Figlus et al., 2011), to the knowledge of the authors the direct role of waves in dune face growth has not been previously recognized. Although wave-driven dune accretion was only explicitly documented for the fall 2016 period, the morpho-stratigraphic approach implies this accretional process is not infrequent and may contribute between 9% (up to $TWL_{2\%}$) and 38% (up to TWL_{max}) to annual dune growth. This is in contrast to the conventional viewpoint of geomorphic responses to the collision regime using Sallenger's (2000) Storm Impact Scaling model, requiring a shift away from the paradigm in which collisional wave impacts are unconditionally erosional. As LBP is relatively unique among coastal systems in that it is prograding, high energy, and low sloping, wave-driven dune accretion may be limited to end-member dissipative systems where the swash zone is dominated by low frequency processes (Cohn & Ruggiero, 2016; Ruessink et al., 1998).

Aeolian and ecological processes have a larger control on overall dune dynamics accounting for between 62% and 91% of ΔV_{dune} over the twenty-year record. Aeolian processes also cannot be fully excluded as a depositional source below TWL_{max} without addi-
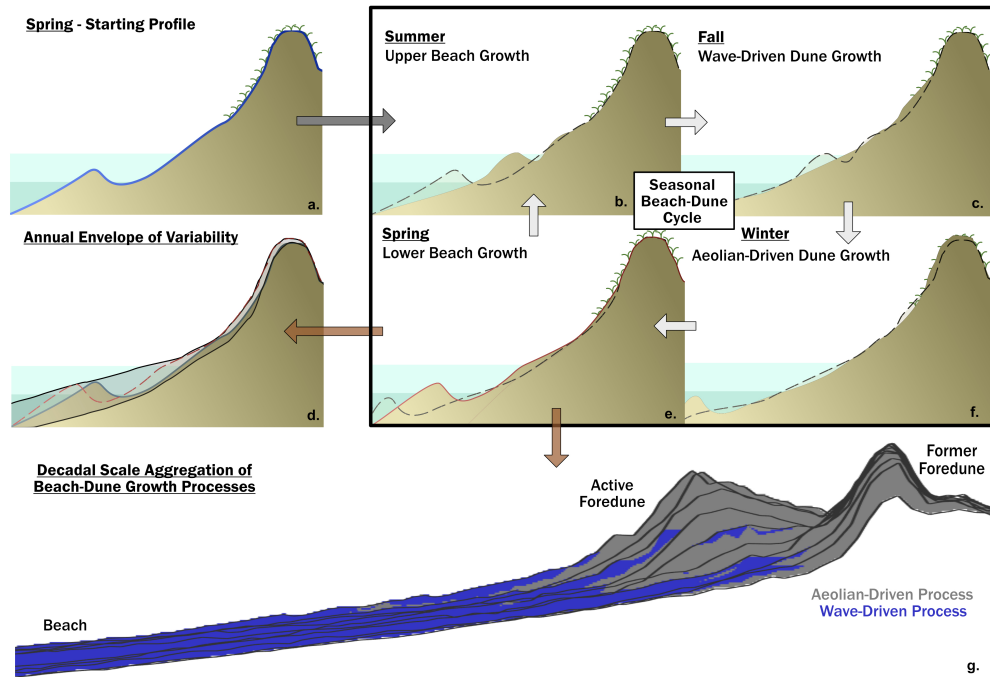
Figure 2.5: Conceptual model of beach and dune evolution at Oysterville, WA showing the inferred predominant seasonal transport modes and geomorphic changes (a,b,c,e,f) and annual envelope of bed elevation change (d). Seasonal process aggregation over a decadal period using the morpho-stratigraphic approach is shown in panel g, where each black line represents net geomorphic changes over one year with aeolian (grey) and wave-driven (blue) contributions highlighted.

tional field observations. However, the lack of observed dune erosion despite the frequency of TWLs in the collision regime (~250 hrs/yr) is indirect evidence that high TWLs are not necessarily destructive to the dunes. While wave processes are assumed to dominate depositional signatures below $TWL_{2\%}$, higher thresholds show similar results. Only for threshold durations above $TWL_{7.5\%}$, corresponding to ~2 hrs/day in the collision regime, does the morpho-stratigraphic approach indicate that aeolian processes are the sole contributor to dune growth (not shown).

Driven by the field observations, a conceptual model of the inferred seasonal sediment cycling and its relationship to long-term coastal evolution is presented in Figure 2.5.

Spring is characterized by lower beach growth, summer by upper beach growth via IBW, fall by wave-driven lower dune growth, and winter by aeolian-driven upper dune growth. The repeat cycling of these seasonal processes drives interannual dune growth; a cycle in which foredune growth is temporally de-coupled from beach and nearshore sediment supply (Figure 2.4d). Based on these detailed field observations, the synchronization hypothesis (Houser, 2009) does not appear to be valid for LBP and may be limited in its ability to explain the dynamics of sediment-starved systems and/or systems where wind and wave climates are not seasonally in-phase.

2.5   Conclusions

Morphologic measurements spanning time scales of days to decades provide new insights into processes driving dune growth at a dissipative, prograding beach. Beach and dune growth at Oysterville, WA are not synchronized in time. While onshore intertidal sandbar migration drives beach growth in spring and summer, maximum dune growth instead occurs in winter coincident with the most eroded beach state and the highest wind speeds. It is demonstrated, perhaps for the first time, that elevated TWLs can cause dunes to accrete – in contrast to conventional frameworks that relate water levels above the dune toe solely to foredune erosion.

Acknowledgements

Chapter 3: The influence of seasonal to interannual nearshore profile variability on extreme water levels: Modeling wave runup on dissipative beaches

Nicholas Cohn and Peter Ruggiero

Abstract

Wave runup, an important contributor to storm-induced extreme water levels, is commonly predicted via empirical formulations that parameterize coastal morphology using simple metrics such as the foreshore beach slope. However, spatially and temporally complex nearshore morphology, such as subtidal sandbars, have the potential to alter surf zone wave dissipation patterns and therefore influence setup, swash, and runup levels observed at the shoreline. In this study, a suite of numerical experiments using XBeach demonstrate reasonable skill in reproducing wave runup observations in dissipative settings, explore the relative influence of seasonal to interannual variability in nearshore morphology on runup and its constitutive components, and illustrate differences between empirical and numerically modeled estimates of runup. The numerical model results show that interannual variability in sandbar configuration, associated with net offshore sandbar migration, has a larger influence on wave runup than does seasonal sandbar variability. Although the particular configuration of sandbars was estimated to influence runup by as much as 0.18 m during storm conditions, natural variability in subaerial beach topography has a stronger influence on runup than subtidal morphology. XBeach demonstrates that both wave setup and infragravity swash have morphologic controls. In experiments simulating storm conditions in which both nearshore and beach morphology was varied, natural interannual variability in beach topography explained about 80% of the variance in runup and its constituents. While XBeach predictions of setup, swash, and runup compare favorably with empirical predictors for low wave conditions, the numerical model predicts higher runup levels for storm-conditions on dissipative beaches raising potential concerns about coastal hazards assessments that use these empirical models to estimate extreme total water levels.

3.1 Introduction

Storm-induced, elevated water levels pose a major hazard to low-lying coastal communities, occasionally generating severe backshore flooding and erosion. Recent events such as Hurricanes Katrina and Sandy have highlighted community vulnerability to anomalous high water events which can result in substantial environmental and economic damages

(Benimoff et al., 2015; Vigdor, 2008). While wind-driven storm surge can dominate damages during large landfalling hurricanes, often one of the most important components of storm-induced extreme total water levels (TWLs) is wave runup (e.g., Stockdon et al., 2007). In a recent U.S. West Coast study, Serafin & Ruggiero (2014) showed that wave runup contributed approximately 60% of the TWL during the maximum high water level event on record. In more than half of the ~150 events (~5 events per year) included in that studies' extreme value analysis, wave-induced water levels accounted for >50% of the TWL signal.

Many studies have related runup, and its constituent components of setup and swash, to local beach characteristics and to the incident wave climate (e.g., Holman, 1986; Ruessink et al., 1998; Stockdon et al., 2006). For example, working on high energy dissipative beaches in the U.S. Pacific Northwest (PNW), Ruggiero et al. (2001) [henceforth R01] found that >95% of swash variance was in the infragravity band and related the 2% exceedance elevation of runup maxima, $R_{2\%}$, as

$$R_{2\%} = 0.27 \sqrt{\beta_f H_o L_o} \qquad \text{(EQ 3.1)}$$

where β_f is the foreshore slope, H_o is the deep-water significant wave height, and L_o is the deep-water wavelength. Stockdon et al. (2006) synthesized video data from 10 field experiments at 6 different beaches, including the dissipative beach data from Ruggiero et al. (2001), and generated empirical models relating wave setup ($\bar{\eta}$), incident band swash (S_{INC}), infragravity band swash (S_{IG}), and $R_{2\%}$ to offshore wave conditions and characteristics of the coastal profile. The general form of the Stockdon et al. (2006) model [henceforth SG06] for extreme wave runup is given as

$$R_{2\%} = 1.1 \left(\bar{\eta} + \frac{\sqrt{S_{INC}^2 + S_{IG}^2}}{2} \right) = 1.1 \left(0.35\beta_f \sqrt{H_o L_o} + \frac{\sqrt{H_o L_o \left(0.563\beta_f^2 + 0.004 \right)}}{2} \right)$$
$$\text{(EQ 3.2)}$$

For data with Iribarren numbers (ξ_o; Battjes, 1974) less than 0.3, Stockdon et al. (2006) developed a formulation specific to dissipative beaches [henceforth SD06]

$$R_{2\%} = 0.043 \sqrt{H_o L_o} \qquad\qquad \text{(EQ 3.3)}$$

While the SD06 relationship is independent of the beach profile, SG06 and R01 both have dependencies on β_f, which is defined as the mean slope between $\bar{\eta} \pm$ twice the standard deviation of the swash time series. Stockdon et al. (2006) explored $\bar{\eta}$, S_{INC}, S_{IG}, and $R_{2\%}$ dependencies on other metrics representing the nearshore profile, such as the surf zone slope, yet found no statistically significant relationships. However, a number of field studies have suggested that complex nearshore morphology, such as the presence of sandbars, may influence swash processes (e.g., Brodie et al., 2012; Cox et al., 2013; Guedes et al., 2012; Sénéchal et al., 2013) and therefore β_f alone may not fully explain the morphologic control on runup.

Nearshore sandbars act as a perturbation to the coastal profile causing waves to break further offshore during storm events, potentially limiting coastal erosion by dissipating wave energy away from the beach face (Castelle et al., 2007; Holman & Sallenger, 1985; Shand et al., 2006). Likewise, temporal variability in tides on a barred beach alters surf-zone wave breaking patterns which may also in turn influence swash processes (e.g., Holman & Sallenger, 1985). For example, Guedes et al. (2011) found that runup height could vary by up to a factor of 2 between high tide (no waves breaking on a bar) and low tide (waves breaking on a bar) on an intermediate, micro-tidal beach. Similarly, Sénéchal et al. (2013) found a 30% reduction in runup during low tide caused by a reduction in infragravity energy associated with sandbar-induced wave breaking. Although these observations support the notion that sandbars influence wave runup, developing field datasets that directly link the influence of nearshore bathymetric variability to setup and swash statistics has proven challenging. For this reason, numerical models have increasingly been used to explore runup and its relationship to variable morphology. For example, using the Thornton & Guza (1983) wave transformation model, Stephens et al. (2011) demonstrated that, in the presence of a sandbar, the nearshore profile could explain at least as much variance on $\bar{\eta}$ as H_o. Using XBeach (Roelvink et al., 2009), Cox et al. (2013) [henceforth C13] found that S_{IG} is reduced when waves break over a bar relative to a non-barred beach profile. Based on these model results, C13 presented the following empirical model for infragravity swash

$$S_{IG} = 0.08F \sqrt{H_o L_o} \qquad \text{(EQ 3.4)}$$

where F is 0.71 on a non-barred beach (collapsing to the SG06 relationship for S_{IG} in Equation 3.2) and is equal to $\left(\frac{h_{bar}}{h_{nobar}}\right)^{0.39}$ on a barred beach, which represents the ratio of the bar depth (h_{bar}) to the local water depth in the absence of the bar (h_{nobar}). Conversely, using a nonlinear shallow water equations solver Soldini et al. (2013) found little difference in maximum predicted runup for a barred beach profile as compared to an equilibrium beach profile with the same onshore topography. Collectively, these studies indicate that the presence of nearshore sandbars, and their inherent variability, may influence $\bar{\eta}$, S_{IG}, and maximum runup in as yet unexplained ways.

To deepen understanding of the influence of nearshore morphological variability on wave runup, here we present a series of numerical XBeach experiments performed on observed and simulated beach profiles from the PNW. This region contains long stretches of sandy coast characterized by flat, dissipative beaches with wide surf zones and multiple nearshore sandbars (Haxel & Holman, 2004; Ruggiero et al., 2005). Since much of this coastline is characterized as a morphodynamic end-member (Wright & Short, 1984) and sandbars in the region have been shown to vary significantly both spatially and temporally on seasonal to interannual time scales (Di Leonardo & Ruggiero, 2015), the PNW is an ideal region to explore the influence of coastal morphology on swash zone hydrodynamics. Here we first demonstrate that XBeach skillfully reproduces runup statistics on high energy dissipative beaches by simulating conditions from the High Energy Beach Experiment (HBE) at Agate Beach, OR (Ruggiero et al., 2004). We then turn our focus to investigating the implications of natural variability in nearshore bathymetry and topography on $\bar{\eta}$, S_{IG}, runup, and TWLs along a characteristic dissipative beach. A wide range of wave conditions are simulated in order to analyze the general behavior of the model and to assess relationships between the coastal profile and wave driven components of TWLs.

The paper is organized as follows. Descriptions of the study sites, Agate Beach, OR and Long Beach, WA, are given in Section 3.2. In Section 3.3 the modeling approaches for five distinct numerical experiments are described, each of which explore runup behavior under differing environmental forcing conditions and nearshore morphological configurations.
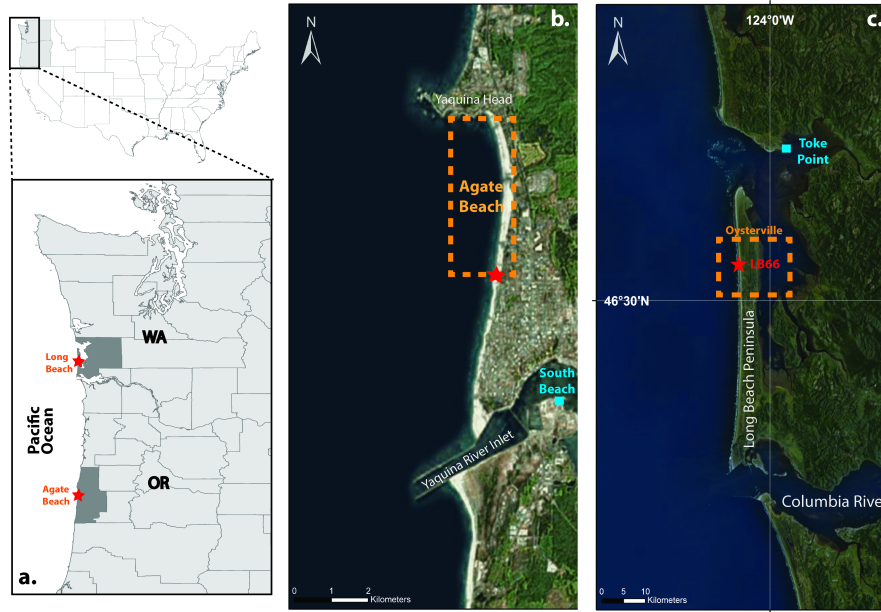
Figure 3.1: (a) Regional map of the U.S. Pacific Northwest with the two field sites identified. Zoomed in images of (b) Agate Beach and (c) Long Beach Peninsula show the coastal morphology measurement locations (red stars) and other geographic points of interest.

Results of these numerical modeling simulations are presented in Section 3.4 followed by comparisons of the results to existing empirical predictors of runup from the literature in Section 3.5. Concluding thoughts are provided in Section 3.6.

3.2   Study Sites

Classically, beaches have been defined as being in a dissipative state when the Iribarren Number, $tan(\beta_f)/\sqrt{H_o/L_o}$, is less than approximately 0.3 (Wright & Short, 1984). During storms this criteria is often satisfied because of large H_o while on beaches with very low β_f this criteria is satisfied under most sea states. Many PNW beaches are modally dissipative as a result of characteristically flat, low sloping profiles (Ruggiero et al., 2005). The PNW also has one of the most energetic wave climates in the world, with average annual H_o of about 2.4 m with peak wave periods of about 10.8 s and typically experiences about three

storm events per year with wave heights exceeding 8 m (Allan & Komar, 2002; Allan et al., 2006).

For this study, two relatively similar, meso-tidal, high energy, dissipative PNW beaches are investigated (Figure 3.1). The High Energy Beach Experiment took place at Agate Beach, OR in 1996, providing a runup dataset during dissipative conditions with H_o up to 3.1 m. Agate Beach is a 2.5 km sandy, bluff-backed stretch of coast located at the northern end of the Newport littoral cell in Newport, OR (Figure 3.1b). Repeat topographic surveys reveal large seasonal variability at Agate Beach, with an estimated 31.4±8.5 m^3/m of beach sediment lost to the nearshore during the winter and reworked onshore during summer (Haxel & Holman, 2004). Over the longer term the beach is net progradational, with an average shoreline change rate of about 2 m/yr between 1967 and 2002 (Ruggiero et al., 2013). While Argus image analysis indicates a dynamic nearshore with sandbars migrating onshore in summer and offshore in winter (Alexander & Holman, 2004), long-term in-situ observations of nearshore morphology do not exist for this site.

To take advantage of an existing PNW long-term dataset of in-situ coastal morphology measurements, our second study site is on the Long Beach Peninsula (LBP), part of the Columbia River Littoral Cell (CRLC). The CRLC is a dissipative, progradational coastal system that spans the Oregon and Washington border. The 165 km sandy coastal system consists of four barrier plain sub-cells bisected by 3 large estuaries – with the Columbia River being the largest historical source of sediment to the system (Kaminsky et al., 2010). Each of these barriers is generally characterized by wide, gently sloping beaches with broad surf zones and multiple dynamic subtidal and intertidal sandbars.

The shoreline along LBP (Figure 3.1c), just north of the mouth of the Columbia River, prograded at an average rate of 4.7±0.3 m/yr between the 1980s and 2002 (Ruggiero et al., 2013). More recent coastal change in the CRLC has been extensively documented via bathymetric and topographic beach surveys completed annually since 1998 as part of the Southwest Washington Coastal Erosion Study (SWCES) (Gelfenbaum & Kaminsky, 2010). Hundreds of cross-shore transects, extending from ~-12 m to ~+10 m, that have been collected throughout the CRLC provide insight into the regional sediment dynamics of this dissipative coastline. The annual surveys confirm that the high rates of progradation

(~4.0 m/yr in the Oysterville region of LBP) have continued through 2014. Quarterly topographic beach profiles also reveal a rapidly changing coastal system where there is significant seasonal and interannual variability in morphology (Ruggiero et al., 2005). In Oysterville, measurements show fairly alongshore-uniform sandbars that exhibit a trend of net offshore sandbar migration (NOM) with a return period of about 2.4 years (Cohn et al., 2014). This trend of NOM has been observed in numerous parts of the world whereby sandbars form in the inner surf zone, cyclically migrate offshore, and eventually dissipate in form on the shoreface (Plant et al., 1999; Ruessink & Kroon, 1994; Wijnberg & Terwindt, 1995).

Long Beach Peninsula profile 66 (LB66), a representative profile for the Oysterville region from the SWCES dataset (Figure 3.2a), typically contains two to three nearshore sandbars that conform to the cyclic NOM behavior (Cohn et al., 2014). These bars are generated close to shore, migrate offshore at an average (and maximum) rate of about 150 m/yr (405 m/yr) in Oysterville and deepen at an average (and maximum) rate of 1 m/yr (2.7 m/yr) (Figure 3.3b,c). Between 1998 and 2013 the profile data reveals a vertical envelope of over 4 m associated with the migration of these sandbars. Additionally, the data shows that the beach was always low sloping, with β_f at LB66 varying between 0.013 and 0.02 and having an average of 0.015 (Figure 3.3a).

3.3   Methods

To explore the influence of seasonal to interannual variability in coastal morphology on wave runup and its components, five discrete XBeach numerical modeling experiments were performed (Table 3.1). First, to demonstrate the model's skill in simulating $\overline{\eta}$, S_{IG}, and wave runup in highly dissipative settings, Experiment 1 hindcasts these parameters for the observed hydrodynamics during HBE. Experiments 2, 3, and 4 investigate the role of seasonal (Experiment 2) to interannual (Experiments 3 and 4) varying morphology on the components of runup at LBP. To isolate the relative influence of nearshore morphology (<-2.0 m MSL) versus beach morphology (>-2.0 m MSL) on runup, Experiment 3 varies nearshore morphology while holding beach morphology fixed between simulations while Experiment 4 varies both nearshore and beach morphology concurrently. Finally, in or-
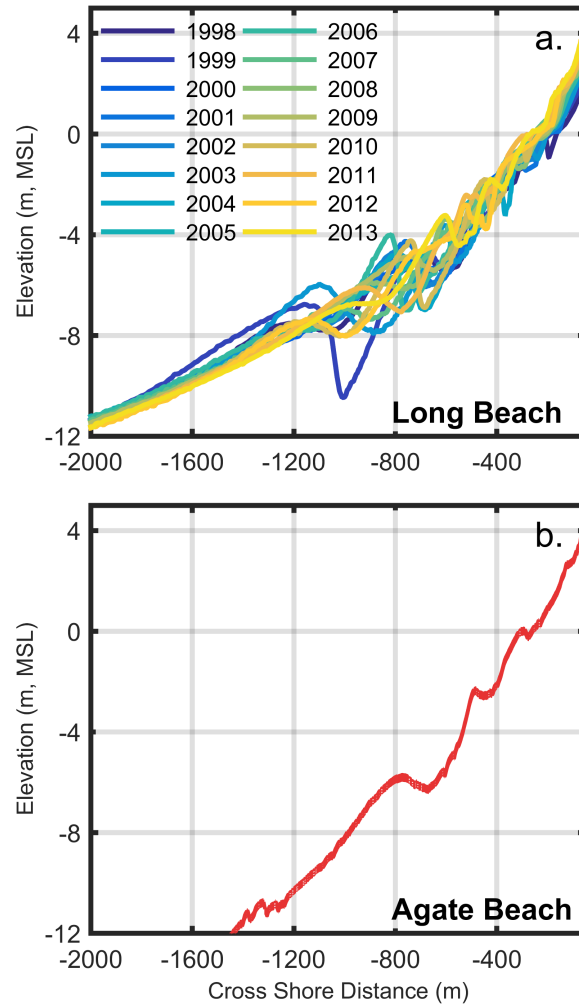
Figure 3.2: Coastal profiles measured at (a) LB66 from 1998 to 2013 and (b) Agate Beach in 2012.
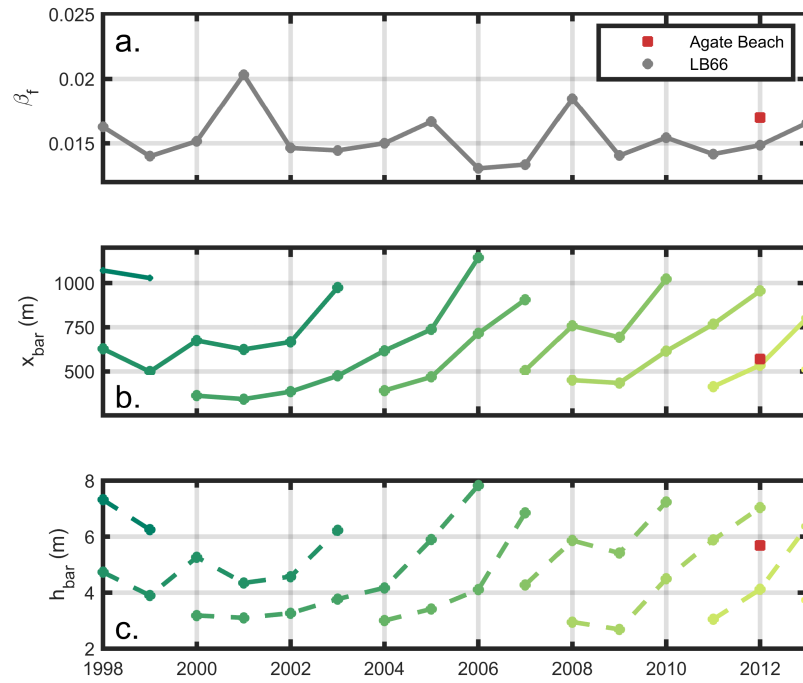
Figure 3.3: (a) Foreshore beach slope measured at LB66 (lines with circle markers) from 1998 to 2013. Alongshore-averaged (b) cross-shore location (x_{bar}) and (c) water depth (h_{bar}) of sandbars in Oysterville, WA showing a trend of interannual net offshore sandbar migration (modified from Cohn et al., 2014). In each panel the red squares indicate the equivalent morphometrics extracted from the 2012 Agate Beach profile.

der to explore potential implications of the results from these numerical experiments on coastal vulnerability assessments, a year-long TWL hindcast is generated at LBP in Experiment 5. Specific details of model setup and the experiments are described in the following subsections.

3.3.1 Hydrodynamic Model Overview

XBeach is a phase-averaged, process-based, surface gravity wave model (Roelvink et al., 2009) that is coupled with a non-linear shallow water model accounting for the generation of low frequency motions (Reniers et al., 2006). The model solves two-dimensional, depth-averaged equations for wave propagation and has modules for simulating sediment transport and morphologic change due to waves and wave-driven circulation. XBeach has been applied to a wide range of coastal applications including rip current prediction (Austin et al., 2013), overwash (McCall et al., 2010), dune erosion (de Winter et al., 2015; Splinter & Palmsten, 2012), and wave runup (Stockdon et al., 2014). Since XBeach is a phase-averaged model it does not resolve incident band swash excursions which may be important for the total runup, particularly on moderate to steeply sloped beaches. However, in dissipative settings, such as is the focus for our application, the swash zone is typically dominated by infragravity energy (Holman, 1986; Ruessink et al., 1998; Ruggiero et al., 2004).

XBeach is often applied in 1D, examining predominantly cross-shore processes while neglecting alongshore gradients in energy. The 1D model does not account for alongshore variability in hydrodynamics, does not incorporate wave directional spreading (Van Thiel de Vries et al., 2011), and only resolves the cross-shore directed component of infragravity energy (de Winter et al., 2015). Despite neglecting some potentially important physical processes, the 1D version of XBeach has demonstrated skill in reproducing surf-zone wave transformation (e.g., Stockdon et al., 2014; Geer et al., 2012) and dune erosion (e.g., van Dongeren et al., 2009). It has also provided reasonable estimates of wave runup compared to observational data. For example, model estimates of $\bar{\eta}$ at Duck, NC (Stockdon et al., 2014) using XBeach agree well with observations (RMSE < = 0.17 m with no significant model bias) in both 1D and 2D mode. While XBeach was found to generally underpredict

S_{IG} at Duck – the 1D model agreed better with S_{IG} observations than the 2D model. Here we justify the use of the 1D version of XBeach based on previous model validations (e.g., Stockdon et al., 2014), a model to field data comparison performed at Agate Beach, OR presented in Section 3.4.1, and to allow for exploration of a wide range of environmental and morphologic parameter space. Since 2D XBeach models require significantly more computing resources, thousands of simulations, such as those presented here, would not be possible.

The same general model setup was used for each of the five numerical experiments in this study, with only the bulk wave parameters, tidal elevations, and the coastal profile changed between simulations. For each experiment a 1D, cross-shore grid included elevations from ~-32 m to ~+8 m relative to MSL. Between ~-32 m and -12 m beach profile data was extracted from the NOAA Astoria 1/3 arc second Coastal Digital Elevation Model for all of the numerical experiments (Carignan et al., 2009). For Experiments 1, 3, and 4 profile data collected with the Coastal Profiling System (Ruggiero et al., 2005) and backpack-based RTK GPS was used to define the bed elevation shallower than ~-12 m. For Experiments 2 and 5 modeled bathymetry derived from a UNIBEST-TC [henceforth UTC] (Bosboom et al., 2000) simulation (to be further described in Section 3.2) was used for water depths shallower than ~-12 m and was merged with RTK GPS topographic measurements. Each of the datasets were converted to MSL using VDatum (Xu et al., 2010) and interpolated onto a grid with variable grid spacing of 10 m offshore and finer 0.5 m onshore grid spacing in order to adequately resolve low frequency swash excursions on the beach face. Further details of the topography and bathymetry for each numerical experiment are provided in Section 3.3.3 and Table 3.1.

For all of the numerical experiments, XBeach was run in 1D hydrostatic mode for a total simulation time of two hours. To validate our choice of the 1D model, additional 2D XBeach simulations were made for Experiment 1 assuming an alongshore uniform beach profile and applying the same boundary conditions as the 1D model. For the 2D simulations, the model domain extended 10 km in the alongshore dimension with high resolution (10 m) spacing in the center of the domain and increasing grid size (>100 m) near the lateral boundaries. This approach was taken to adequately resolve alongshore variability

Table 3.1: Environmental and morphology conditions used to define the run matrix for XBeach numerical modeling experiments 1 through 5.

Experiment #	Description	Site	Morphology		Waves	Water levels	# of simulations
			Subtidal (<-2 m)	Onshore (>-2 m)			
1	High Energy Beach Experiment	Agate Beach	Measured 2012 (1 profile)	Measured during HBE	Measured	Measured	14
2	Seasonally variable subtidal morphology	LBP	UTC modeled (12 profiles, seasonal)	Measured 2011	48 generic conditions	MSL	576
3	Interannually variable subtidal morphology	LBP	Measured 1998–2013 (16 profiles, annual)	Measured 2011	48 generic conditions	MSL	768
4	Interannually variable onshore and subtidal morphology	LBP	Measured 1998–2013 (16 profiles, annual)		48 generic conditions	MSL	768
5	Simulation of daily maximum conditions	LBP	UTC modeled (344 profiles, daily)	Measured 2011	SWAN modeled (hindcast)	Measured	344

in swash motions along the center 1 km of the domain while avoiding boundary effects. For all simulations morphological updating was turned off and default model settings were used for other model parameters not described herein.

For Experiments 1 to 4 the deepwater wave conditions were characterized by a generic JONSWAP spectrum utilizing a directional spreading coefficient of 2 (cosine power formulation) and a peak enhancement factor of 3.3. These spectra were shoaled over a planar slope to the water depth at the seaward edge of the XBeach grid using the Simulating Waves Nearshore (SWAN) model (Booij et al., 1999). For Experiment 5, XBeach was forced using bulk wave parameters derived from a regional wave model hindcast (García-Medina et al., 2014) extracted at the offshore XBeach model boundary. A JONSWAP spectrum based on these bulk wave parameters was input directly into XBeach for these simulations. The *random* variable in XBeach is set to zero in all experiments in order to sample the wave spectrum similarly for each simulation. This approach allows the influence of morphological variability on wave runup to be isolated rather than confounding the results due to the effects of the randomness of incoming wave groups.

In Experiments 2 to 4 the tidal level is held constant at MSL while tidal variability is included in Experiments 1 and 5. In Experiment 1 tides were obtained from the nearby NOAA South Beach tide gauge (Station 9435380, Figure 3.1b) for the period of HBE. Tides for Experiment 5 were derived from the nearby NOAA Toke Point tide gauge (Station 9440910, Figure 3.1c).

For all five experiments the model was run for two hours, where the first hour consisted of model spin-up and only data from the second hour was used for subsequent analysis. Water surface elevation was exported for the entire model grid at one second time intervals for this second hour. Runup time series were generated based on the landward most location where the instantaneous water surface exceeded 1 cm. For the 1D model simulations a single runup time series is generated, whereas for the 2D model simulations data every 10 m in the alongshore from the middle 1 km of the domain were exported. For each shoreline location, the mean of these runup time series is taken as $\overline{\eta}$, whereas the variations around that mean value are the low frequency swash excursions. Consistent with the approach

of Stockdon et al. (2006), the significant infragravity swash height is calculated from the demeaned runup time series and is given as

$$S_{IG} = 4 \sqrt{\sum_{f=0Hz}^{0.05Hz} PSD(f)\,df}$$

(EQ 3.5)

To distinguish the fact that XBeach model results exclude contributions from incident swash, we define the two percent exceedance value of infragravity runup as

$$R_{2\%,IG} = 1.1 \left(\bar{\eta} + \frac{S_{IG}}{2} \right)$$

(EQ 3.6)

Equation 3.6 therefore takes the same form as Stockdon et al. (2006) (Equation 3.2) with the exception that S_{INC} is neglected.

3.3.2   Estimated Seasonal Morphologic Variability

In coastal systems with strongly seasonal wave climates, such as the PNW (Allan & Komar, 2002, 2006), nearshore subtidal morphology typically exhibits seasonal variability (Alexander & Holman, 2004; Walstra et al., 2012). Since field measurements of nearshore bathymetry are collected only once per year in the CRLC, we simulate seasonal sandbar variability using UTC. UTC is a 1DH, wave-averaged hydrodynamic, sediment transport, and bed evolution model which has previously been applied to simulate seasonal to interannual sandbar migration (e.g., Pape et al., 2010; Ruessink et al., 2007; Ruessink & Kuriyama, 2008; Walstra et al., 2012). Roelvink et al. (1995) and Ruessink et al. (2007) found that the angle of repose (tanφ), breaker delay parameter (λ), and a current-related roughness factor (kc) were among the most important calibration parameters for realistically simulating cross-shore sandbar evolution. These site-specific tuning parameters are necessary to accurately represent the cross-shore distribution of wave energy dissipation (λ), suspended sediment concentrations (kc), and the maximum bar crest to trough relief (tanφ) (Ruessink et al., 2007). Using UTC, Walstra et al. (2012) developed an optimization procedure for tanφ, λ, and kc to successfully model NOM at Nordwijk, the Netherlands.

Here we follow the same approach as Walstra et al. (2012) running a suite of 500 UTC simulations to optimize these three parameters for the LBP study site.

UTC was initialized with a measured bathymetric profile from 9 August 2010 at profile LB66, a characteristic dissipative profile located approximately 30 km north of the mouth of the Columbia River (Figure 3.1c). A horizontally variable cross-shore grid with coarse resolution offshore (> 100 m) and finer resolution in the nearshore (5 m) was used. The model was run at hourly time steps using wave parameters derived from a regional wave hindcast (García-Medina et al., 2014) and measured water levels from NOAA tide gauge 9440910 (Toke Point, WA; Figure 3.1c). A median grain size (D_{50}) of 163 microns and a D_{90} of 230 microns were input to the model as derived from a sediment sample taken from the beach. During the simulations, the subtidal morphology was allowed to evolve freely in water depths between -12 m to -2 m and was held fixed in deeper and shallower water depths since our focus was on simulating subtidal sandbar behavior only.

UTC was run for 344 days, from 9 August 2010 until 19 July 2011, corresponding to the date of the subsequent bathymetric survey at LB66. From the suite of 500 simulations (with varying parameter combinations), the individual simulation yielding the lowest summed squared error between the model result and the measured 2011 bathymetric profile was classified as having the optimum free parameter combination for the study site. The optimized UTC free parameter values were found to be $\tan\varphi = 0.177$, $\lambda = 1.4$, and $k_c = 0.0102$ m, values which compare well with previously reported values (ranging from 0.102 to 0.466, 1 to 2.76, and 0.0056 m to 0.061 m, respectively) for barred beaches (Bosboom et al., 2000; Ruessink et al., 2007; Walstra et al., 2012). During this simulation both the outer and inner sandbars migrated offshore and increased in relief in response to high waves and strong near bottom velocities during the winter. The summer had comparatively lower wave energy which drove a slow onshore migration of the bars. Over the full year simulation there was a net 215 m offshore sandbar migration of the initial inner bar, agreeing well with the 180 m migration observed from field measurements. Model simulations also suggest an approximately 3 m vertical envelope of variability that bounds the seasonal evolution of these sandbars (Figure 3.4).
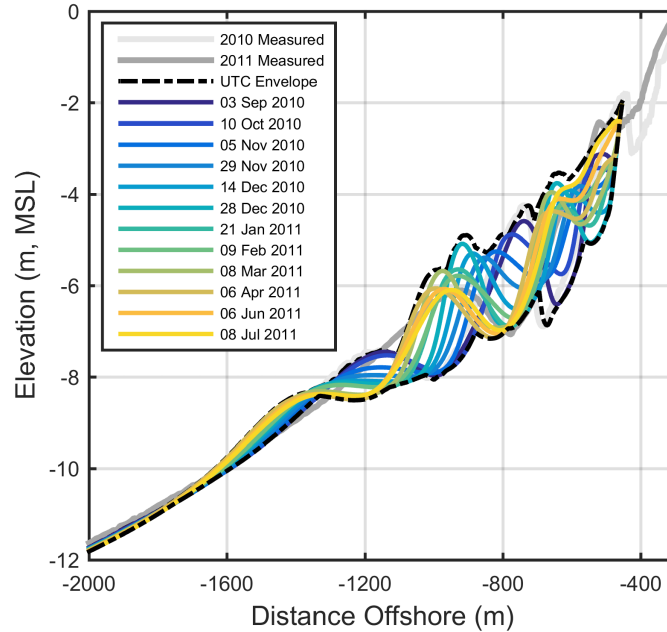
Figure 3.4: Representative profiles (solid colored lines) and envelope of variability (dotted black line) from UTC modeled seasonal sandbar configuration at LB66. The measured 2010 (light grey) and 2011 (medium grey) profiles are shown for comparison.

In Experiment 2, the time-varying best-fit UTC simulated nearshore morphology was subset to 12 representative end-member profiles using an automated K-Means/Maximum Dissimilarity clustering algorithm (Camus et al., 2011) (shown in Figure 3.4). For Experiment 5, a bathymetric profile was extracted once a day from the UTC model for input into XBeach.

3.3.3 Numerical Experiments

3.3.3.1 Experiment 1: High Energy Beach Experiment

To demonstrate the suitability of XBeach for modeling runup in high energy dissipative beach environments, simulations were completed that hindcast the conditions observed during HBE (Ruggiero et al., 2004). Experiment 1 consisted of 14 simulations with ob-

served significant wave height, and peak wave period (Stockdon & Holman, 2011) and water levels from the nearby NOAA South Beach tide gauge (Figure 3.1b). Since a complete nearshore profile was not collected during HBE, a 2012 Coastal Profiling System survey at the study site was used to define the nearshore bathymetry for input to the model. Above 0 MSL a planar foreshore beach slope ranging from 0.012 to 0.023, based on HBE observations, was combined with the bathymetric profile for each of the 14 simulations. For Experiment 1, and all other numerical experiments presented herein, the bathymetry for water depths greater than 12 m were extracted from the NOAA Astoria DEM.

3.3.3.2 Experiment 2: Seasonally variable nearshore morphology

In the absence of detailed observations of seasonally varying nearshore morphology at either study site, the optimized UTC model was used to simulate seasonal sandbar evolution at LBP (Figure 3.4). The 12 representative profiles extracted from the UTC simulation, as described in Section 3.3.2, were each merged with the measured LB66 2011 topographic profile. XBeach was run for a set of 48 generic wave conditions comprised of deepwater significant wave heights ranging from 1 to 8 m (ΔH_o = 1 m) and peak wave periods (T_p) from 6 to 16 s (ΔT_p = 2 s). This suite of wave conditions covers the range of the sea states that are typically seen on an interannual basis in the PNW (Allan & Komar, 2002, 2006). For simplicity, in all Experiment 2 simulations the mean incident wave direction was shore normal and water levels were held constant at MSL. Combining the 12 representative profiles with the 48 wave conditions resulted in 576 individual simulations (Table 3.1).

3.3.3.3 Experiment 3: Interannually variable nearshore morphology

At interannual time scales, nearshore bathymetric variability in LBP is dominated by a cycle of net offshore bar migration (Cohn et al., 2014). The influence of interannual variability in nearshore morphology, while holding beach morphology constant, is explored in Experiment 3. For this suite of simulations, measured bathymetric profiles (< -2 m MSL) from 1998 to 2013 at LB66 are used in conjunction with constant topography from the measured LB66 2011 profile. Experiment 3 uses the same wave and tide conditions as in

Experiment 2, resulting in 768 total simulations for the 16 different observed beach profiles.

3.3.3.4   Experiment 4: Interannually variable nearshore and beach morphology

Although the range of observed temporal variability on the subaerial beach in the CRLC is relatively small (Figure 3.3a), even small topographic changes have the potential to influence runup due to the well documented β_f dependence. In Experiment 4, both bathymetric and topographic data from 1998 to 2013 at LB66 are varied to investigate the influence of interannually varying nearshore and beach morphology on runup. The same wave and water level conditions are used as for Experiments 2, again resulting in a total of 768 simulations. Taken together, Experiments 3 and 4 are used to isolate the influence of beach morphology on runup.

3.3.3.5   Experiment 5: Daily maximum TWL simulations

While Experiments 2 to 4 explore the role of variable morphology on runup for select wave conditions, tides were excluded from these simulations. However, tides are an important contributor to TWLs and tidal stage has also been suggested to have important implications on runup (e.g., Brinkkemper et al., 2013; Brodie et al., 2012; Guedes et al., 2011; Sénéchal et al., 2013). Not only do variable tidal levels influence wave breaking patterns due to subtidal sandbars (e.g., Guedes et al., 2011), but increased still water levels result in a swash zone higher up on the beach where there is a potentially higher foreshore slope. In Experiment 5, XBeach is used to simulate TWLs to assess differences between numerical modeling results and empirical runup formulations and to consider potential implications on coastal vulnerability.

Wave runup and TWLs were simulated at LB66 from 9 August 2010 to 19 July 2011. For each of the 344 days in this time period, a single XBeach simulation was completed using the time-variable UTC model results for that same day to define the nearshore morphology and utilizing the static 2011 LB66 topography. The same wave and tide time series

as used to force UTC (as explained in Section 3.3.2) were used for Experiment 5, although only one static environmental condition per calendar day was selected. For each day the maximum H_o, maximum T_p, maximum tidal elevation, and minimum wave direction (D_p) relative to shore normal were selected from the environmental time series to represent the worst case daily conditions (Figure 3.5). Consistent with the other numerical experiments, in Experiment 5 each XBeach simulation was run for 2 hours using constant environmental conditions (both waves and tides) with only the second hour of data used to calculate wave runup statistics.

3.4   Results

3.4.1   Experiment 1: High Energy Beach Experiment

In Experiment 1 the environmental conditions observed during HBE were hindcast to demonstrate XBeach model skill at predicting runup on a dissipative PNW beach. Model comparisons to observed HBE swash metrics are shown in Figure 3.6 and bulk statistics are provided in Table 3.2. In general, both the 1D and 2D XBeach models slightly overpredict $\overline{\eta}$ and underpredict S_{IG} relative to the field observations. The mean error ($\Delta \mu$) and root mean squared differences (RMSD) between XBeach and the observations are smaller for both $\overline{\eta}$ and S_{IG} than SG06 but higher than that of SD06. Overall the 1D XBeach simulations exhibit almost no bias for R$_{2\%,IG}$ ($\Delta \mu$= -0.01m), with a RMSD of 0.23 m. The bias of these 1D results is less than or equal to the biases from R01, SD06, and SG06 and with similar RMS differences for $R_{2\%,IG}$, whereas the 2D model shows a positive bias ($\Delta \mu$= 0.16 m ± 0.06 m) and a larger RMSD (0.26 m ± 0.05 m) on average.

While both numerical models reproduce field observations of $\overline{\eta}$, S_{IG}, and $R_{2\%,IG}$ skillfully, this analysis suggests that the 1D version of the model using the default model settings provides comparable (for S_{IG}) or better (for of $\overline{\eta}$ and $R_{2\%,IG}$) results than the 2D model for low-sloping, dissipative beaches. These results are consistent with Stockdon et al. (2014) who found closer agreement between 1D XBeach simulations for $\overline{\eta}$ and S_{IG} at Duck, NC than 2D simulations. Together, these findings provide confidence in the ability of XBeach to simulate wave runup in 1D.
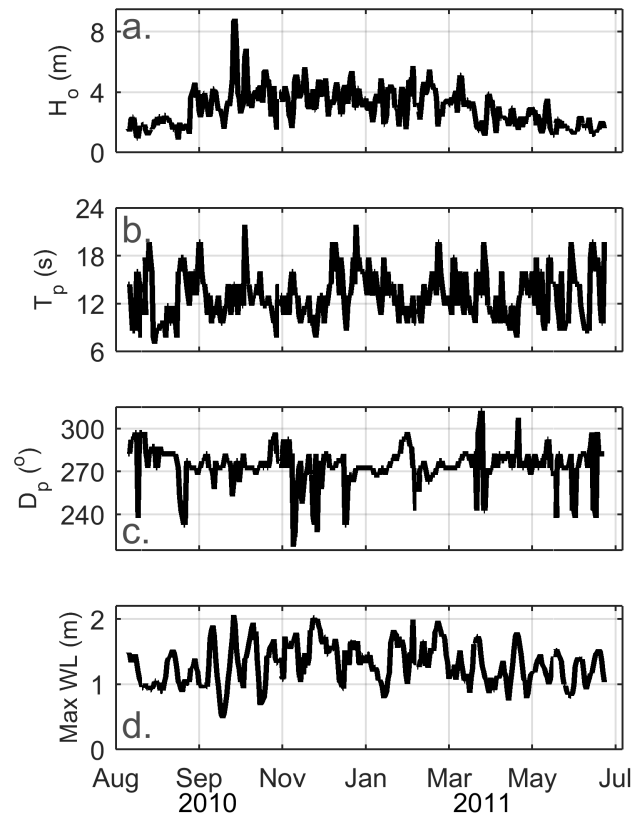
Figure 3.5: Time series of (a) deepwater significant wave height, (b) peak wave period, (c) offshore wave direction, and (d) maximum daily water level which were used to define the daily maximum TWL conditions for Experiment 5.
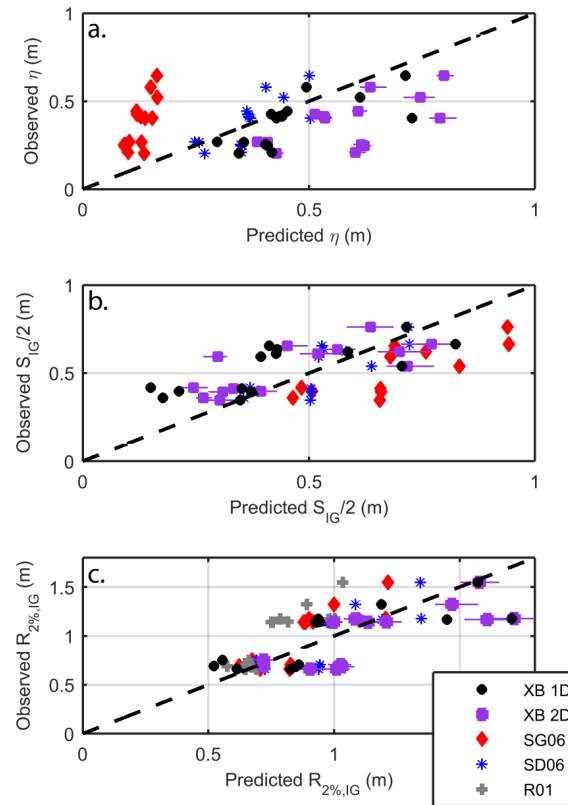
Figure 3.6: XBeach and empirical model predictions of $\bar{\eta}$, S_{IG}, and $R_{2\%,IG}$ compared to measurements from the High Energy Beach Experiment at Agate Beach, OR (Ruggiero et al., 2004). The range of alongshore varying predicted values are provided (by the horizontal bars) for the 2D XBeach simulations.

Table 3.2: Bias and RMSD between model results and HBE observations for Experiment 1.

	Model	$\Delta\mu$ (m)	RMSD (m)
$\overline{\eta}$	SD06	-0.01	0.09
	SG06	-0.25	0.28
	XB 1D	0.08	0.13
	XB 2D	0.21 ± 0.02	0.24 ± 0.02
$S_{IG}/2$	SD06	<0.01	0.09
	SG06	0.16	0.19
	XB 1D	-0.09	0.16
	XB 2D	-0.06 ± 0.04	0.14 ± 0.02
$R_{2\%,IG}$	R01	-0.22	0.28
	SD06	-0.01	0.18
	SG06	-0.10	0.20
	XB 1D	-0.01	0.23
	XB 2D	0.16 ± 0.06	0.26 ± 0.05

3.4.2 Experiments 2 to 4: Seasonal to interannual variability in morphology

The results described below demonstrate the relative effect of variable seasonal (Experiment 2) to interannual (Experiments 3 and 4) morphology on wave runup. Among these three numerical experiments a total of 2,112 simulations were completed using 48 generic wave conditions over a range of profile configurations. The results indicate that XBeach simulated $\overline{\eta}$, S_{IG}, and $R_{2\%,IG}$ all increase with both H_o and T_p and that $\overline{\eta}$ contributes more to $R_{2\%,IG}$ than S_{IG} for most wave conditions. For the $H_o = 2$ m, $T_p = 10$ s wave case, which most closely approximates the average annual wave condition, and using the observed 2011 LB66 observed profile (Experiments 3 and 4), XBeach predicts $\overline{\eta} = 0.33$ m, $S_{IG}/2 = 0.23$ m, and $R_{2\%,IG} = 0.61$ m (Figure 3.7). A representative PNW storm condition (8m at 14 s) results in 1.41 m, 1.44 m, and 3.13 m for the same metrics, respectively.

These general trends are consistent across all of the simulations, although the predicted values of $\overline{\eta}$, S_{IG}, and $R_{2\%,IG}$ vary between profiles. Within each numerical experiment across all morphologies (12 for Experiment 2 and 16 each for Experiments 3 and 4) and individually for each of the 48 wave conditions, the range of results is calculated as the difference between the maximum and minimum simulated $\overline{\eta}$, S_{IG}, and $R_{2\%,IG}$ and are pre-
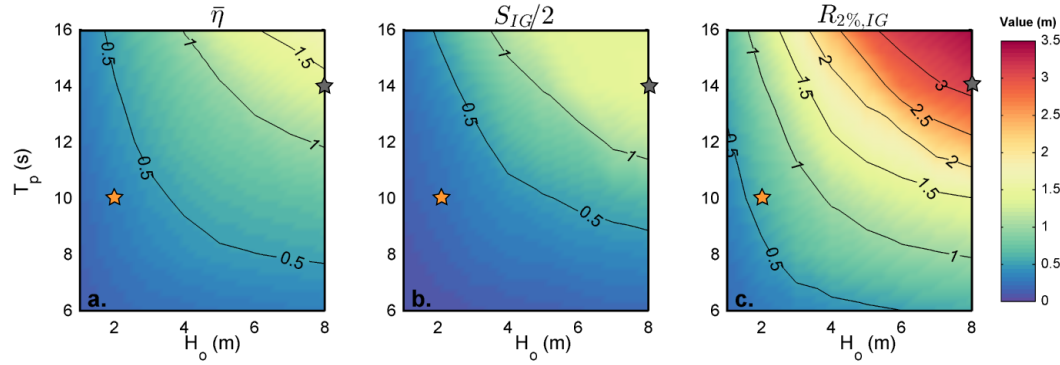
Figure 3.7: Example XBeach predictions of $\bar{\eta}$, $S_{IG}/2$, and $R_{2\%,IG}$ for 48 wave simulations completed for the 2011 LB66 profile. Orange and grey stars highlight the mean annual (H_o = 2 m, T_p = 10 s) and representative storm (H_o = 8 m, T_p = 14 s) wave conditions.

sented in Figure 3.8. For example, the 8 m, 14 s storm event is estimated to result in $R_{2\%,IG}$ as little as 3.07 m and as much as 3.16 m (range of 0.09 m) by varying only the subtidal morphology in Experiment 3. In Experiment 2 (Figure 3.8a,b,c) the maximum range in modeled $R_{2\%,IG}$ for any wave condition is only 0.05 m (0.04 m and 0.03 m for $\bar{\eta}$ and $S_{IG}/2$, respectively) suggesting that seasonal variability in sandbar configuration does not greatly alter swash zone hydrodynamics regardless of the incident wave conditions. Similarly, when wave conditions are below the annual average, the range of results is always less than 0.05 m for Experiment 3 (Figure 3.8d,e,f). However, during long period waves and during storm conditions depth-limited wave breaking occurs further offshore and in these cases the influence of interannual nearshore bathymetric variability is more important. XBeach results indicate that there is up to a 0.18 m difference in $R_{2\%,IG}$ (0.11 m and 0.09 m for $\bar{\eta}$ and $S_{IG}/2$, respectively) across the interannually varying nearshore profiles, suggesting that large oscillations in nearshore morphology associated with NOM can enhance or weaken the magnitude of wave runup.

The ranges for Experiment 4 (Figure 3.8h,i,g) are substantially higher than those for Experiments 2 and 3, highlighting the relatively larger importance of beach topography on $\bar{\eta}$, S_{IG}, and $R_{2\%,IG}$. Similar to the other experiments the largest ranges occur for the most energetic conditions. However, the predicted range of $R_{2\%,IG}$ exceeds 0.1 m for all simula-
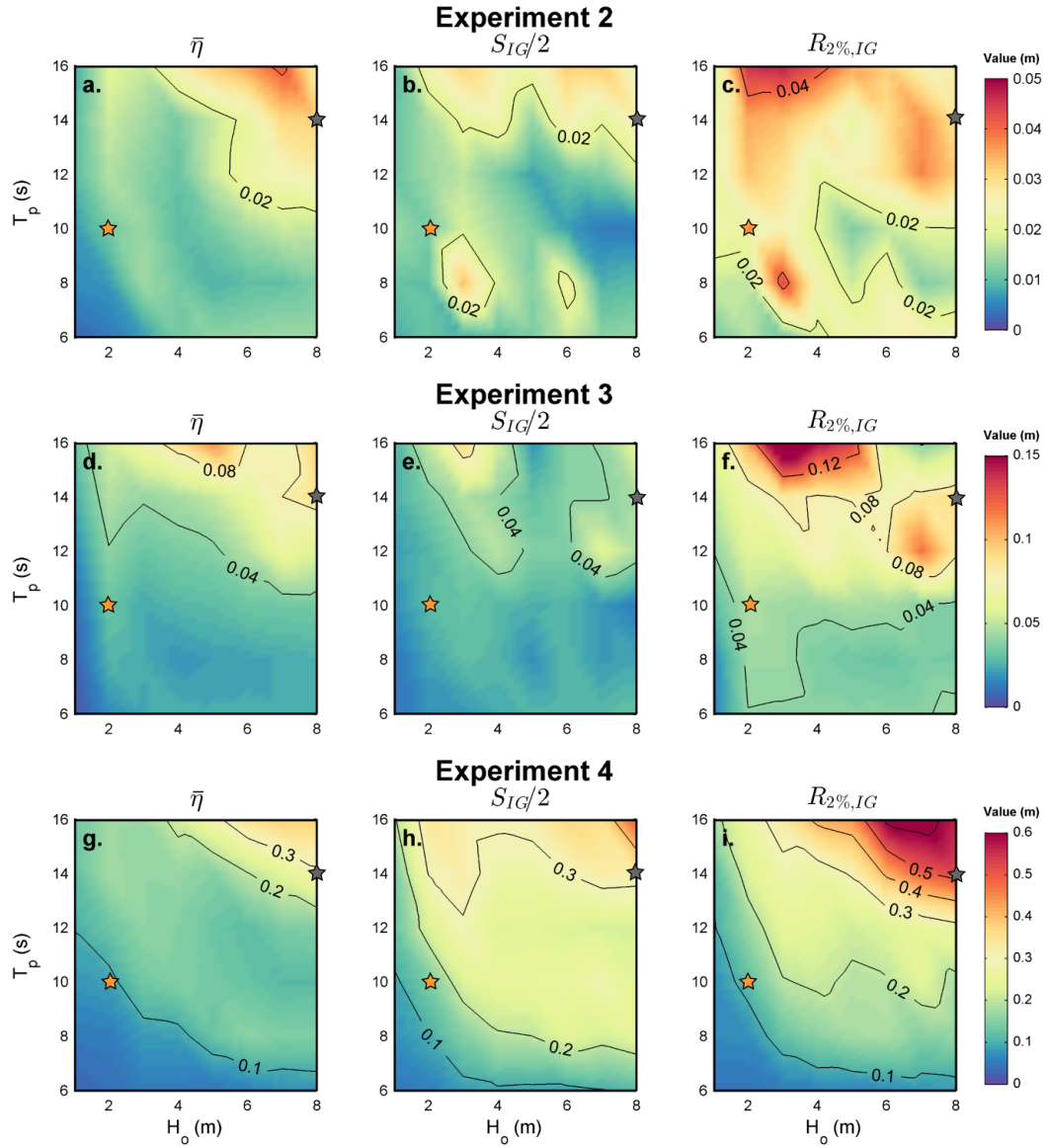
Figure 3.8: Difference between maximum and minimum simulated values of $\overline{\eta}$, $S_{IG}/2$, and $R_{2\%,IG}$ for Experiments 2 to 4 for all 48 wave conditions.

tions where H_o or T_p are greater than the average annual PNW waves. The maximum range of $R_{2\%,IG}$ (and $\overline{\eta}$ and $S_{IG}/2$, respectively) among the 48 wave conditions for Experiment 4 is 0.64 m (0.38 m and 0.49 m) which is 13.4 (9.1 and 15.0) and 3.5 (3.3 and 5.3) times larger than the maximum ranges in Experiments 2 and 3, respectively.

The numerical framework for Experiments 3 and 4 allow the relative effects of bathymetry versus topography on runup to be distinguished from one another. In Experiment 3 the beach morphology is held constant between all simulations, thus any variance in the modeled runup signature between different profiles for the same wave condition can be attributed purely to a bathymetric influence. However, in Experiment 4 both topography and bathymetry are varied. Therefore by subtracting the results for Experiment 3 from Experiment 4 for equivalent wave conditions and equivalent subtidal morphologies, the relative topographic control on $\overline{\eta}$, S_{IG}, and $R_{2\%,IG}$ can be inferred. Figure 3.9 reveals the model predicted mean contribution of topographic variability on the overall vertical variability of $\overline{\eta}$, S_{IG}, and $R_{2\%,IG}$.

When $H_o > 3$ m or $T_p > 8$ s topographic changes explain a significant majority of the variability in results. For an 8 m, 14 s storm event, about 80% of the variability in the three runup metrics are explained on average by the topography alone. Model results suggest that topographic variability has a relatively stronger influence on S_{IG} than on $\overline{\eta}$ (Figure 3.8d,e,g,h and Figure 3.9a,b), which largely disagrees with previous observations. Stockdon et al. (2006) had found no statistical correlation between the beach morphology and infragravity swash – with their observed dependence relying solely on $\sqrt{H_o L_o}$. The modeling results of this present study suggest that there may in fact be a morphologic dependence for S_{IG} (Figure 3.8), although perhaps not linearly dependent with β_f, similar to the findings of Ruggiero et al. (2001).

3.4.3 Experiment 5: Simulation of daily maximum conditions

A year-long time series of daily maximum TWL conditions was simulated in Experiment 5. During the analysis period (9 August 2010 to 19 July 2011) the largest wave conditions occurred between October and December, with H_o up to 8.9 m and T_p up to 21.9 s (Fig-
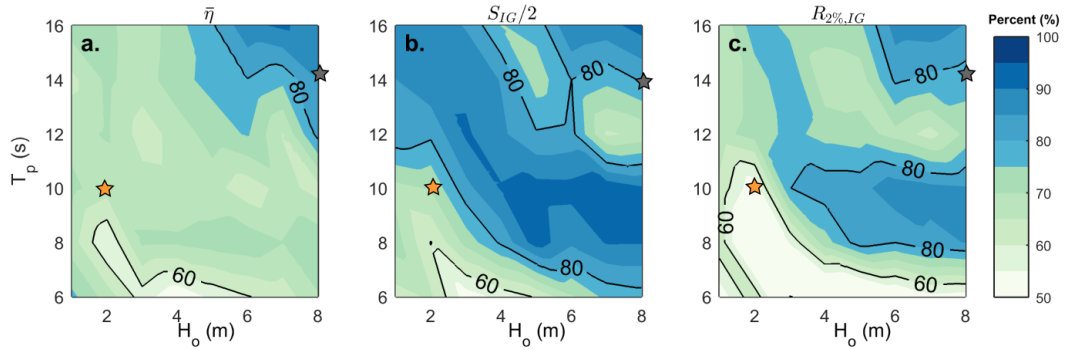
Figure 3.9: Mean percentage contribution of topographic variability to modeled runup variability for $\bar{\eta}$, $S_{IG}/2$, and $R_{2\%,IG}$

ure 3.5). While long period ocean swell can occur year round in the PNW, wave heights drop substantially during the summer.

Over the course of the year, the largest hindcast values of $\bar{\eta}$, $S_{IG}/2$, $R_{2\%,IG}$, and TWL were 1.74 m, 2.16 m, 4.29 m, and 5.68 m, respectively, which all occurred during a storm event on 2 November 2010 ($H_o = 6.3$ m, $T_p = 21.9$ s, $D_p = 270°$, and still water level [SWL] = 1.39 m) (Figure 3.10). For these same conditions R01, SD06, and SG06 predict maximum TWLs of 3.71 m, 4.34 m, and 4.07 m, respectively. With the dune toe at LB66 located at approximately 4 m above MSL, during this storm event R01 predicts no dune impact, SD06 and SG06 estimate the maximum extent of runup occurring near the base of the dune, and XBeach predicts that the dune is in the collision regime of the Sallenger (2000) storm impact scale. Overall, XBeach, R01, SD06, and SG06 predict the collision regime will occur 11 days, 3 days, 3 days, and 2 days, respectively, over the year.

While the storm impact scale gives a proxy for whether coastal change will occur, Sallenger (2000) does not directly relate total water levels to the magnitude of potential erosion. A recent laboratory study by Palmsten & Holman (2012) found that $R_{16\%}$ is a better proxy for dune erosion than $R_{2\%}$, suggesting that the relative contributions of SWL, setup, and swash to the TWL may be important for storm-induced backshore changes. Based on all of the XBeach simulations in Experiment 5, $\bar{\eta}$, $S_{IG}/2$, $R_{2\%,IG}$, and SWL respectively contributed 23%, 19%, 46%, and 54% to the TWL, on average. The relative contribution of
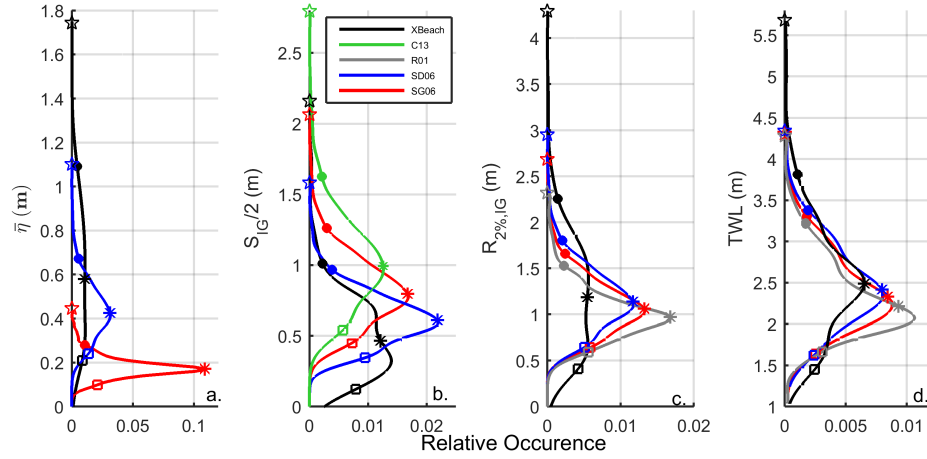
Figure 3.10: Probability distribution of (a) $\overline{\eta}$, (b) $S_{IG}/2$, (c) $R_{2\%,IG}$, and (d) TWLs for XBeach (black), SG06 (red), SD06 (blue), R01 (grey), and C13 (green). The 5th percentile (square), 50th percentile (asterisk), 95th percentile (circle), and maximum (star) values are marked on each line.

these wave-driven components to the TWL also varies depending on the deep-water wave conditions. For H_o greater than 6 m, $\overline{\eta}$, $S_{IG}/2$, $R_{2\%,IG}$, and SWL contribute 27%, 33%, 66%, and 34%, respectively, to the TWL – unsurprisingly indicating an increasingly important wave driven component to TWL with increasing wave energy. Similarly, these relative contributions to the TWL vary for the empirical models (Table 3.3). The XBeach simulations also show that wave direction influences these TWL contributions, with increasing wave obliquity decreasing both $\overline{\eta}$ and S_{IG}, which the empirical models do not capture.

3.5 Discussion

Many previous studies have shown a link between morphology (usually in the form of β_f) and wave runup (e.g., Stockdon et al., 2006). The 1D numerical modeling results presented here support this notion while confirming that topographic variability has a more significant influence on runup than nearshore bathymetric variability. However, subtidal morphology was shown to have a non-zero influence on $\overline{\eta}$, S_{IG}, and $R_{2\%,IG}$, during energetic conditions. In the following sections we explore simple scaling relationships for wave runup and its

Table 3.3: Percentage contribution of $\bar{\eta}$, S_{IG}, and $R_{2\%,IG}$ to TWL in Experiment 5.

	Model	All conditions	$H_o > 2$ m	$H_o > 4$ m	$H_o > 6$ m
$\bar{\eta}$	SD06	17.5%	18.1%	19.2%	21.9%
	SG06	7.6%	7.6%	8.1%	9.7%
	XB	22.9%	25.1%	27.2%	26.9%
$S_{IG}/2$	SD06	25.2%	26.0%	27.6%	31.5%
	SG06	33.9%	35.1%	37.3%	42.6%
	XB	19.1%	20.1%	22.4%	33.2%
$R_{2\%,IG}$	R01	43.6%	44.7%	47.7%	55.7%
	SD06	47.0%	48.5%	51.5%	58.7%
	SG06	45.6%	46.9%	49.9%	57.5%
	XB	46.2%	49.7%	54.6%	66.1%

components, compare model results to both field data and to existing empirical formula, and discuss implications of our results to coastal vulnerability assessments.

3.5.1   Model Comparison to Measurements

XBeach was shown to compare skillfully ($|\Delta \mu| \leq 0.1$ m, RMSD ≤ 0.23 m) to measurements from the High Energy Beach Experiment. The bias and RMSD between the 1D XBeach results and the HBE observations are both lower for $\bar{\eta}$ and S_{IG} relative to the same statistics for SG06 (Figure 3.6 and Table 3.2). However, there were deviations between the XBeach model results and the observations, with differences of up to 0.32 m for $\bar{\eta}$, 0.27 m for S_{IG}, and 0.53 m for $R_{2\%,IG}$. These differences could have resulted from a number of factors. First, the offshore wave conditions for HBE were measured from a buoy 100 km south of the study site and no directional data were available (Ruggiero et al., 2004). A poor characterization of the offshore wave climate, including not adequately accounting for directional spreading (Guza & Feddersen, 2012) or two dimensionality in the infragravity wave field (Herbers et al., 1995) in the case of the 1D simulations, has the potential to negatively influence the model predictions. Another potential discrepancy may arise from the use of a beach profile collected in 2012 for a 1996 hindcast. Although the 2012 beach was likely similar to that in 1996, even small differences in the coastal profile have the potential to influence runup predictions (Figure 3.8). While alongshore uniformity was assumed

within XBeach, complex nearshore and subaerial morphology, such as is present at Agate Beach (Alexander & Holman, 2004; Haxel & Holman, 2004), also has the potential to alter swash processes (e.g. Guedes et al., 2012). Additionally, other factors such as wind (e.g. Vousdoukas et al., 2011) and infiltration (Villarroel-Lamb et al., 2014) may be important for swash processes but were not accounted for within this model application.

The most energetic condition observed during HBE was a 3.1 m wave at 14.3 s which resulted in observed $\bar{\eta}$ of 0.65 m, $S_{IG}/2$ of 0.76 m, and $R_{2\%,IG}$ of 1.55 m. The range of results from Experiment 3 showed that for a similar wave condition (H_o = 3 m, T_p = 14 s), variability in the nearshore subtidal morphology could explain up to 0.04 m, 0.05 m, and 0.08 m variability in $\bar{\eta}$, $S_{IG}/2$, and $R_{2\%,IG}$, respectively. Similarly, the difference between the Experiment 3 and 4 results indicate that variability in subaerial beach morphology could explain differences of up to 0.16 m, 0.35 m, and 0.29 m for $\bar{\eta}$, $S_{IG}/2$, and $R_{2\%,IG}$, respectively, for the same wave condition. Therefore, assuming that Agate Beach experiences similar morphologic variability as observed at LBP, natural variability in the coastal profile could potentially explain the differences between model results and observations for S_{IG} and about half of the potential maximum error for both $\bar{\eta}$ and $R_{2\%,IG}$.

3.5.2 Runup Scaling Relationships

Previous field studies have found differing relationships between observations of runup and environmental variables. As examples, Battjes (1974) suggested a scaling of (dimensional) runup with $H_o \xi_o$, (which is equivalent to $\beta_f \sqrt{H_o L_o}$), SD06 found a linear relationship with $\sqrt{H_o L_o}$, and R01 related runup to $\sqrt{\beta_f H_o L_o}$. Many variants of these proposed relationships exist, but nearly all incorporate some combination of H_o, L_o, and β_f. The model output from Experiments 2 to 4 similarly show that $\bar{\eta}$, S_{IG}, and $R_{2\%,IG}$ are all highly dependent on H_o and T_p (or L_o) (Figure 3.11). Linear regressions through the data indicate that $\sqrt{H_o L_o}$ explains 85%, 68%, and 78% of the variance for $\bar{\eta}$, S_{IG}, and $R_{2\%,IG}$, respectively. Scatter among these results for identical wave conditions suggests that there is some morphologic control on runup that may explain the remaining variance. Comparison of the model predicted runup values to $\beta_f \sqrt{H_o L_o}$ and $\sqrt{\beta_f H_o L_o}$ both yield more statistically significant relationships, providing evidence of this morphologic control. However, neither $\beta_f \sqrt{H_o L_o}$

nor $\sqrt{\beta_f H_o L_o}$ fully explains the variance in $\overline{\eta}$, S_{IG}, or $R_{2\%,IG}$. This suggests that β_f alone does not fully describe the morphologic features of the coastal profile, although attempts (not shown) to fit the data with slopes other than β_f did not yield more statistically significant linear relationships. For example, despite a 4 m envelope of variability at LB66 resulting from NOM, the surf zone slope (β_{surf}) remains nearly constant with time and therefore β_{surf} does not improve linear fits to runup metrics over β_f. Similarly, describing the variance based on h_{bar}/h_{nobar} does not explain the subtidal morphologic control on runup at LB66. It is unlikely that a single morphodynamic descriptor can fully describe coastal profiles and their influence on swash processes.

3.5.3   Model Comparison to Empirical Formulations

Empirical formulations are easy to apply and as such have been widely used to predict the wave driven component of TWLs as part of coastal erosion and flooding assessments (e.g., Birchler et al., 2014). Empirical model predictions of $\overline{\eta}$, S_{IG}, and $R_{2\%,IG}$ are compared to the XBeach results from Experiments 2 to 4 in Figure 3.12. XBeach predicts higher $\overline{\eta}$ than both SD06 (RMSD = 0.27 m) and SG06 (RMSD = 0.61 m), with these deviations increasing with increasing wave energy. S_{IG} predictions compare reasonably well with Stockdon et al. (2006), with a RMSD across all 2,112 simulations of 0.29 m for SG06 and 0.20 m for SD06. SD06 matches XBeach results S_{IG} more closely for lower energy conditions ($H_o < 4$ m or $T_p < 12$ s), while SG06 compares better to the numerical model during more energetic conditions.

While the C13 formulation for S_{IG} was originally developed using an idealized, single barred beach profile, here we apply it to each of the conditions in Experiments 2 to 5. Consistent with the approach taken by Cox et al. (2013), an equilibrium profile (Dean, 1991) was fit between the shoreline and the trough location of the first significant subtidal sandbar (bar height > 0.5 m) and extended to the location of the bar crest to allow for the computation of h_{nobar}. The form of Equation 3.4 indicates that when $0.42 < h_{bar}/h_{nobar} < 1$ C13 S_{IG} predictions will be higher than those of SG06. At LB66 the h_{bar}/h_{nobar} ratio varied between 0.64 and 1 and consequently, C13 predicts infragravity swash that is typically higher than both SG06 and XBeach for the conditions of Experiments 2 to 4 (Figure 3.12,
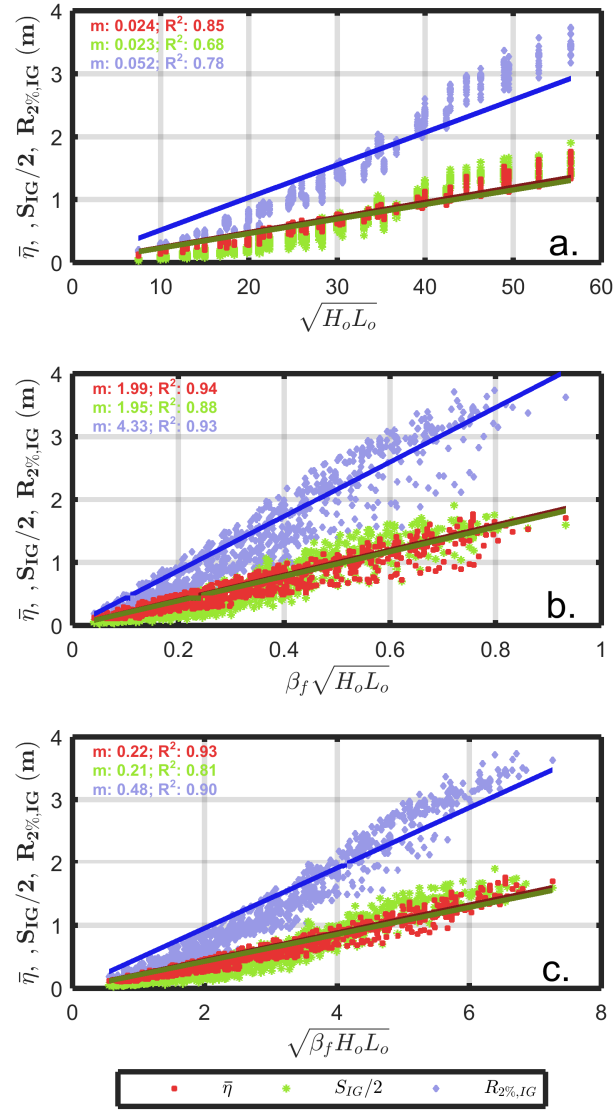
Figure 3.11: XBeach simulations of $\overline{\eta}$ (red), $S_{IG}/2$ (green), and $R_{2\%,IG}$ (blue) from Experiments 2 to 4 compared to (a) $\sqrt{H_o L_o}$, (b) $B_f \sqrt{H_o L_o}$, and (c) $\sqrt{B_f H_o L_o}$. In each panel the best fit line (with y-intercept set to zero) and corresponding slope and R^2 values are shown
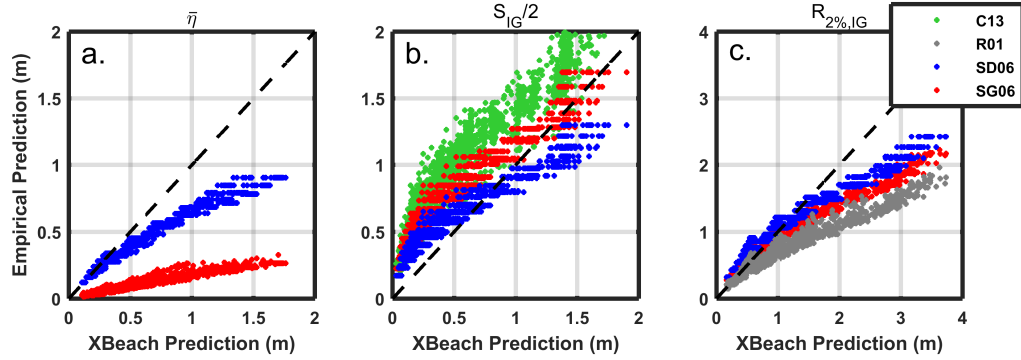
Figure 3.12: XBeach simulations of (a) $\bar{\eta}$, (b) $S_{IG}/2$, and (c) $R_{2\%,IG}$ compared to empirical estimations by R01 (grey), SD06 (blue), SG06 (red), and C13 (green) for Experiments 2 to 4.

$\Delta\,\mu = 0.45$ m and RMSD = 0.47 m). Similar results are found when the C13 model is applied to the outer bar (not shown) of the typically multi-barred nearshore profiles. While the results shown here agree with the Cox et al. (2013) finding that nearshore bars influence S_{IG}, in the PNW this does not appear to be controlled solely by the ratio h_{bar}/h_{nobar}. This may be a reflection of the modally dissipative nature of the study site or the presence of multiple sandbars.

For $H_o < 4$ m or $T_p < 12$ s SG06 (RMSD = 0.07 m), SD06 (RMSD = 0.14 m) and R01 (RMSD = 0.15 m) predictions of $R_{2\%,IG}$ compare reasonably well with the numerical predictions (Figure 3.6c). However, for larger wave conditions XBeach predicts higher values than any of the empirical models and the overall comparative statistics become worse when considering the entire dataset (RMSD > 0.4 m for all three empirical models).

Similar to findings from Experiments 2 to 4, the differences between the empirical and numerical modeling predictions from Experiment 5 are typically larger for $\bar{\eta}$ than S_{IG} (Table 3.4 and Figure 3.10). The largest deviations of S_{IG} occur when the incident waves are highly oblique. In these circumstances XBeach predicts low S_{IG} while the empirical models are unaffected by wave direction – contributing to relatively large mean and RMS differences between XBeach and SD06 and SG06. Similarly to Experiments 2 to 4, C13 had the largest differences ($\Delta\,\mu = 0.52$ m) for $S_{IG}/2$ relative to XBeach in Experiment 5.

Table 3.4: Bias and RMSD between XBeach results and empirical model predictions for Experiment 5.

	Model	$\Delta\mu$ (m)	RMSD (m)
$\overline{\eta}$	SD06	-0.17	0.24
	SG06	-0.43	0.50
$S_{IG}/2$	C13	0.52	0.55
	SD06	0.12	0.21
	SG06	0.31	0.35
$R_{2\%,IG}$	R01	-0.21	0.51
	SD06	-0.05	0.36
	SG06	-0.12	0.42
TWL	R01	-0.21	0.51
	SD06	-0.05	0.36
	SG06	-0.12	0.42

Overall, SD06 matches the XBeach TWL results most closely, underpredicting XBeach on average by 0.05 m and having an absolute RMSD of 0.36 m. Both R01 and SG06 have larger biases and RMSD for $R_{2\%,IG}$ and TWL. Differences in these model predictions could arise in part because these empirical models were developed using limited observations under high energy and dissipative conditions. For example, SD06 was fit to observations where wave heights were less than 4 m and runup did not exceed 2 m (Stockdon et al., 2006; Stockdon & Holman, 2011). Half of the SD06 calibration dataset was from HBE, explaining the close agreement between SD06 to the HBE observations (Figure 3.6 and Table 3.2) but not necessarily implying that it is broadly applicable for other sites or other environmental conditions. For example, Shand et al. (2011) found that R01, SD06, and SG06 underpredicted runup by over 39% on average during storms at two South Pacific beaches even though these equations performed well at lower runup levels. Therefore, while these empirical formulations do agree well with many field and lab observations (e.g., Suanez et al., 2015), the wave and morphology conditions in the empirical equations are parameterized and do not necessarily capture the full complexity of the coastal zone.

3.5.4 Implications for Coastal Vulnerability Assessments

Coastal managers often rely on the simple empirical tools described above to estimate storm induced TWLs for coastal planning, evacuation route determinations, and hazard mapping. Therefore, the potential that these approaches might be underestimating coastal flooding hazards could be a detriment to coastal stakeholders. Comparisons of XBeach predicted $\bar{\eta}$, S_{IG}, and $R_{2\%,IG}$ to field data from HBE demonstrate that the numerical model performs skillfully for dissipative beaches, at least for the conditions observed. Furthermore, data from the various numerical experiments indicates a reasonable agreement with empirical predictors of S_{IG}. However, XBeach predictions of $\bar{\eta}$, $R_{2\%,IG}$, and TWL are typically higher than those of R01, SD06, and SG06 for simulations at LB66 (Figure 3.10 and Table 3.4). These differences are most pronounced for extreme events, consistent with the findings of Shand et al. (2011) described above. For example, the 95th percentile (and maximum) TWLs predicted by XBeach, R01, SD06, and SG06 are 3.81 m (5.68 m), 3.22 m (4.28 m), 3.38 m (4.34 m), and 3.30 m (4.31 m), respectively (Figure 3.10). In the Experiment 5 hindcast, XBeach predicts about 5 times as many days with dune collision as SG06. As these empirical models are widely used in predicting TWL return levels (e.g., Serafin & Ruggiero, 2014) and coastal change hazards (e.g., Birchler et al., 2014), underestimating the magnitude of extreme TWLs may exacerbate risk to low lying coastal systems if policy and zoning decisions are made with guidance from these formulations alone.

The results of Palmsten & Holman (2012) suggest that the elevation of the dynamic still water level (still water level + $\bar{\eta}$) relative to the dune toe, may be more important for inducing erosion than extreme swash levels alone, and therefore that equivalent magnitude TWLs may induce different erosional responses along the same beach if the magnitude of the components vary. In another example, Theuerkauf et al. (2014) documented that a year characterized by calm wave conditions but positive sea level anomalies resulted in higher erosion rates than a period with hurricane conditions. While the importance of the relative contributions of SWL, $\bar{\eta}$, S_{IG}, and S_{INC} individually to net sediment transport has not yet been thoroughly documented, these observations highlight that accurate predictions of the constituents that make up TWLs are potentially important for adequately characterizing coastal vulnerability. Consistent underprediction of $\bar{\eta}$ (Figure 3.6a) and overprediction of

S_{IG} (Figure 3.6b) by SG06 for HBE demonstrates that even if runup and TWL are predicted well, the physical and environmental limitations of empirical model predictions need to be better understood.

More observational data, particularly during times of high wave energy, are necessary to further substantiate the numerical model predictions presented here, but our results do provide some indication that simple empirical equations for wave runup may, by themselves, be insufficient for predicting storm-induced extreme TWLs along dissipative coasts. This is perhaps not surprising given both the lack of physical processes included within the empirical models and the limited number of measurements during high wave events that are included in the formulation of these equations.

3.6   Conclusions

XBeach was applied to U.S. Pacific Northwest beaches to investigate morphological controls on setup, infragravity swash, and extreme wave runup. A suite of numerical experiments demonstrated the suitability of XBeach for simulating wave runup on dissipative beaches, explored the relative influence of seasonal to interannual variability in nearshore bathymetry and beach topography on $\overline{\eta}$, S_{IG}, and $R_{2\%,IG}$, and compared numerical simulations of wave runup to simple empirical predictors.

Results of this study suggest that while $\overline{\eta}$, S_{IG}, and $R_{2\%,IG}$ all generally scale well with $\sqrt{H_o L_o}$ there is also a morphologic control on runup processes on dissipative beaches. Interannual variability in nearshore morphology at a representative PNW beach profile was predicted to modestly influence $R_{2\%,IG}$ by up to 0.18 m, whereas seasonal variability in sandbars had less influence on $\overline{\eta}$, S_{IG}, and $R_{2\%,IG}$. While the larger vertical envelope of profile variability associated with interannual net offshore sandbar migration contributes to these results, factors such as sandbar geometry and profile rugosity likely also influence the bathymetric control on runup and its components. Results of this study suggests a non-zero bathymetric influence on runup, yet confirm a much larger influence on runup and its components from intertidal and supratidal morphology. Natural variability in beach topography was shown to modify $R_{2\%,IG}$ by up to 0.64 m under storm wave conditions. Therefore, con-

sistent with previous observations, beach topography appears to play a significant role in influencing extreme runup (e.g., Stockdon et al., 2006).

Due to the spatial (and temporal) complexity of coastal morphology, characterized by bedforms with a wide range of scales (e.g., ripples to sandbars) and large local gradients in slope, a single morphologic descriptor cannot fully describe coastal profiles and their influence on swash processes. Process-based numerical models, such as XBeach, can more readily account for these variable features, improving our ability to (1) fully understand the factors which influence wave runup and (2) predict TWLs and corresponding coastal vulnerability. As numerical models are also increasingly used operationally for storm hazards predictions (e.g., Barnard et al., 2014; Vousdoukas et al., 2012), the findings of this study suggest that an adequate characterization of the intertidal and supratidal morphology is more important than detailed bathymetric measurements for suitably modeling $\bar{\eta}$, S_{IG}, $R_{2\%,IG}$, and TWLs along dissipative coasts. Therefore, despite the fact that nearshore bathymetry is often poorly characterized (Holman et al., 2014), the increasingly availability of high-resolution, frequent topographic measurements (e.g., Klemas, 2011) should allow for appropriate morphology boundary conditions for these operational models along dissipative shores.

Overall, XBeach generally predicts similar S_{IG} but higher $\bar{\eta}$ values than both the generic and dissipative form of Stockdon et al. (2006). During modest waves ($H_o < 4$ m and $T_p < 12$ s) the differences in these values are relatively small, resulting in $R_{2\%,IG}$ RMS differences of less than 0.15 m. However, during high energy conditions $R_{2\%,IG}$ predictions deviate considerably between XBeach and commonly used empirical models, with maximum differences exceeding 0.5 m. While further validation of the numerical model during high energy events is necessary, the results presented here highlight the potential for underestimating TWLs for extreme events using simple empirical formulations, a finding that has important implications for the prediction of coastal flooding and erosion hazards.

Acknowledgements

Chapter 4: Environmental and morphologic controls on wave-induced dune response

Abstract

The Pacific Northwest of the United States exhibits complex spatial patterns of storm-induced coastal foredune erosion. Using oceanographic and morphologic data from three field sites encompassing a range of subaqueous and subaerial coastal profile configurations, a relationship is found between morphologic characteristics and dune volume changes during storm events producing high water levels. The data suggests that dune erosion increases with increasing backshore beach slope and that, under particular oceanographic forcing conditions, wave-driven processes can grow the lower portion of dunes on low sloping, dissipative beaches. These observations of environmental and morphologic controls on storm-induced dune impacts are further explored using XBeach, a state of the art numerical model capable of simulating interactions between hydrodynamics and morphology. Consistent with the field data, model simulations indicate that wave-driven dune growth may occur on low sloping beaches in cases where the dynamic still water level (still water level plus wave setup) is lower than the dune toe. However, these accretional processes are restricted to events where limited incident wave energy impacts the dune. Cases with steep backshore beach slopes or dynamic still water levels exceeding the dune toe instead typically result in dune erosion. Additionally, the model suggests that morphologic properties of the shelf, nearshore, and the dune itself also influence storm-induced dune volume change.

4.1 Introduction

Coastal erosion poses a major threat to coastal communities by limiting beach access, endangering backshore infrastructure, and impacting ecologically important environments.

The preservation of coastal foredunes, features which provide the first line of defense for limiting backshore flooding, is of particular interest as a valuable form of green infrastructure (Sutton-Grier et al., 2015). However, rising water levels along the coast from sea level rise (SLR) and, potentially, changing patterns of storminess are generally expected to increase the frequency of ocean waves impacting dunes (Pachauri et al., 2014) – raising questions regarding the long-term resilience of these landforms.

Coastal dune formation reflects the aggregation of aeolian, wave-driven, and ecological processes, with post-storm dune recovery typically spanning numerous years (Houser, 2009; Walker et al., 2017). The erosion of dune systems is primarily driven by wave processes and is often conceptualized by the frequency of the total water level (TWL) exceeding the dune toe (collision regime), how often the TWL is higher than the dune crest (overwash regime), and when the still water level (SWL) exceeds the dune crest (inundation regime) (Sallenger, 2000). These impacts typically occur during storms due to the combined influence of storm surge and wave runup. In areas prone to tropical cyclone impacts storm surge is a particularly important contributor to dune erosion (e.g., van de Graaff, 1977). However, the relative contributions of non-tidal residuals (including storm surge), tides, and waves to extreme TWLs vary regionally based on climatic, oceanographic, and morphologic controls (Serafin et al., 2017). For example, the wave-driven component of TWLs is particularly important on the west coast of the United States resulting from intense wave energy and a narrow continental shelf, which limits storm surge.

The wave-driven component of TWLs is referred to as wave runup and includes both the time-averaged elevated mean water level driven by cross-shore gradients in radiation stresses (wave setup, $\overline{\eta}$) and the time variable swash component with energy across a range of incident (< 20 s, S_{INC}) and infragravity time scales (≥ 20 s, S_{IG}) (Holman & Sallenger, 1985). Low gradient, dissipative beaches tend to be dominated by swash in the infragravity band (e.g., Ruessink et al., 1998), whereas steeper beaches are generally characterized by proportionally larger S_{INC}. Previous studies have found that wave runup is predominantly dependent on offshore wave height (H_o), wavelength (L_o), and the foreshore beach slope (β_f) (e.g., Ruggiero et al., 2001; Stockdon et al., 2006). Among the most commonly applied wave runup formulations is that of Stockdon et al. (2006) which parameterizes runup as:

$$R_{2\%} = 1.1 \left(\overline{\eta} + \frac{\sqrt{S_{INC}^2 + S_{IG}^2}}{2} \right) = 1.1 \left(0.35\beta_f \sqrt{H_o L_o} + \frac{\sqrt{H_o L_o \left(0.563\beta_f^2 + 0.004 \right)}}{2} \right)$$

$$(EQ\ 4.1)$$

where $R_{2\%}$ is the 2% exceedance level of wave runup maxima. Although the sole morphologic control of runup in Stockdon et al. (2006) was found to be from the local beach slope within the swash zone, other studies have revealed that subtidal morphology also influences wave runup processes (Cohn & Ruggiero, 2016; Cox et al., 2013; Sénéchal et al., 2013).

Field observations show that coastal erosion impacts are often highly variable during individual storm events (e.g., Stockdon et al., 2007; Splinter et al., 2018). This variability in storm response has been partially attributed to alongshore variability in wave energy (Cooper et al., 2004; Costas et al., 2005), differences in grain size (Nelson, 1991), local influence of rip-channel embayments (Revell et al., 2002; Thornton et al., 2007), and the presence of hard engineered structures (Irish et al., 2013). Geometric properties of the dune, including the dune face slope, pre-storm dune toe elevation, and dune crest elevation (Burroughs & Tebbens, 2008; Houser, 2013; de Winter et al., 2015; Splinter et al., 2018), and morphologic properties of the nearshore, such as nearshore slopes or the presence/absence of sandbars (Carter & Balsillie, 1983; Castelle et al., 2015; de Winter et al., 2015; Biel et al., 2017), have also been shown to influence storm-induced dune erosion. However, the primary morphologic control on variable dune responses has been related to beach slope. Steep (narrow) beaches have been shown to be more vulnerable to dune erosion relative to low sloping (wide) beaches (Saye et al., 2005; Thornton et al., 2007; Burroughs & Tebbens, 2008; Splinter et al., 2014). Decreased susceptibility to dune erosion on low sloping beaches appears to be related in part to feedbacks associated with β_f reducing S_{INC} and TWLs (e.g., Stockdon et al., 2006, 2007). On an infragravity-dominated, low sloping beach it has recently been shown that TWLs exceeding the dune toe contribute positively to lower dune growth (Cohn et al., 2018). This observed wave-driven accretion

is in contrast to conventional viewpoints of an erosional response to TWLs in the collision regime (e.g., Sallenger, 2000; Stockdon et al., 2007).

To characterize and simulate dune response to high water levels, numerous analytical models (e.g., Vellinga, 1986; Kriebel & Dean, 1993; Komar et al., 1999; Larson et al., 2004; van Gent et al., 2008; Palmsten & Holman, 2012) have related hydrodynamic and morphologic controls to volumetric dune erosion. Consistent among these models is that increases in wave energy, TWLs, or the frequency of wave impact to the dune will all increase the magnitude of dune erosion. However, the predictive skill of these models varies for different field sites (e.g., Splinter & Palmsten, 2012; Mull & Ruggiero, 2014), in part because of model simplifications of the physical processes driving dune erosion. Furthermore, no analytical framework for wave-driven dune response currently has the ability to simulate wave-driven dune growth.

Process-based numerical models, which include the relevant physics of wave transformation, sediment transport, and morphology change, have also been widely utilized to simulate coastal profile change. While numerous process-based models have shown skill at simulating storm-induced foredune erosion (e.g., Larson & Kraus, 1989; Johnson et al., 2012), the XBeach model (Roelvink et al., 2009) has been among the most widely used tools for this purpose (e.g., van Dongeren et al., 2009; Lindemer et al., 2010; McCall et al., 2010; Splinter et al., 2014; de Winter et al., 2015; Palmsten & Splinter, 2016). XBeach is a phase-averaged hydrodynamic, sediment transport, and morphology change model which resolves infragravity wave processes that are typically important during energetic storm conditions (Roelvink et al., 2009) and on low sloping beaches (Vousdoukas et al., 2012; Roelvink et al., 2018). As an example of the model's skill, McCall et al. (2010) reproduced spatial patterns of both dune erosion and overwashing from a major hurricane along a barrier island in the U.S. Gulf of Mexico using XBeach. As another example, de Winter et al. (2015) utilized XBeach to simulate alongshore variability in dune scarping and slumping from a major storm event at a field site in the Netherlands, demonstrating that the pre-storm dune face steepness had the largest control on the magnitude of dune response, with secondary effects from alongshore variability in nearshore bathymetry. Numerous

other studies have shown that XBeach has reasonable skill at simulating both accretive and erosive coastal profile changes (e.g., Pender & Karunarathna, 2013; Splinter et al., 2014).

In this study, we aim to understand the primary controls on spatio-temporal variability in storm-induced dune impacts along dissipative coasts – including the drivers of both accretive and erosive responses. Since the recent observation of wave-driven dune accretion at an end-member dissipative beach (Cohn et al., 2018) is in contrast to the many global observations of wave-driven dune erosion, we hypothesize that there is a morphologic control on the processes contributing to wave-driven dune growth. In order to test this hypothesis, both field datasets and process-based numerical modeling are utilized to characterize the environmental and morphologic controls on the magnitude and direction (accretion or erosion) of wave-driven dune response.

The chapter is organized such that morphology data from three field sites in the U.S. Pacific Northwest (PNW) are first used to identify controls on alongshore variability of storm-induced dune response in Section 4.2. These event-scale field measurements indicate a morphologic control on high water induced dune responses, including the potential for dune accretion directly through wave-driven processes at all three field sites under particular environmental forcings. Due to the paucity of observations available, and the complexity of the dune erosion processes the data reveal, XBeach is then used to further assess the factors controlling the environmental and morphologic controls driving high water level induced dune response. In Section 4.3, the modeling methodology is presented, which includes a comparison of XBeach model hindcasts of high water events at the three PNW field sites to demonstrate that the model is capable of simulating both accretion and erosion of coastal foredunes. Additional model simulations are completed which (1) alter details of the shelf, nearshore, beach, and dune morphology in order to isolate morphologic controls on dune response and (2) investigate a wide range of oceanographic forcing (varying still water levels and waves) to determine the physical drivers of wave-driven erosion and accretion for a low sloping dissipative beach. Results of the exploratory numerical modeling simulations are presented in Section 4.4. A discussion and summary of the environmental and morphologic controls based on these observations and modeling results are presented in Sections 4.5 and 4.6, respectively.

4.2 Field Observations of Wave-Driven Dune Response

4.2.1 Field Setting

The U.S. Pacific Northwest (PNW) is a tectonically active coast defined by a high energy, seasonally varying wave climate and a wide variety of beach morphologies (Peterson et al., 1991; Ruggiero et al., 2005). The region has among the most intense wave climates in the world, with the average annual storm event having significant wave heights (H_s) exceeding 10 m (Ruggiero et al., 2010). These storms typically occur in boreal fall and winter, coinciding with seasonally elevated SWLs resulting from region-wide wind-induced sea level anomalies and thermal expansion (Komar et al., 2011). These high TWL conditions drive corresponding erosion of the beach (e.g., Ruggiero et al., 2005). Many of the largest erosional events occur during El Niño Southern Oscillation (ENSO) periods which alter storm frequency, intensity, and direction in the region (Barnard et al., 2011, 2015, 2017; Allan & Komar, 2002) which can increase the frequency of TWLs impacting the dune and export sediment via spatial gradients in longshore sediment transport. For example, there was significant beach erosion documented across much of the PNW during the 1997-1998 El Niño (e.g., Allan & Komar, 2002; Revell et al., 2002). However, even more widespread erosion and damages occurred during the energetic 1998-1999 La Niña the following winter (Komar et al., 2001; Allan & Komar, 2002; Ruggiero et al., 2005). This is likely due in part to a lack of beach recovery from the previous intense winter, resulting in a narrower (steeper) beach and leaving the dunes more vulnerable to erosion via elevated TWLs.

While seasonal to decadal topographic beach changes throughout the Pacific Northwest have been well characterized through beach monitoring (Allan et al., 2013; Ruggiero et al., 2005) and airborne lidar surveys, assessments of sub-seasonal change measurements in the region have been less common until recently (e.g., Barnard et al., 2017; Cohn et al., 2015, 2017). These efforts have included measurements of beach and dune morphology at nominally monthly scale at three sandy, dune-backed field sites: South Beach, OR (SBSP), Netarts Littoral Cell, OR (NLC), and Oysterville, WA (OYST) (Figure 4.1).

Figure 4.1: (a) Overview map showing the three field sites (triangles), local wave buoys (orange stars), and tide gauges (blue squares) and local maps of Oysterville, WA (OYST, b), South Beach, OR (SBSP, c), and Netarts Littoral Cell, OR (NLC, d) sites with the circles indicating the survey locations used in this analysis.

4.2.1.1   South Beach, OR (SBSP)

South Beach State Park (SBSP) in Newport, OR is located adjacent to the Yaquina River Inlet South Jetty (Figure 4.1c). The jetty structure has historically impeded northerly directed longshore sediment transport, leading to a modern short-term shoreline change rate (STSCR), measured between 1967 and 2002, of ~2 m/yr within 500 m of the jetty (Ruggiero et al., 2013). Further to the south, the STSCR has been close to zero or slightly erosional (~ -1 m/yr). In response to these shoreline changes, the beach is widest near the jetty and decreases in width towards the south. The whole field site is characterized by vegetated foredunes backing the beach.

4.2.1.2   Netarts Littoral Cell, OR (NLC)

Netarts Littoral Cell is a 12 km long headland bounded stretch of coastal in central Oregon (Figure 4.1d) which includes vegetated dunes, scarped dunes, and bluff-backed regions. As a result of counter-clockwise shoreline rotation from a multi-decadal shift in wave direction offshore the PNW (Anderson & Ruggiero, 2015), STSCR at the southern portion of NLC has been approximately -2 m/yr (Ruggiero et al., 2013). This rate is higher than the littoral cell average STSCR of -1 m/yr. These recent shoreline trends have contributed to spatially variable beach characteristics, with beaches generally being narrower in the southern portion of NLC and wider towards the north.

4.2.1.3   Oysterville, WA (OYST)

Oysterville, WA (OYST) on the Long Beach Peninsula is a wide, flat coastal system which has low gradient ($\beta_f \sim 0.025$), heavily vegetated foredunes backing the beach (Figure 4.1b). The system is rapidly prograding (STSCR ~4-5 m/yr; Ruggiero et al., 2013), with sediment sourced from the Columbia River located ~ 30 km to the south and delivered to the site predominantly via longshore sediment transport processes (Ruggiero et al., 2016). The coastal dunes are prograding at similar rates to the shoreline (~3-4 m/yr; Ruggiero et al., 2016) and a new foredune has formed over the past decade resulting from these large sediment

inputs (Moore et al., 2016). This site has been the focus of a long-term (1997 to present) coastal monitoring program (Ruggiero et al., 2005), with recent work focused on characterizing sub-seasonal nearshore, beach, and dune dynamics (Cohn et al., 2017, 2018). Field observations at OYST have shown that elevated TWLs in the collision regime contribute positively (~1-5 m^3/m/yr) to lower dune growth at Oysterville, WA (Cohn et al., 2018).

4.2.2 Field Methods

Coastal monitoring programs have measured coastal change throughout the PNW. The methodologies for collection and interpretation of these morphologic datasets, in conjunction with oceanographic data which drives these coastal changes, are presented below.

4.2.2.1 Morphology Measurements

Recent field surveying efforts at SBSP, NLC, and OYST have characterized sub-seasonal beach and dune evolution. At each site cross-shore topographic transects are measured using backpack-based real time kinematic (RTK) global positioning systems (GPS) from wading depth to the foredune crest. Additional bathymetric surveys using the Coastal Profiling System (CPS; Ruggiero et al., 2005) have also been completed at a subset of these surveyed topographic lines in summer months.

At SBSP, topographic surveys were completed approximately monthly or more frequently at 22 cross-shore locations covering a 1.7 km length of beach between January 2014 and October 2017 (Figure 4.1c; Susa et al., 2014; Cohn et al., 2015). The most recent CPS bathymetry measurements were collected in summer 2015. Numerous storm events occurred throughout the 4 year topographic record at SBSP, while the event with the largest offshore wave conditions occurred during the 2015-2016 El Niño. During the 2015-2016 El Niño period, topographic data was also collected along the entire 12 km stretch of the NLC at nominally monthly intervals. Data from 29 transects along a 6.6 km extent of Netarts spit backed by dunes is utilized for the analysis presented in this paper. A littoral cell wide bathymetric survey using the CPS was completed in 2011 on the same topographic transect lines; these data are used to characterize the nearshore morphology at NLC. Numerous

storm events impacted the dune throughout the measurement period, with a 10 December 2015 storm event being the most severe. Topographic and bathymetric data were also collected intermittently at OYST over a one-year period between 2016 and 2017 at time scales ranging from 1 day to every 2 months (Cohn et al., 2018). For the full year, 13 cross-shore transects were measured at least every 2 months along a 500 m alongshore stretch of coast.

From these cross-shore profile data the dune slope (β_{dune}) is calculated from the dune crest (D_{crest}) to the 4 m NAVD88 contour, which is used to approximate the dune toe (D_{toe}) elevation regionally (e.g., Mull & Ruggiero, 2014), for each transect. All vertical references henceforth are relative to the NAVD88 datum, where 0 m NAVD88 is ~coincident with the mean lower low water (MLLW). Dune volume changes (ΔV_{dune}) are calculated between subsequent topographic surveys from the 4 m to 7 m contour positions. This upper limit corresponds to the highest estimated TWL at any of the three field sites during the morphology measurement period, above which bed level changes likely do not reflect the influence of marine processes. Therefore, higher elevations are purposely excluded from the volumetric analysis to limit the inclusion of aeolian-driven dune growth as much as possible and to reduce compounding volumetric error estimates associated with topographic surveying of the spatially variable (e.g., hummocky, steeper sloped) upper dune. Uncertainty in the ΔV_{dune} estimates, resulting from GPS and other vertical measurement errors (e.g., Ruggiero et al., 2005), is approximately 1-5 m^3/m depending on the horizontal distance between the 4 and 7 m contours.

Aeolian processes may also contribute to morphology changes between 4 and 7 m. However, to limit aeolian influences on ΔV_{dune}, data are only used for periods when TWLs were predicted to reach at least the 4 m contour and where ~monthly scale morphology measurements were made. Given that the time scale of dune growth is typically long (>months) (e.g., Houser & Hamilton, 2009), we assume that any observed dune changes during these high water level events reflects a proportionally larger wave signal than aeolian-driven accumulations in the depositional record (e.g., Cohn et al., 2018).

Additional morphometrics are also calculated from the field datasets. The backshore beach slope ($\beta_{backshore}$) is defined between the 4 m contour and mean high water (MHW, 2.1 m), whereas the surf zone slope ($\beta_{nearshore}$) is derived from the CPS bathymetric data

and is calculated as the average slope from the MHW contour to the -12 m contour. The shelf slope (β_{shelf}) is the average slope from -50 m to -12 m calculated from regional NOAA bathymetric digital elevation models (DEM) (Carignan et al., 2009).

Observations of alongshore varying ΔV_{dune} are assessed in detail for the highest TWL event for each of the three field sites. Data from all available topographic surveys collected at the storm time scale are further analyzed to investigate relationships between dune volume change and local morphometrics and oceanographic conditions.

4.2.2.2 Oceanographic Conditions

A number of wave buoys and tide gauges operated by the National Oceanic and Atmospheric Administration (NOAA) National Data Buoy Center (NDBC), the NOAA Tides and Currents program, and the Coastal Data Information Program (CDIP), collect continuous oceanographic measurements within the PNW. Measurements from NDBC buoy 46050 (Stonewall Bank) and NDBC buoy 46029 (Columbia River Bar) (Figure 4.1a), located in proximity to SBSP (46050), NLC (46050), and OYST (46029), are used to characterize the wave climate in this study. Still water levels (SWL) measurements, which include the effects of tides, seasonal sea level anomalies, storm surge, and other non-tidal residuals, are obtained from nearby tide gauges NOAA 9435380 in South Beach, OR (SBSP), NOAA 9437540 in Garibaldi, OR (NLC), and NOAA 9440581 in Cape Disappointment, WA (OYST) (Figure 4.1a). Wave and SWL measurements were obtained for periods when morphologic measurements were collected. These time series data are used to understand the forcing conditions driving the observed coastal dune response and as boundary conditions for model hindcast simulations.

To characterize the general oceanographic attributes within the PNW, a thirty two year time series of H_s, peak wave period (T_p), and wave direction (D) derived from the NDBC 46050 buoy and still water levels from NOAA 9435380 was also developed, where data gaps were filled in from other nearby stations when available (Figure 4.2). These variables exhibit significant seasonality, with the most energetic waves and highest water levels typically occurring in January and December (Figure 4.2f,g,i). This long oceanographic record
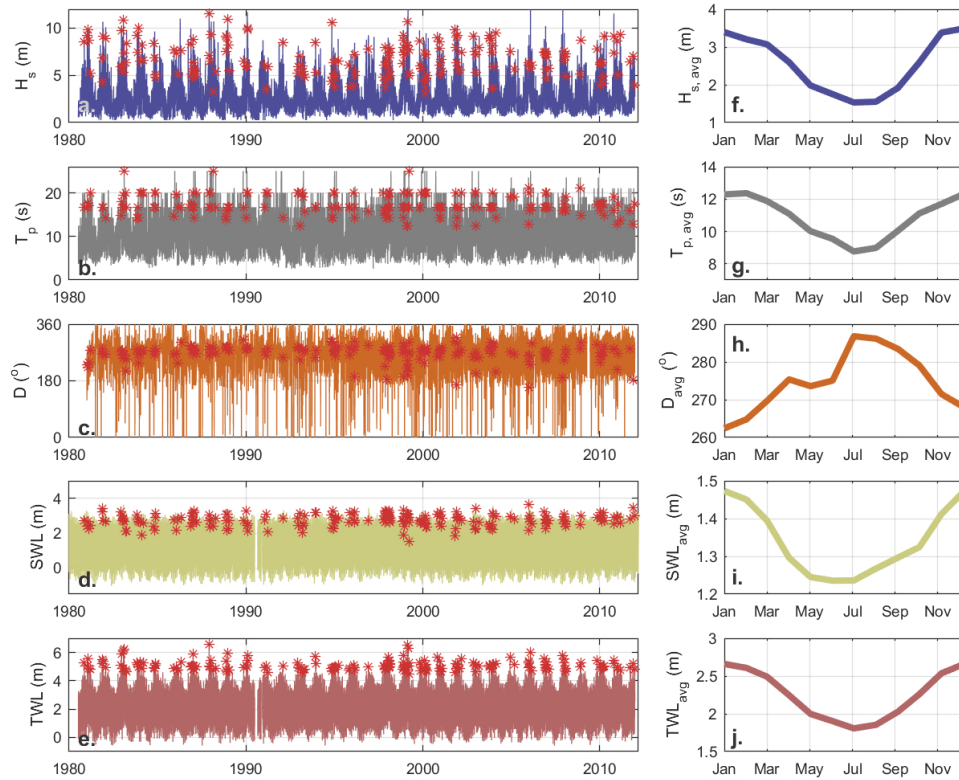
Figure 4.2: Regionally representative 32 year (1980 2012) environmental conditions time series and monthly averages of deep water significant wave height (a/f), peak wave period (b/g), dominant wave direction (c/h), still water levels (d/i), and empirically estimated TWLs assuming a $\beta_{backshore}$ of 0.02 (e/j), with the oceanographic characteristics associated with the five largest events per year shown with red asterisks.

is used to generate generic PNW storm hydrographs for use in exploratory numerical model simulations.

4.2.3 Field Results

4.2.3.1 SBSP Coastal Response (Single Event)

The most erosive event to the foredunes in the 4 year SBSP record occurred on 10 December 2015 when a storm with maximum H_s of 9.5 m coincided with an elevated SWL (3.3 m at the peak H_s). The waves approached obliquely from the south which limited wave sheltering effects from the jetty. A pre-storm survey had been completed at SBSP on 22 November 2015 and a post-storm survey was completed on 21 December 2015. Using Stockdon et al. (2006) to calculate runup and utilizing $\beta_{backshore}$ for β_f, maximum TWLs during this event were predicted to be between 5.7 m (shallowest $\beta_{backshore}$) and 6.4 m (steepest $\beta_{backshore}$).

The steepest $\beta_{backshore}$ (0.037) prior to this storm was measured at line 21 (Figure 4.3c) at the southern extent of the SBSP field site. At line 21 a ~1 m high, near-vertical scarp developed (Figure 4.3h,i) resulting in ΔV_{dune} of -21.8 m^3/m (Figure 4.3e). Conversely, within 250 m of the jetty, including line 5 (Figure 4.3c), pre-storm $\beta_{backshore}$ were less than 0.023. At these northern transects negligible or net positive ΔV_{dune} of up to 3.1 m^3/m were measured. At SBSP there is a positive relationship between ΔV_{dune} and $\beta_{backshore}$ (R^2 = 0.34 for a linear trend), with shallower sloped beaches generally experiencing less dune erosion or in some cases positive ΔV_{dune}.

While the southerly wave approach during the December 2015 storm should have resulted in similar wave conditions outside of the surf zone across the study site, the jetty structure would have blocked longshore sediment transport to the north during this, and other, events. Consequently, longshore transport gradients may have increased the local sediment budget near the northern portion of the study site. However, as the largest longshore sediment transport rates are generally thought to coincide with the largest longshore current velocities (e.g., Bailard, 1981), which occur far from the dune face, at the storm time scale we assume that these external sediment inputs do not contribute to ΔV_{dune}.
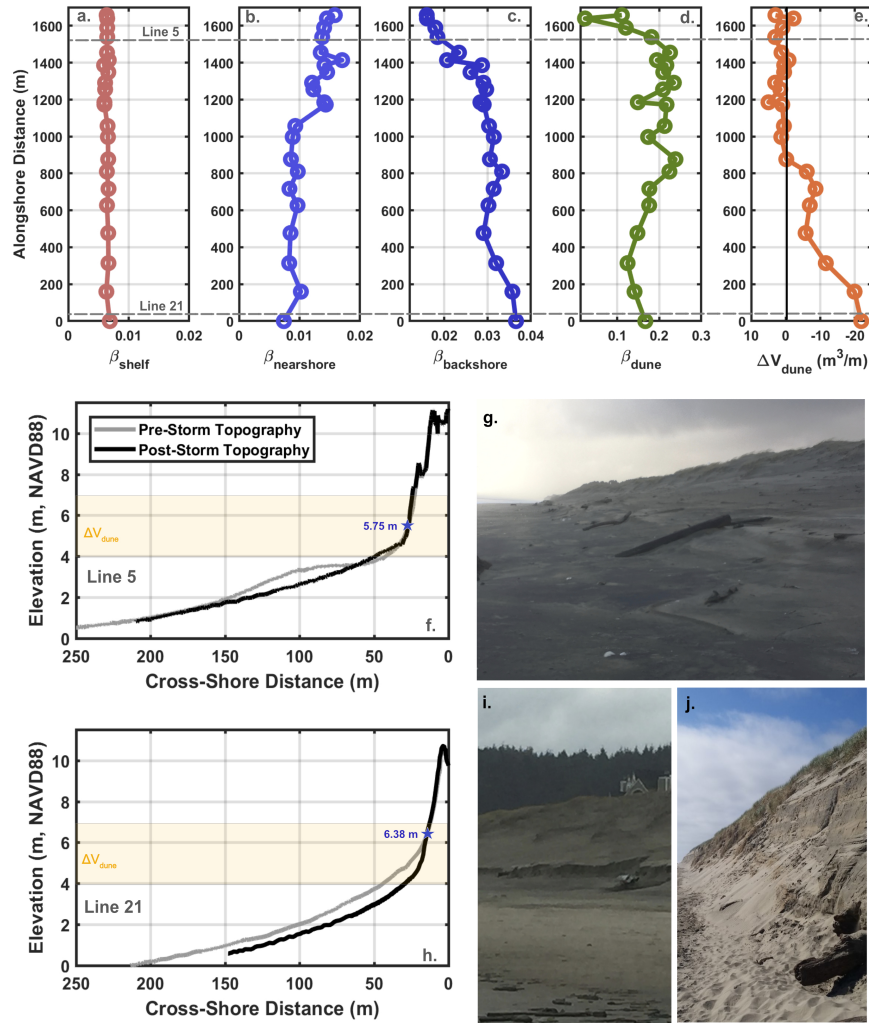
Figure 4.3: Alongshore variability in beach morphometrics (a-d) and measured dune volume changes (e) from a 10 December 2015 storm event at SBSP, cross-shore profile change from before the storm (22 November 2015) and after the storm (21 December 2015) (f/h). The elevation of the estimated maximum TWL during the storm event is shown as a blue star for each transect (f/h). Post-storm pictures of scarp development at line 21 (i) and no apparent erosion near line 5 (g) were taken on 21 December 2015. The continued development of the 1 m scarp to a 3 m near-vertical scarp at line 21 throughout the 2015-2016 El Niño is shown in photo (j) taken on 9 April 2016.

It is important to note that while the 10 December 2015 storm was the largest TWL event between the two survey dates, this early winter period was generally characterized by high wave energy and elevated SWLs. During the period between 23 November 2015 and 15 December 2015, TWLs exceeded the 4 m contour 11% (lowest $\beta_{backshore}$) to 22% (steepest $\beta_{backshore}$) of the time at SBSP. Thus, while ΔV_{dune} likely primarily reflects the impacts of the largest TWL event, impacts from additional high water events may also have induced an erosional or accretional response. Additionally, aeolian recovery could have also occurred in this time period – masking signs of marine-induced erosion. However, as the post-storm survey was completed within 10 days of the end of the storm, aeolian-driven dune recovery on these time scales is hypothesized to be minimal.

4.2.3.2 NLC Coastal Response (Single Event)

In the one year coastal change record at NLC, the most erosive event to the foredunes also coincided with the storm event on 10 December 2015. The maximum SWL at NLC during this storm was 3.3 m based on the Garibaldi, OR tide gauge. Pre- and post-storm topographic data was collected on 23 November 2015 and 15 December 2015, respectively. During this storm event, maximum TWLs reached between 6.2 m and 6.7 m, depending on $\beta_{backshore}$. At Line 8, located approximately 1.5 km north of the Cape Lookout headland (Figure 4.1d), -17.6 m³/m was lost from the dune and a prominent scarp developed (Figure 4.4h,j). This scarp was continuous for hundreds of meters, as demonstrated in the comparable ΔV_{dune} for transects adjacent to Line 8 (Figure 4.4e). The scarping was coincident with some of the steepest beach slopes ($\beta_{backshore} \sim 0.037$) on the barrier. Conversely, in the north-central portion of the study site, no dune erosion was observed (Figure 4.4f,j). Instead, these transect locations accreted up to 4.7 m³/m (Figure 4.4e). These accretional areas coincided with some of the shallowest sloping backshores at this field site ($\beta_{backshore} <$ 0.03). The data shows that there is a relationship between ΔV_{dune} and $\beta_{backshore}$ ($R^2 = 0.82$) at NLC.

As the post-storm survey was completed within 4 days of the end of the storm, similarly to the interpretation at SBSP aeolian-driven post-storm dune recovery is hypothesized to be minimal in this time frame. This is supported by the presence of logs and debris which
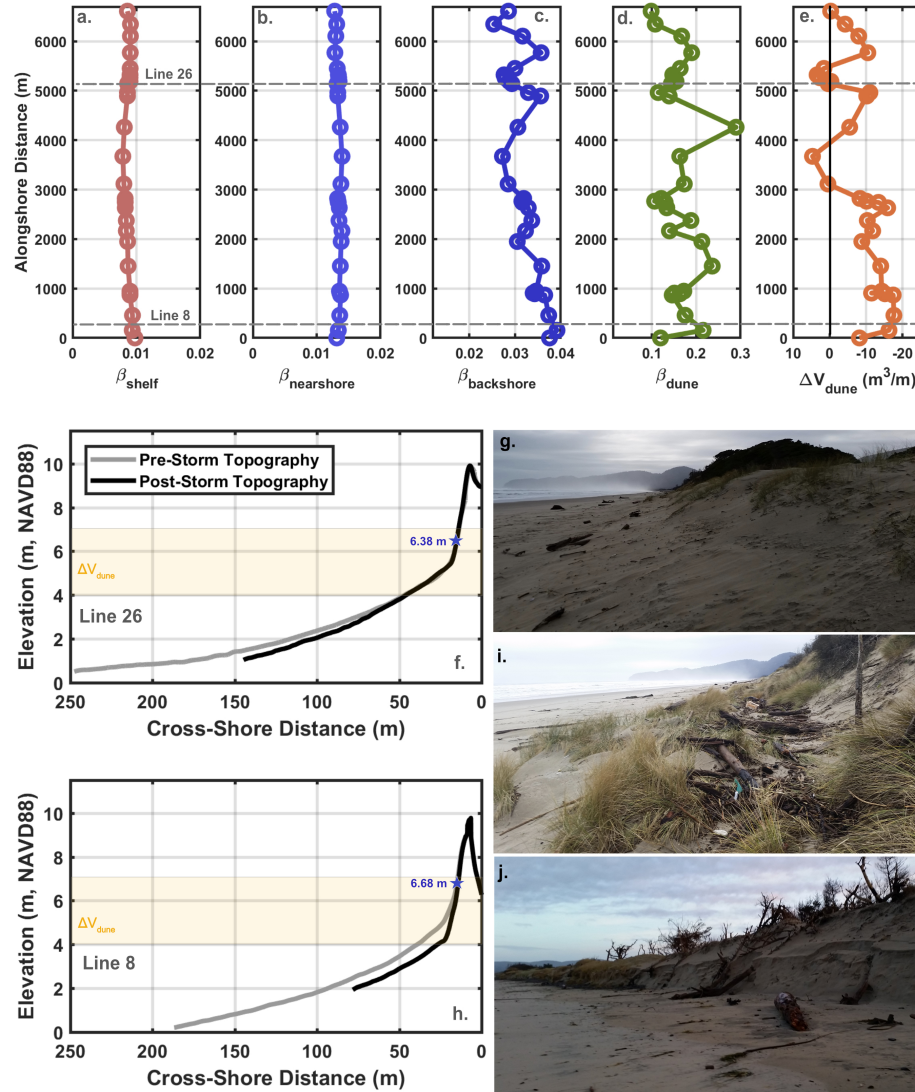
Figure 4.4: Alongshore variability in beach morphometrics (a-d) and measured dune volume changes (e) from a 10 December 2015 storm event at NLC, cross-shore profile change from before the storm (23 November 2015) and after the storm (15 December 2015) (f/h). The elevation of the estimated maximum TWL during the storm event is shown as a blue star for each transect (f/h). Pictures of scarp development at line 8 (j), no dune erosion at line 26 (g), and new debris/logs washed into the base of the dune near line 22 (i; alongshore distance 3.5 km) taken on 15 December 2015.

washed up at the base of the dune/bluffs during the storm event and which did not show evidence of post-storm aeolian accumulations by the time of the post-storm survey (e.g., Figure 4.4i). Therefore, foredune growth during this period is thought to be primarily from wave-driven processes. However, since TWLs exceeded the 4.0 m contour 21% (lowest $\beta_{backshore}$) to 29% (steepest $\beta_{backshore}$) of the time during this energetic period between the 23 November 2015 and 15 December 2015 surveys, additional wave-driven dune erosion or deposition may have also occurred beyond just the response to the 10 December 2015 storm event.

4.2.3.3   OYST Coastal Response (Single Event)

A high water level event on 15 November 2016 with H_s of 4 m and T_p of 17 s coincided with a spring high tide and a positive sea level anomaly which led to TWLs sufficient to reach the dune toe at OYST (TWLs predicted between 5.1 and 5.2 m). During this event a temporary Argus camera (Holman & Stanley, 2007) provided visual confirmation on the evolution of water levels during the storm revealing that TWLs reached at least 5 m, exceeding the dune toe elevation (Figure 4.5h). Based on topographic surveys from 8 November 2016 and 8 December 2016, during which period the TWL was predicted to exceed 4 m about 9% of the time, dune volume growth of up to 8.6 m^3/m occurred (Figure 4.5e,f). Over the 500 m stretch of coast studies the beach and dune morphometrics are relatively alongshore uniform, with an average $\beta_{backshore}$ of 0.025. As discussed in Cohn et al. (2018), accretion during this high water event is attributed primarily to a wave-origin rather than aeolian processes, demonstrated by the presence of fresh, uncovered macrophyte algae (kelp) at the base of the dune and the lack of aeolian-driven deposition at any elevations landward of the kelp (Figure 4.5g). A detailed study of dune evolution by Cohn et al. (2018) shows that wave-driven dune accretion processes contribute between about 10 to 40% of lower dune growth at OYST, indicating that the impacts from the November 2016 storm event are not anomalous.
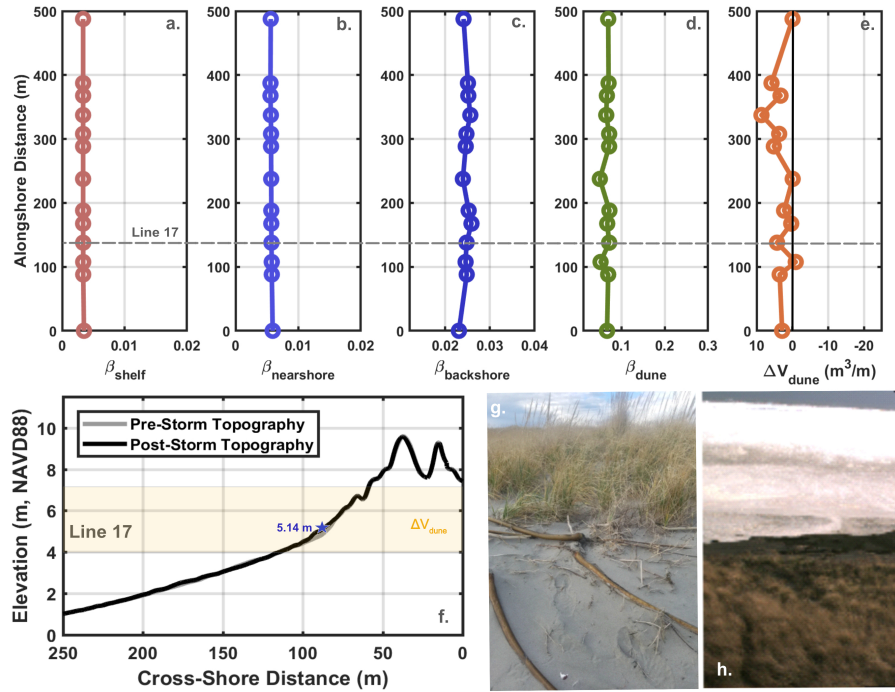
Figure 4.5: Alongshore variability in beach morphometrics and measured dune volume changes (a-e) from a 15-16 November 2016 storm event at OYST, cross-shore profile change from before the storm (8 November 2016) and after the storm (8 December 2016) (f), picture of kelp deposited at base of dune from high water event (picture taken 8 December 2016) (g), and Argus composite brightest image collection from 16 November 2016 taken during daylight hours showing water levels reaching the base of the dune (h).

4.2.3.4 Combined Coastal Response Data (Multiple Events)

While the individual high water level events described above shed light on the controls of spatially varying dune response, high water level events reach the dune toe relatively frequently in the PNW. Additional coastal foredune change measurements at ~monthly scale at SBSP (61 topographic surveys at 22 transects over 4 years), NLC (13 surveys at 23 transects over 1 year), and OYST (50 surveys at 13 transects over 1 year) are analyzed to explore additional dune responses under a wide range of oceanographic forcing conditions. ΔV_{dune} was calculated between consecutive surveys for any period where the time between

surveys was less than 2 months apart. These data are then compared to β_{shelf}, $\beta_{nearshore}$, $\beta_{backshore}$, and β_{dune}, which are computed for each period using data from the first of each survey pair (Figure 4.6a,b,c,d and Table 4.1).

The maximum wave height ($H_{s,max}$) and maximum TWL (TWL_{max}) between the survey pairs was extracted from the oceanographic time series from the closest wave buoy and tide gauge to each site (Figure 4.6e,f). For this analysis TWLs are calculated utilizing the $\beta_{backshore}$ measured at each transect from each topographic survey using the Stockdon et al. (2006) equation for wave runup. The duration that TWLs exceed a particular contour has been previously related to beach and dune impacts (e.g., Ruggiero et al., 2001; Wahl et al.,
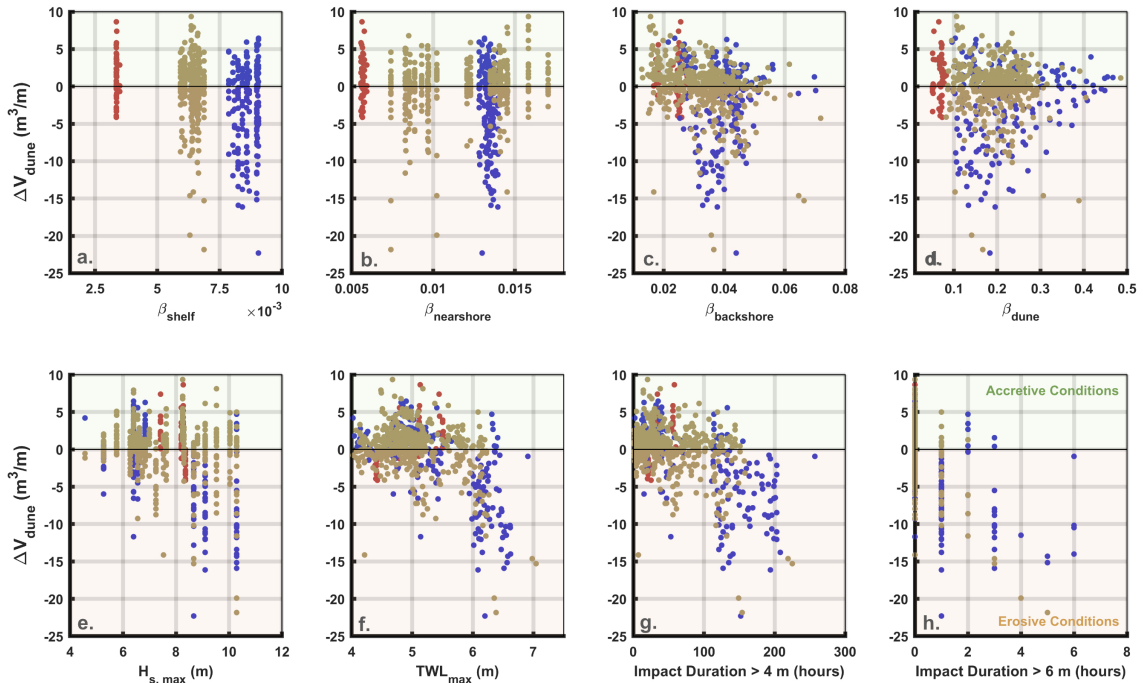
Figure 4.6: Field observations of dune volume change compared with relevant profile morphometrics (a-d), maximum wave height calculated between topographic survey dates (e), maximum TWL calculated between topographic survey dates (f), duration of TWLs above 4 m (g), and duration of TWLs above 6 m (h) at the three field sites (SBSP tan; NLC, blue; OSYT, red).

Table 4.1: Morphometric values for three field sites across all available measurements (including non-storm cases). For each morphometric the range is given, with the mean value in parentheses.

Morphometric	SBSP	NLC	OYST
β_{shelf}	0.0059 – 0.0069 (0.0064)	0.0079 – 0.0098 (0.0089)	0.0034 – 0.0035 (0.0034)
$\beta_{nearshore}$	0.0074 – 0.017 (0.0118)	0.0128 – 0.014 (0.0136)	0.0056 – 0.0059 (0.0057)
$\beta_{backshore}$	0.011 – 0.123 (0.029)	0.021 – 0.076 (0.038)	0.017 – 0.030 (0.023)
β_{dune}	0.018 – 0.875 (0.202)	0.096 – 0.622 (0.215)	0.050 – 0.102 (0.075)

2016). Here the impact duration above the 4 m and 6 m contours are also calculated using the TWL time series between each set of surveys (Figure 4.6g,h).

Dune volume change measurements are compared to these morphologic and oceanographic variables in Figure 4.6 for all periods where the inter-survey TWL_{max} exceeded D_{toe} (4 m). This results in 572 records of ΔV_{dune} across the three field sites. While the majority of these observations show dune erosion coincident with high TWLs (Figure 4.6), 20% of these 572 storm measurements show dune growth greater than 2 m^3/m between consecutive surveys in which water was impacting the dune toe. The largest accretional events occurred on low sloping $\beta_{backshore}$ (<0.03), although positive ΔV_{dune} were measured across the full range of measured $\beta_{backshore}$ (Figure 4.6c). Collectively, these observations suggest that TWLs in the collision regime do not necessarily drive widespread erosion on these low sloping beaches.

Similar to previous studies, the combined PNW field data provide some evidence for both environmental and morphologic controls on sub-seasonal dune response. Weak relationships exist between ΔV_{dune} and β_{shelf} (R^2 = 0.07), ΔV_{dune} and $\beta_{backshore}$ (R^2 = 0.08), and $H_{s,max}$ (R^2 = 0.09). Dune volume changes have more variance explained by TWL_{max} (R^2 = 0.25), the 4 m impact duration (R^2 = 0.28), and, although infrequent, the 6 m impact duration (R^2 = 0.33). However, further insights are hard to ascertain directly from the field data in part because of the regularity that TWLs reach D_{toe} in the PNW (Figure 4.6f,g,h) and due to the relatively small number of observations available at the high water level event

time scale. Therefore, a numerical model is utilized to further explore controls on spatially variable dune responses and to better understand the drivers of wave-driven dune accretion and erosion. XBeach is specifically utilized for these purposes as the model has previously shown skill at resolving dune responses for a range of oceanographic and morphologic conditions (e.g., McCall et al., 2010; Splinter et al., 2014; Vousdoukas et al., 2012).

4.3 Numerical Simulations of Wave-Driven Dune Response

The XBeach model is used to explore factors contributing to wave-driven dune erosion and accretion. The following sub-sections provide detail on the modeling methodology, including a validation of XBeach at the three field sites and the development of exploratory simulations to assess environmental and morphologic controls on wave-induced dune responses.

4.3.1 Numerical Model Overview

XBeach is an open-source, process-based numerical model which simulates wave transformation, wave-driven current generation, subaqueous sediment transport, and corresponding morphology change (Roelvink et al., 2009). Using the hydrostatic version of the model, the time dependent, short wave action balance equation solves for the wave group envelope and is coupled with the non-linear shallow water equations to resolve mean currents and infragravity waves. Sediment transport is modelled using a depth-averaged advection-diffusion equation (Galappatti & Vreugdenhil, 1985) and morphology change is calculated based on gradients in sediment transport at each time step. Dune erosion in XBeach occurs directly from these transport gradients, as well as from avalanching which is induced when a critical angle of repose is exceeded. Model formulations are described in detail in Roelvink et al. (2009) and Roelvink et al. (2015) and are not repeated here. XBeach has been extensively validated for erosional dune processes in numerous coastal settings (e.g., McCall et al., 2010; Harley et al., 2011a; Smallegan et al., 2016; Splinter & Palmsten, 2012; Splinter et al., 2014).

4.3.2   Model Comparison to PNW Field Observations

4.3.2.1   Model Hindcast Setup

Since XBeach is sensitive to details of model configuration (e.g., Simmons et al., 2017), a validation of XBeach using the hydrostatic model was completed to demonstrate model capabilities of simulating storm-induced dune responses along the high energy PNW outer coast. XBeach was run for a single storm event for each of the three field sites: the 10 December 2015 El Niño storm event at SBSP and NLC and the 15 November 2016 high water level event at OYST. For each simulation the offshore boundary was forced with wave time series from the closest wave buoy (Figure 4.1a), where the bulk wave parameters were linearly transformed from the buoy depth to the -50 m contour and input to XBeach using a JONSWAP spectrum. Time series of measured water levels from nearby tide gauges were also input into the models.

For each field site, 1D cross-shore grids were developed for input into XBeach for each field measurement transect for the TWL$_{max}$ event at each site (22 transects at SBSP, 29 at NLC, 13 at OYST), resulting in 63 total simulations. Each grid utilized measured pre-storm topography and the most recent available CPS nearshore bathymetry. As the nearshore bathymetry typically only extends to ~12 m water depth, bathymetric data further offshore (to -50 m) was extracted from NOAA DEMs. XBeach grids with variable cross-shore resolution from 50 m (offshore) to 1 m (on the beach and dune) were developed. For all cases the models were run with a constant random seed number to allow for numerical repeatability (*random* = 0) and Snell's law was used to transform the mean wave direction of the waves as they shoal (*dtheta* = 360). Furthermore, a single grain size distribution (D50 = 0.2 mm, D90 = 0.3 mm) was assumed for all simulations in this study, generally representative for the region (Ruggiero et al., 2005). Otherwise, default model settings have been assumed.

Output from each 13 hour model simulation (including 1 hour of spin-up time), which encompasses the peak TWL portion of the storm time series, are compared to the post-event topographic measurements – collected a few days to a few weeks following the event. As described previously, additional high water events impacted the dune between the surveyed
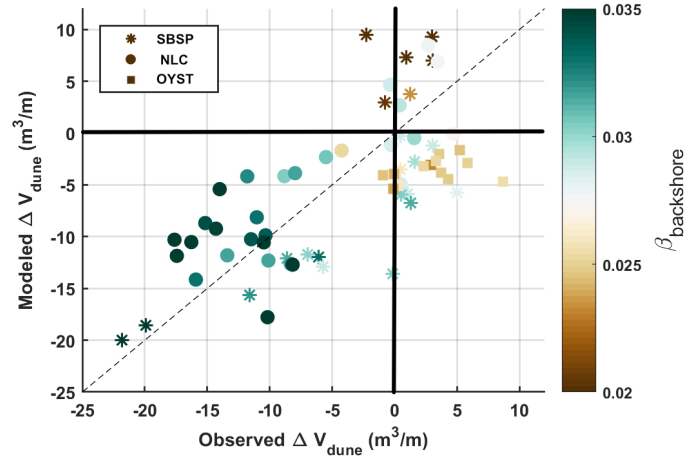
Figure 4.7: Field measurements to model simulations comparison of dune volume change before and after select storm events at SBSP (asterisks), NLC (open circles) and OYST (solid squares). Colors represent the pre-storm measured backshore slope at each transect line.

profile dates. However, for this analysis only the largest TWL event in the monthly period was simulated. Consistent with the field data analysis methods, dune volume changes from the model simulations are calculated as the integrated change from the initial 4 m and 7 m contours, before and after the storm event.

4.3.2.2 Model Hindcast Results

The model hindcasts at SBSP, NLC, and OYST agree well with field data (Figure 4.7), with a root mean square error of 6.4 m^3/m and a mean erosion overprediction of 3.6 m^3/m. The model predicts the highest dune volume losses occurring at the steepest coastal segments for both SBSP and NLC (Figure 4.7), with profile changes also generally qualitatively agreeing between the observations and model simulations (e.g., Figure 4.8). Consistent with the field observations, the model also predicts positive dune growth for many of the lowest sloping transects. XBeach simulates wave-driven dune growth for 21% of the 28 field profiles where dune growth was documented in the field data. The model does not accurately simulate dune growth at all sites where storm-induced dune accretion was ob-

served, especially at the OYST site. This may reflect a poor description of model boundary conditions for this particular storm event (e.g., characterization of wave spectrum, outdated morphology, not accounting for vegetation) or unresolved model physics (e.g., incident band swash processes).

The field measurements of dune growth most likely also contain some aeolian driven-component, although as previously described (1) the high inter-survey water levels, (2) the typically slow time scale of dune recovery, and (3) anecdotal evidence of wave-driven dune accretion at the field sites (e.g., kelp and logs deposited in the dunes) together support a
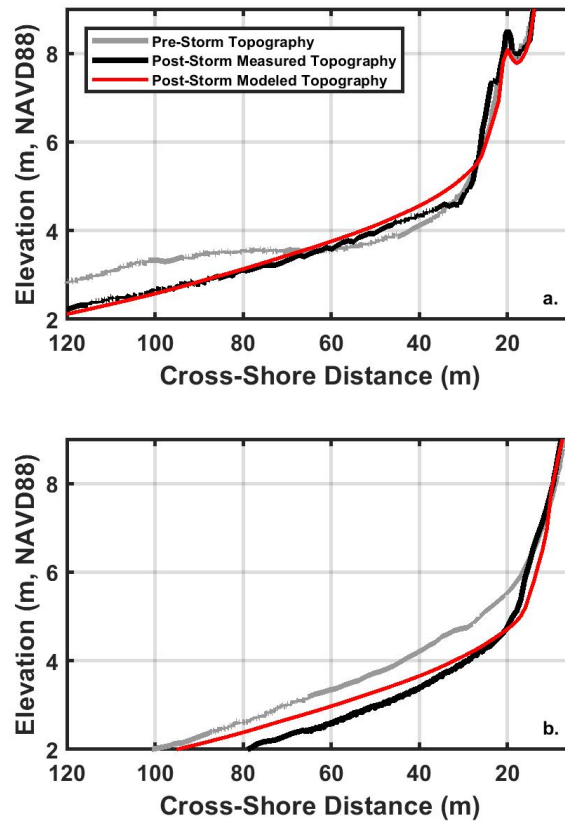
Figure 4.8: Example XBeach predicted profile change (red lines) compared to field observations for the 10 December 2015 storm event at (a) line 5 and (b) line 21 at SBSP.

primarily wave-driven origin of these sediments. Given the general agreement between model results and field observations, including the apparent influence of backshore slope on the dune response and the ability for the model to simulate positive dune growth from wave-driven processes, lends confidence in the models skill at simulating wave-induced dune responses for PNW beach and dune systems.

4.3.3   Numerical Experiments of Wave-Driven Dune Response

Based on reasonable model skill at hindcasting coastal behavior in a variety of morphologic settings within the PNW, XBeach is next applied for a range of oceanographic conditions and profile configurations in order to ascertain fundamental controls on the magnitude and direction (accretion or erosion) of wave-driven dune response. To do so, generic environmental and profile configurations were developed to drive the boundary conditions for these model simulations. Details of the generic boundary and profile conditions are first explained, followed by the details of the numerical experiments.

4.3.3.1   Generalized Boundary Conditions

4.3.3.1.1   Environmental Control: **Synthetic Storm Hydrographs**

Characterizing the time evolution of TWLs, driven by tides and non-stationarity of wave properties and non-tidal residuals, is crucial for accurate prediction of storm-induced dune response. An environmental time series from the central PNW is used to generate a single storm hydrograph that is representative of typical extreme storm events in the PNW. Using the 32 year environmental time series, extreme high water level events (Figure 4.2, red asterisks) were identified from the environmental record using a peak over threshold approach following the methods of Serafin & Ruggiero (2014), with the defined threshold corresponding to an average of five extreme TWL events per year over the length of the record (Figure 4.2). TWLs were calculated from the time series data using the Stockdon et al. (2006) runup equation assuming a $\beta_{backshore}$ of 0.02. Events were required to be at least 3 days apart (the approximate time scale of northeast Pacific extratropical storms)

to ensure independence of each storm system (Ruggiero et al., 2010). In general, for the largest TWL events on record, wave heights were between 3-14 m, wave directions were between 200-300 degrees from true north, and peak periods were between 12-25 seconds. Extreme TWLs generally occurred during high tide and usually, but not always, when the still water level (SWL) was above 2 m. It is important to note that identified extreme TWL events are not necessarily defined by the largest significant wave height event, but rather are often associated with periods of high still water levels.

For each selected extreme TWL event, the time series (including 6 hours before and 6 hours after the maximum TWL) of storm wave heights, wave periods, and SWLs were normalized based on the maximum value of each metric during that storm. The mean representative storm hydrograph, as shown in Figure 4.9, is calculated as the mean value of each oceanographic variable for each hour from the normalized time series. Although there is significant variability in the evolution of wave characteristics during individual storms, in general there is a ramp up and ramp down of wave height and wave period throughout PNW storms. The mean normalized hydrographs of wave height, wave period, and water level are then used to define the time evolution of hydrodynamic boundary conditions for storms within XBeach. Using this approach any chosen wave height/period/water level combination can be multiplied by these normalized hydrograph curves to generate synthetic storm cases. Because the normalized hydrographs represent an average, they do not have maximum values of 1 for all parameters. This indicates that the maximum wave height and wave period do not always coincide with the peak TWL across all Northeast Pacific storms. For example an 8 m, 18 s wave results in a hydrograph with maximum 7.4 m, 17.5 s waves. This approach aims to accurately characterize the TWL evolution during the storm rather than just the maximum wave conditions. While wave direction also varies considerably for storms, for simplicity here all simulated storms are assumed to follow the mean storm track derived from the selected extreme events which shifts ~7° during the evolution of the storm (not shown). These hydrographs are used to describe the time evolution of H_s, T_p, and SWL for all exploratory model simulations.
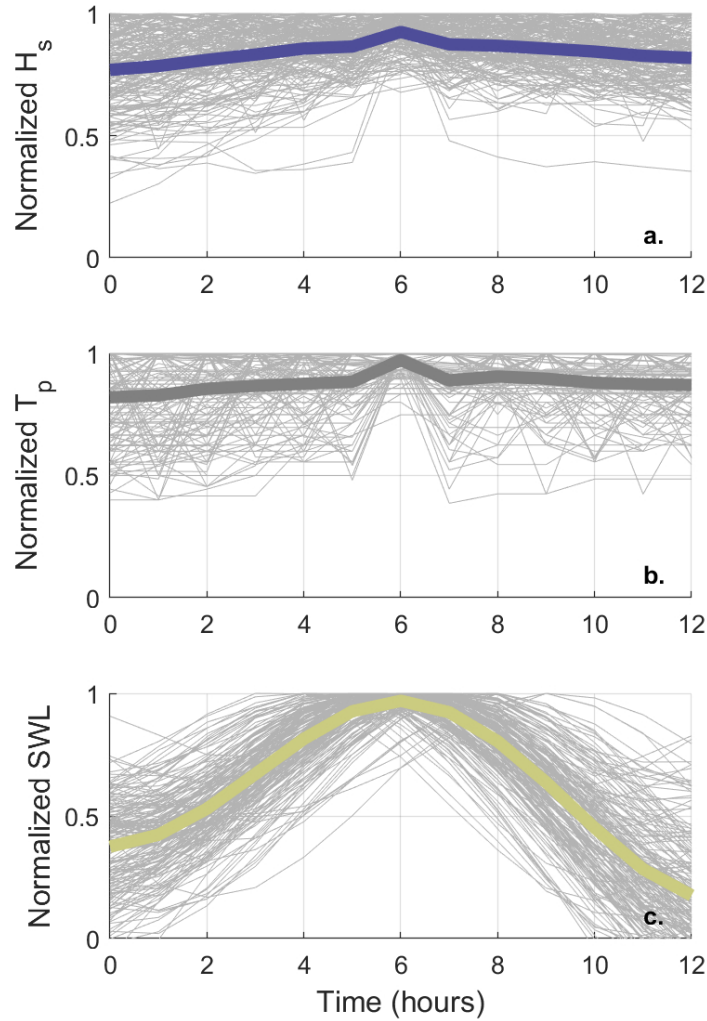
Figure 4.9: Normalized (a) wave height, (b) wave period, and (c) still water level hydrographs derived from the high water level events from the 32 year environmental time series. The light grey lines indicate the normalized hydrographs for all 191 selected high water events. Bold lines indicate the mean normalized hydrograph which is used for parameterizing model boundary conditions.

Table 4.2: Morphometric quantities of the baseline and exploratory composite slope scenarios.

Morphometric	Baseline Value	Exploratory Morphology Simulations		
		Minimum Value	Maximum Value	Number of Simulations
β_{shelf}	0.003	0.002	0.01	9
$\beta_{nearshore}$	0.0075	0.005	0.016	12
$\beta_{backshore}$	0.025	0.01	0.065	12
β_{dune}	0.07	0.05	0.45	12
D_{toe} (m)	4	3.25	6	12
D_{crest} (m)	9.5	6	16	11
V_{berm} (m^3/m)	N/A	0	100	12

4.3.3.1.2   Morphologic Control: Composite Slope Profiles

Simplified coastal profile shapes are generated to avoid the influence of subtidal sandbars and complex morphology associated with actual measured profiles and to isolate the individual geomorphic controls on dune response. A composite slope profile which has linear (fixed slope) segments for the shoreface (-50 m to 12 m), surf zone (-12 m to 2.1 m), beach (2.1 m to D_{toe}), and dune (D_{toe} to D_{crest}) are developed. A baseline composite profile is created to approximate a characteristic low sloping PNW beach, with the morphometrics of this baseline profile provided in Table 4.2 and shown in Figure 4.10 (grey lines). This profile has characteristics similar to that of OYST (Table 4.1). Additional composite slope profiles are generated for the exploratory morphologic simulations as described in Section 4.3.3.3. For all exploratory cross-shore simulations, the grids for use in XBeach have cross-shore variable grid resolution, with a coarse resolution (dx = 50 m) offshore and finer resolution (dx = 1 m) on the beach and dune. For simplicity, the elevation landward of the foredune crest is assumed to be a constant elevation of D_{crest} for all model simulations.
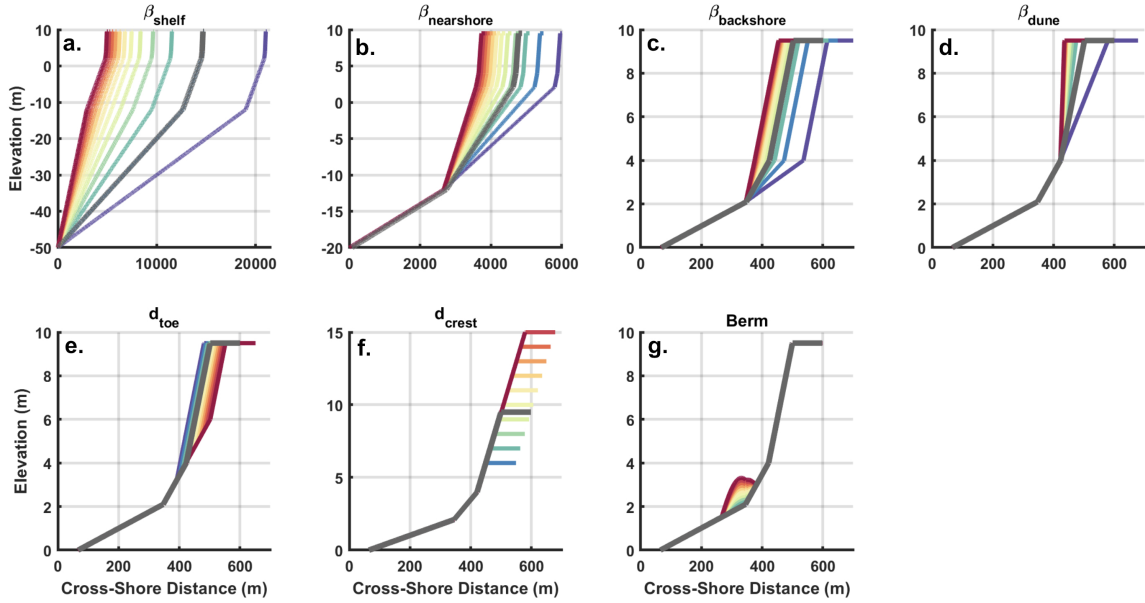
Figure 4.10: Composite sloped profiles varying shelf (a), nearshore (b), backshore (c), and dune (d) slopes and altering the dune toe elevation (e), dune crest elevation (f), and berm volume (g). The grey line in each panel represents the baseline case for comparison.

4.3.3.2 Numerical Experiment Setups

4.3.3.2.1 Environmental Controls on Dune Response

On the single baseline composite slope profile, numerous synthetic storms utilizing the normalized hydrographs are simulated. In total 10 wave height (1 m to 10 m) and 9 wave period (8 s to 24 s) conditions are simulated resulting in 90 offshore wave scenarios. Additionally, 3 still water level conditions which approximate a normal high tide (2 m), a spring high tide (3 m), and an extreme water level condition (4 m) are simulated for each wave scenario, resulting in 270 total model scenarios. These conditions generally cover the range of oceanographic conditions within the Pacific Northwest (Figures 4.2 and 4.11a,b,c). The maximum wave and water level conditions defined here are used in conjunction with the storm hydrographs to drive the time-evolving model boundary conditions. Consistent with the validation simulations, each exploratory model simulation is run for 13 hours (includ-

ing 1 hour of spin-up time). Because some TWLs in this set of simulations exceeded 7 m, dune volume changes from the exploratory simulations are calculated as the volumetric change from the initial D$_{toe}$ location to the landward extent of the model grid.

For each simulation the TWL is calculated in 30 minute increments from the model output. For each time interval, the land-water interface is tracked every 1 s and decomposed into its SWL signature, wave setup, and swash components, where swash is calculated according using the same approach as Stockdon et al. (2006). The significant infragravity swash height for each 30 minute period is calculated from the demeaned runup time series as:
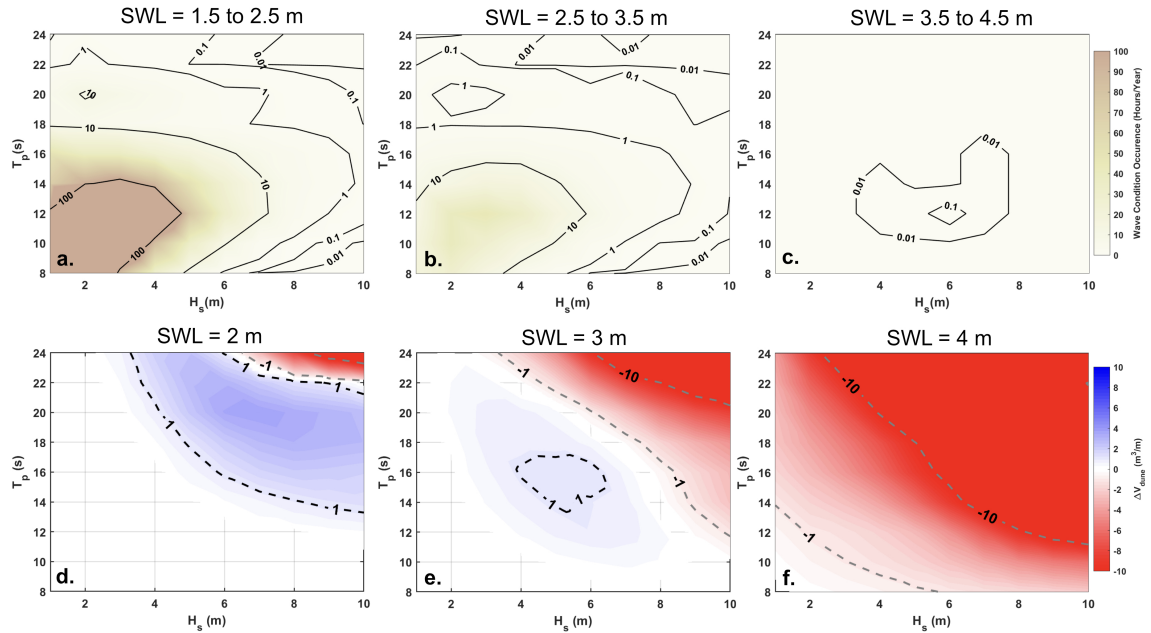
Figure 4.11: Average hours per year occurrence frequency of wave height and wave period combinations grouped by still water levels, (a) 1.5 to 2.5 m, (b) 2.5 m to 3.5 m, and (c) 3.5 m to 4.5 m, derived from the 32 year environmental time series. Model predicted dune volume change for the baseline profile for the 90 wave conditions for SWLs conditions of (c) 2 m, (d) 3 m, and (e) 4 m. Note that the colorbar axes on the model output plots are limited to highlight the accretional conditions; ΔV_{dune} of up to -74.2 m^3/m was simulated.

$$S_{IG} = 4 \sqrt{\sum_{f=0Hz}^{0.05Hz} PSD(f)\,df} \qquad\qquad \text{(EQ 4.2)}$$

Where f is the frequency and PSD is the power spectral density. Note that in XBeach there some energy in the incident band (f > 0.05 Hz) despite the model being a phase-averaged model. Here, consistent with the methods of Stockdon et al. (2014), S_{INC} is also calculated from the model results for f > 0.05 Hz to avoid under-reporting the TWL. The decomposed TWL is calculated as the sum of the SWL and $R_{2\%}$ [EQ4.1], where runup includes $\bar{\eta}$, S_{INC}, and S_{IG}, for each 30 minute period. The TWL_{max} from each simulation is calculated as the maximum 30 minute TWL occurring within the 13 hour storm event.

4.3.3.2.2 Morphologic Controls on Dune Response

To explore which portions of the coastal profile have the largest control on storm-induced dune response, a series of generic cross-shore beach profiles are generated to specifically investigate morphologic controls on dune response. Following the methodology presented in Section 4.3.3.1.2, a series of additional cross-shore profiles are developed. Slopes within particular segments of the baseline profile are individually altered based on the range of morphometrics (β_{shelf}, $\beta_{nearshore}$, β_{beach}, β_{dune}) observed at the three field study sites. The range of values investigated for each morphometric is given in Table 4.2 and shown in Figure 4.10. Additionally, as D_{toe} and D_{crest} are both thought to influence resulting dune responses (Splinter et al., 2018; Stockdon et al., 2009), these morphometrics are also altered within ranges characteristic of the PNW (Mull & Ruggiero, 2014; Table 4.2).

The presence of a beach berm is typical in summer months at many locations within the PNW (Diez et al., 2018) and it has been suggested that berms may have an influence on foredune impacts (e.g., Cohn et al., 2018). Additional model simulations were completed in which between 10 m³/m to 100 m³/m of sediment are added to approximate the presence of a berm by adding a sine wave crest distributed between the 1.5 m and 3 m contours (Figure 4.10g), the typical elevation of summer berms in the PNW (e.g., Diez et al., 2018).

In order to isolate the role of each of these morphometrics from the shelf to the dune on influencing ΔV_{dune}, XBeach was used to simulate a single environmental scenario on each

new cross-shore profile. For this single event we simulate the approximate average annual storm event in the region which consists of a 10 m significant wave height, 20 s peak wave period, and a still water level of 3 m – resulting in an extreme TWL event that exceeds the 4 m contour for the full range of PNW beach slopes.

4.4   Numerical Experiment Results

4.4.1   Environmental Controls on Dune Response

For the 2 m SWL case, H_s above 4 m and T_p of 12 s or longer result in TWLs reaching above the dune toe and inducing changes in dune morphology (Figure 4.11d). For a wide range of oceanographic conditions in which dune changes occur, when wave periods are less than 22 s or wave heights are less than 6 m, TWLs only briefly impact the dune and the model simulates sediment accumulation (up to 3.8 m^3/m) of the lower portion of the dune. When either wave heights are above 6 m or wave periods longer than 22 s, the model simulates dune erosion for the 2 m SWL case. When the SWL is increased to 3 m, a smaller range of wave conditions promote dune growth (Figure 4.11e). Instead, most large wave height and long period wave conditions (approximately $H_s > 8$ m or $T_p > 20$ s) induce dune erosion. For the 4 m SWL scenarios only dune erosion is simulated by XBeach with ΔV_{dune} of -4.6 m^3/m for the H_s of 6 m and T_p of 12 s case (Figure 4.11f). Dune erosion as large as -74.2 m^3/m was simulated for extreme wave conditions (H_s = 10 m, T_p = 24 s) co-occurring with an extreme SWL (4 m), although that combination of oceanographic forcings has not been observed in the historical environmental record (Figure 4.11c).

In general dune erosion increases with increasing TWLs (Figure 4.12). However, not all TWLs are created equal, as the erosional response (or lack of accretion) is generally higher for cases where the SWL contribution to the TWL is larger. For example, for TWL$_{max}$ approximately equal to 7 m, ΔV_{dune} ranges from ~+4 m^3/m (SWL=2 m) to ~-20 m^3/m (SWL=4 m). Although waves are functionally responsible for the physical process of dune erosion, the SWL controls where short wave dissipation and the corresponding short wave-induced sediment transport occurs. We define the mean swash level as the dynamic still water level (DSWL), which is the combination of the SWL and $\bar{\eta}$. Figure 4.13 reveals
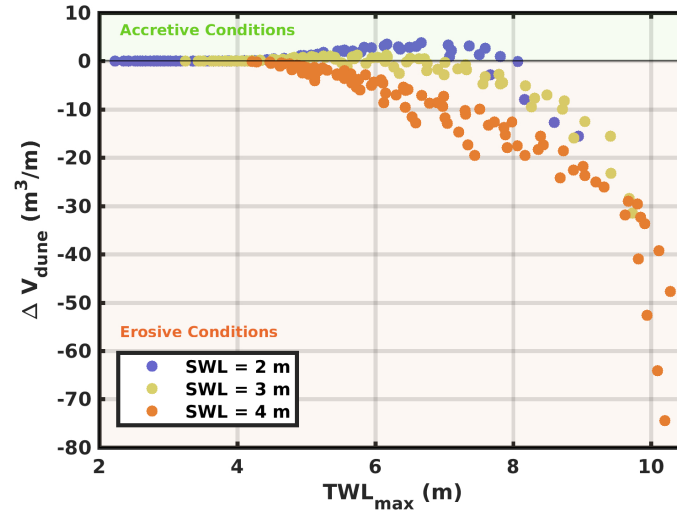
Figure 4.12: Modeled dune volume change compared to XBeach modeled maximum TWLs for 270 environmental conditions (same conditions as in Figure 10) categorized by SWL.

that accretive conditions are always simulated when the TWL_{max} reaches the dune but the DSWL is lower than D_{toe}. As DSWLs increase, the duration that TWLs are at or above the dune toe also increases (Figure 4.13a) and in response the average short wave energy (over the course of the entire event) at the initial dune toe elevation ($E_{w,toe}$) increases (Figure 4.13b). In almost all cases where the DSWL exceeds the D_{toe}, dune erosion is simulated. The only exceptions to this occur when the DSWL is only marginally above D_{toe} (< 0.7 m) and both the inundation duration and $E_{w,toe}$ are low, the combination of which also leads to simulated accretion (Figure 4.13ab). These results indicate that infragravity swash can be a constructive process for lower dune growth in low gradient beach settings, particularly when swash is only occasionally impacting the dune (DSWL $< D_{toe}$).

4.4.2 Morphologic Controls on Dune Response

To explore the morphologic controls on dune response, numerical experiments were completed using the approximate conditions of the annual storm event. In the case of large wave heights and long period waves, there is significant interaction with the bottom seaward of
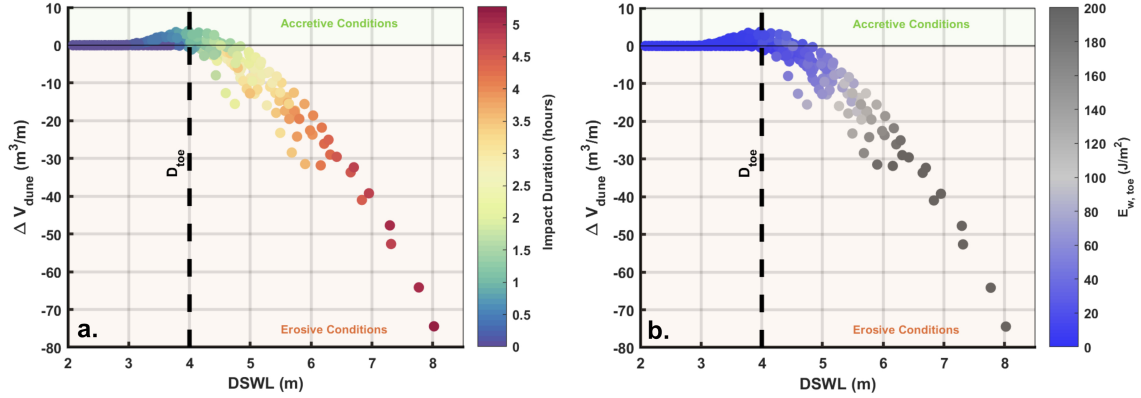
Figure 4.13: Dynamic still water level compared to modeled dune erosion for the 270 environmental condition cases (same conditions as in Figure 10) with colors representing impact hours at the dune toe (a) and mean wave energy at the dune toe location (b).

the -12 m contour. Therefore during the annual storm event the shelf slope in part dictates the cross-shore length of active wave breaking and, as a result, influences incident and infragravity wave energy in the inner surf and swash zone. The model simulations show that lower shelf slopes increase the magnitude and nonlinearity of infragravity energy, which results in a larger infragravity swash signal and therefore higher TWLs (not shown). In response, the model predicts that shallowing of the shelf portion of profile will increase dune erosion, while a steepening of the shelf would decrease TWLs and increase the possibility of wave-driven dune accretion (Figure 4.14a). $\beta_{nearshore}$ has the opposite effect, with steeper surf zone profiles enhancing dune erosion (Figure 4.14b). For the annual storm event this is attributed to an increase in both wave setup and infragravity swash associated with the dissipation of wave energy over a shorter spatial extent (Figure 4.15a). This results in maximum modeled wave runup ($R_{2\%}$) that is 1.6 m higher on the shallowest sloping nearshore profiles than the steepest nearshore profiles. The increased $R_{2\%}$ and TWLs on steeper nearshore profiles results in a longer impact duration above D_{toe} (Figure 4.15b) and more short wave energy at the base of the dune (Figure 4.15c). Based on these morphologic controls on the swash zone hydrodynamics, lower $\beta_{nearshore}$ promotes wave-driven transport to the lower dune whereas progressively steeper $\beta_{nearshore}$ enhances dune erosion.
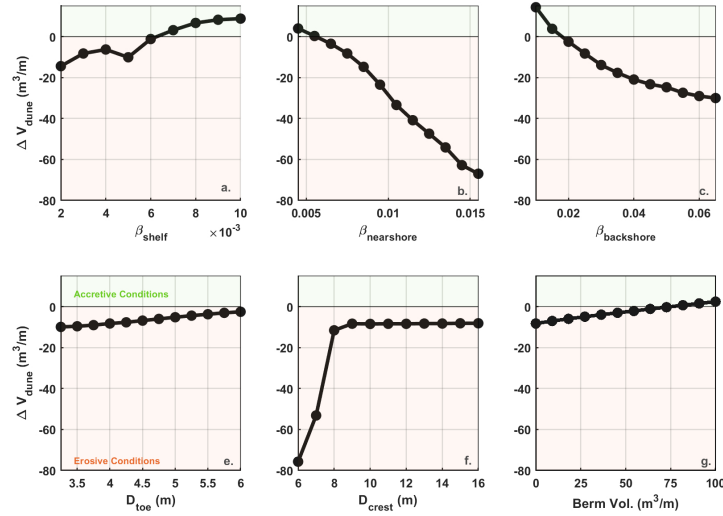
Figure 4.14: Modeled variability in dune response for varying (a) shelf slope, (b) surf zone slope, (c) backshore slope, (d) dune slope, (e) dune toe elevation, (f) dune crest elevation, and (g) berm volume for the annual storm event case.

$\beta_{backshore}$ has a similar control on modeled dune response as $\beta_{nearshore}$, with steeper slopes driving increasing dune erosion (Figure 4.14c). Interrogation of the model outputs shows a small influence of $\beta_{backshore}$ on $\bar{\eta}$ and S_{IG} (Figure 4.15d), resulting in 0.3 m higher $R_{2\%}$ and TWLs on the steepest $\beta_{backshore}$ relative to the shallowest sloping beach profile. While the maximum TWLs are similar between these $\beta_{backshore}$ cases, on steeper beaches slight increases in TWLs and enhanced beach erosion (not shown) result in more impact hours of the dune toe and an increase in short wave energy impacting the dune (Figure 4.15e,f).

The presence of a berm serves to not only limit dune erosion but also can encourage wave-driven sediment delivery to the dune (Figure 4.14g). For the annual storm event there is an approximately linear relationship whereby increases in berm volume leads to a proportional decrease in dune volume loss or an increase in lower dune volume.

Geometric properties of the foredune can also play a considerable role in wave-driven dune response. As expected, when D_{toe} is low (< 4 m) water more frequently impacts the dune, which enhances dune erosion. Progressively higher D_{toe} exhibit more limited dune
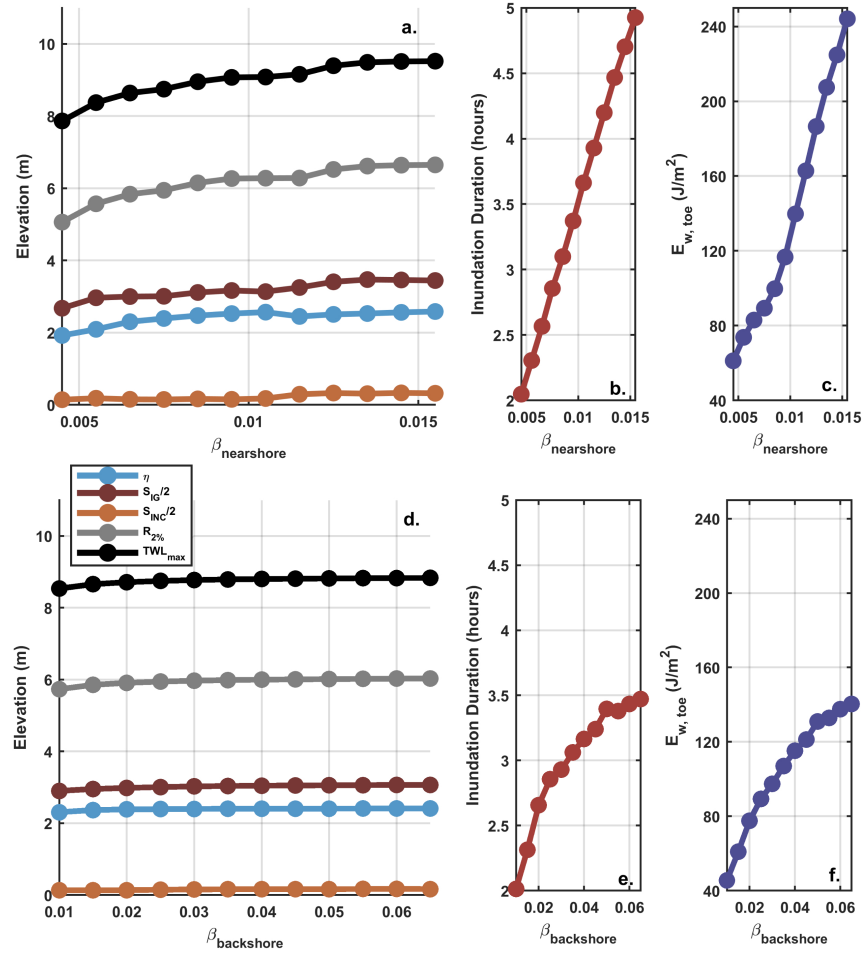
Figure 4.15: Nearshore and backshore slope controls on (a/d) wave setup, infragravity swash, incident swash, $R_{2\%}$, and TWL_{max}, (b/e) impact duration of TWLs at the dune toe, and (c/f) mean short wave energy at the dune toe position for the annual storm case.

response since the dune volume changes represent the integrated volume change landward of the dune toe (Figure 4.14e). This also confirms that while the choice of D_{toe}, which does vary regionally (e.g., Mull & Ruggiero, 2014), has an influence on $\varDelta V_{dune}$ (e.g., Splinter et al., 2018), there are other morphometrics which have a relatively larger influence on $\varDelta V_{dune}$ (Figure 4.14).

When the dune crest is at a low elevation (< 7 m), storm-induced erosion volumes are substantial, reflecting the role of large incident wave energy destroying and/or overwashing the dune. However, there is little influence of D_{crest} on $\varDelta V_{dune}$ when D_{crest} > 9 m for the modeled storm conditions (Figure 4.14f). The front slope of the dune influences the occurrence of avalanching, and therefore steeper β_{dune} also generally promotes increased erosion during high water level events (Figure 4.14d).

The break in slope between the beach and the dune, which occurs at the D_{toe} location in these simulations, has an influence on where sediment can accumulate via waves during high TWL events. If β_{dune} is much steeper than $\beta_{backshore}$ then large swash excursions slam into the dune face and the dune becomes increasingly vulnerable to erosion and avalanching effects. Conversely, in the case that $\beta_{backshore}$ is of similar magnitude to β_{dune} the available accommodation space at D_{toe} is minimized for any further deposition, which also encourages dune erosion when the TWL reaches above D_{toe} for the simulated storm case. Therefore the curve in Figure 4.14d is nonlinear, where high and low values of β_{dune} enhance dune erosion but intermediate values minimize dune erosion.

4.5   Discussion

4.5.1   Primary Controls on Dune Response

Field data from three PNW field sites demonstrate that high TWL events induce longshore variable coastal foredune impacts. At all three field sites, wave-driven dune accretion is observed during some high TWL events, with this phenomenon generally occurring on the lowest sloping segments of the beaches ($\beta_{backshore}$ < 0.03). On steeper beach segments, during the same storm events, only dune erosion is observed. Combined, the morphologic datasets also suggest that there are weak relationships between subtidal and subaerial

morphometrics and ΔV_{dune}. However, the data reveal a stronger control of oceanographic forcing from TWLs on ΔV_{dune} in the PNW. These environmental and morphologic controls are confirmed via additional exploratory numerical simulations.

Numerical simulations demonstrate the importance of the partitioning of the TWL between the DSWL and swash for assessing dune response. The model indicates that a TWL with a proportionally larger infragravity signal can accrete dunes while an equivalent TWL with a larger SWL component can be net erosional. This observation is consistent with previous findings, including that regional seasonal sea level anomalies enhance beach erosion (Theuerkauf et al., 2014). Similarly, the first order importance of storm surge levels on erosional dune impacts have been widely noted (e.g., van Rijn, 2009), reflecting the dominant role of elevated SWLs on dune response. As shown here, the DSWL dictates the amount of short wave energy which reaches at and above the dune toe, which imposes an important control on the magnitude of dune erosion. The cases where dune accretion occurs are limited to the situations where infragravity swash only occasionally impacts the dune toe – leading to small but measurable accumulations of sediment at the upper extent of the swash zone. Limited in-situ measurements exist of infragravity wave-induced swash zone sediment transport, although laboratory measurements by Baldock et al. (2010) demonstrated that long waves will generally promote net onshore transport even when the co-occurring short wave forcings are erosive – consistent with the model simulations discussed here. The dominant onshore transport mechanism to the lower dune within XBeach appears to be related to a net landward sediment flux occurring over the scale of infragravity swash events. This mechanism is likely promoted by the low $\beta_{backshore}$ which limits swash downrush velocities, which are primarily gravity-driven (e.g., Masselink & Puleo, 2006), leading to net deposition from suspended sediment falling out of suspension prior to flow reversal and from net onshore directed bedload transport.

This accretional response is limited to the lowest sloping $\beta_{backshore}$ profiles for the annual storm event. Steeper beach slopes instead promote dune erosion, primarily as a result of morphologic feedbacks on increasing wave setup and incident swash (Stockdon et al., 2006). That is, as $\beta_{backshore}$ increases, the likelihood of wave-driven dune growth decreases – with higher TWLs generally increasing the frequency of wave impact to the dune toe,

entraining dune sediment which is then transported offshore. On relatively steep beaches (Figure 4.14c), or in cases with high DSWLs, model results are consistent with traditional views of erosional response of beach-dune systems during major storm events (e.g., Sallenger, 2000; Stockdon et al., 2009) and the important control of $\beta_{backshore}$ on dune response (e.g., Kriebel & Dean, 1993; Saye et al., 2005; Mull & Ruggiero, 2014). The observed and modeled wave-induced dune growth appears limited to low sloping beaches, which tend to be infragravity energy dominated. However, the sensitivity of these processes to minor changes in slope helps to explain observations of variable backshore responses during a single storm event on low sloping PNW beaches (Figures 4.4, 4.5, and 4.6). Given that $\beta_{backshore}$ in the region generally steepen throughout the winter as the MHW shoreline recedes during extended periods of high wave energy, the established relationship between $\beta_{backshore}$ and ΔV_{dune} suggests that late winter storms (coinciding with high SWLs) are likely to be more damaging to dunes than storms in the early fall following months of beach building (Figure 4.2f,g,i,j). Consistent with other observations (e.g., Dissanayake et al., 2015; Komar et al., 2001), storm sequencing is therefore important for the net annual impacts to the dune. Similarly, dune scarping leads to an increase in β_{dune} and often a reduction in the dune toe elevation (Splinter et al., 2018), both factors which promote increased dune erosion during subsequent storms.

Model findings of storm sequencing susceptibility are also supported by the PNW field observations. For example, the 10 December 2015 event triggered scarping at SBSP line 21 and resulted in a post-storm profile with steeper $\beta_{backshore}$ and steeper β_{dune} (Figure 4.3h). These factors also led to a sharper transition between the beach and dune at the dune toe location. Moderately high wave energy (5 m < H_s < 7 m) coinciding with SWLs of about 3 m in early March 2016 caused ΔV_{dune} up to -15 m^3/m (not shown). These dune losses were comparable to losses from the 10 December 2015 event (Figure 4.3e) at some transects, despite lower wave energy and lower SWLs. The locations that were most impacted were those that were initially scarped in December 2015 (alongshore distance < 200 m; Figure 4.3e). As shown in Figures 4.3i and 4.3j, the ~1 m high scarp at line 21 initially formed during the December 2015 event developed into a larger (~3 m) vertical scarp in response to the March 2016 event.

Beyond the control of subaerial morphometrics, model results also demonstrate that there are subaqueous controls on storm-induced dune response (Figure 4.14). The shelf and nearshore slope have competing roles, with steeper β_{shelf} reducing infragravity energy and steeper $\beta_{nearshore}$ increasing wave setup and, to a lesser degree, increasing infragravity swash. The opposite impacts of shelf and nearshore slopes on infragravity swash appears related to the competing effects of infragravity wave shoaling and break point induced bound long waves (e.g., Bertin et al., 2018; Baldock, 2012) – highlighting the complexity of morphologic controls on nearshore and swash hydrodynamics.

Nearshore and shelf slopes vary on the regional scale (e.g., Figure, 4.3– 4.6) due to alongshore variability in sediment supply and geologic effects. The model results in this study suggest that, when considering these regional scale differences in bathymetry, sub-tidal controls on TWLs and dune susceptibility to erosion may in fact be larger than the backshore controls (Figure 4.14b,c). However, $\beta_{nearshore}$ generally does not vary significantly over short spatial stretches (< a few km). Similarly, given that $\beta_{nearshore}$ represents the average slope from -12 m to MHW (with the nearshore zone typically spanning 1 to 2 km in the cross-shore), the nearshore slope is not sensitive to small volumetric changes. Therefore, according the to definition of $\beta_{nearshore}$ used in this chapter, even though sediment is moved offshore during winter storms, reflected by shoreline retreat and a steepening of $\beta_{backshore}$, seasonal shallowing of $\beta_{nearshore}$ is unlikely to offset the expected increase in dune erosion from seasonal backshore beach steepening (Figure 4.14b,c). Spatio-temporal variability in the backshore slope will therefore generally control local alongshore variability in TWLs or storm-induced dune response. However, this finding is complicated by non–planar morphologies, which were not fully addressed in this study. As other studies have found that the presence of subaqueous sandbars influence both wave setup and swash (Holman & Sallenger, 1985; Cox et al., 2013; Cohn & Ruggiero, 2016; Shand et al., 2006), it is expected that specific sandbar configurations may also influence resulting dune impacts by dissipating short-wave energy and/or decreasing TWLs – similarly to the modelled behavior of the bermed beach profile (Figure 4.14g)

4.5.2 Wave-Driven Contributions to Long Term Dune Growth

Parts of the PNW are unique in that the beaches and dunes are rapidly prograding, in contrast to much of the worlds coastlines (e.g., Luijendijk et al., 2018). The progradation at Long Beach Peninsula is a reflection of sediment delivery via longshore transport gradients and shoreface sediment feeding (Ruggiero et al., 2016) derived from both modern and paleo-sediment sources (e.g., Kaminsky et al., 2010; Peterson et al., 1991). While the positive sediment budget may influence the coastal morphology (e.g., shallower shelf profiles), specific hydrodynamic and aerodynamic processes are responsible for the transport of sediment which drives coastal landscape change. Thus high sediment supply has contributed to, but on its own does has not led to, rapid foredune growth along Long Beach Peninsula.

The model results indicate that the low sloping morphology at OYST encourages dune growth via infragravity swash processes even under energetic offshore wave forcing, particularly because of the uncommon co-occurrence of large wave energy and high SWLs in the PNW (Figure 4.11c). So while foredune growth is more typically related to aeolian processes (e.g., Psuty, 2004), the relative frequency of TWLs in the collision regime but with the DSWLs below D_{toe} supports the assertion of Cohn et al. (2018) that the contribution of infragravity swash processes to dune growth is potentially significant. To quantify the swash contribution to lower dune growth at OYST, the results from the numerical experiments (Figure 4.11d,e,f), which cover the full range of oceanographic conditions within the Pacific Northwest, are utilized.

A three-dimensional lookup table (inputs = H_s, T_p, and SWL, output = ΔV_{dune}) is generated from the environmental model results (Figure 4.11d,e,f). This allows any triplet combination of H_s, T_p, and SWL to be interpolated from the model results to predict storm scale ΔV_{dune} for the simulated baseline profile, which has attributes similar to the OYST profile (Tables 4.1 and 4.2). Next, the H_s, T_p, and SWL conditions corresponding to the maximum TWL for each calendar day from the 32 year representative environmental time series (Figure 4.2) are recorded. The daily maximum oceanographic conditions are run through the lookup table to generate a daily estimated ΔV_{dune}.

Using the lookup table output, the model results indicate that there are 26.9 days on average per year where the TWL exceeds D_{toe} and where there is either an accretional or

erosional dune response. Although there are 5.3 events/year on average which result in erosion (negative ΔV_{dune}), there is only one year out of the 32 year record where net annual dune erosion is predicted via this lookup table approach. This erosional year corresponded to 1983, which included the 1982-1983 El Niño. The lookup table derived model results predict an average 14.9 m^3/m/yr of net wave-driven dune growth at OYST. This value is larger than the magnitude observed in the field at OYST ($\sim$ 1-5 m^3/m/yr; Cohn et al., 2018). This may be due to limitations of the lookup-table approach, including that the same composite slope profile is assumed as the initial condition for each daily estimated ΔV_{dune} (e.g., there is no time evolution of the morphology outside of the storm time-scale). However, the lookup table derived results are consistent with field observations in that wave-driven dune growth occurs several times per year at OYST and potentially serves as an important sediment source for lower dune growth.

4.5.3   Comments on Model Skill and Assumptions

4.5.3.1   Model to Field Comparison

While there is general agreement between field observed and model simulated dune erosion, erosion is slightly over predicted by the model (Section 4.3.2, Figure 4.7). Discrepancies between the magnitude of model and field derived dune volume changes are most likely attributed to the fact that the model was not specifically tuned to each case (Simmons et al., 2017), uncertainty in the boundary conditions (e.g., wave spectrum, exact bathymetry, variability in grain size), additional unresolved model physics (e.g., incident band swash), and excluding the effect of aeolian transport or wave-driven processes outside of the selected TWL$_{max}$ period. Additionally, the lower dune is also often characterized by the presence of dense vegetation in the PNW (Hacker et al., 2012) which may add to accretional processes by dissipating wave energy or limit erosion by altering the soil shear strength (e.g., Sigren et al., 2014). These ecomorphodynamic processes are not accounted for within this numerical exercise but may partially explain model over prediction of erosion (Karanci et al., 2014).

4.5.3.2   Importance of Model Parameter Settings

Phase-averaged models, like the hydrostatic version of XBeach employed here, parameter-ize the processes of wave asymmetry and skewness which are critical for driving onshore transport of sediment and to which the model is sensitive to (De Vet et al., 2015). For the purposes of this study, the model default value for parameterizing short wave asymmetry and skewness (*facua* = 0.1) is used – although tuning of this variable has been found to be important for accurately predicting specific observations of beach evolution, particularly for post-storm beach recovery (e.g., Vousdoukas et al., 2012; Simmons et al., 2017). How-ever, low-sloping, dissipative systems, such as was modelled, are generally infragravity dominated (Ruessink et al., 1998) and therefore infragravity effects will play a dominant role on the transport processes over short wave forcings near the land-water interface on storm time scales. Within XBeach, because the infragravity motions are resolved and in-fluence sediment transport separately from the short waves (Roelvink et al., 2009), the modeled dune accretion results shown here are mostly insensitive to the choice of *facua*. A robust sensitivity analysis exploring implications of non-default XBeach parameter set-tings was not completed for this study, although altering these settings, or other model details (e.g., composite-type profiles), would not be expected to alter the general trends highlighted in this work. However, the simulated magnitudes of ΔV_{dune} would be affected by different parameter choices.

4.6   Conclusions

The U.S. Pacific Northwest is characterized by a range of offshore and beach morpholo-gies, with corresponding variability in observed storm-induced dune responses. By explor-ing a large parameter space of morphologic and environmental conditions using new field datasets and a numerical model applied to the region, this study synthesizes the primary drivers of coastal foredune erosion that previous works have identified for particular sites and/or environmental conditions (e.g., Cooper et al., 2004; Saye et al., 2005; Thornton et al., 2007; Burroughs & Tebbens, 2008; Castelle et al., 2015; Splinter et al., 2018). Con-sistent with these previous studies, the PNW field data and numerical modeling confirm that

beaches with steeper slopes experience more dune erosion during high water level events than shallower, dissipative profiles. Additional new insights into fundamental controls on wave-induced dune response are also found from both the field data and modeling in this study. For example, the documentation of wave-driven dune accretion under a wide range of oceanographic forcing conditions implies that not all TWL events in the collision regime result in an erosional response. The model results indicate that the high TWL conditions with the highest potential for dune erosion occur in cases with anomalously high still water levels and not necessarily the largest wave energy. Therefore, conditions in which sea level anomalies, storm surge, or spring tides elevate the SWL may be the most damaging to the backshore, suggesting that dune erosion will be further compounded by an increase in the mean SWL through sea level rise.

Acknowledgements

Chapter 5: Sediment exchanges between the nearshore, beach, and dune due to combined marine and aeolian processes: Insights from a coupled numerical model

Abstract

Coastal landscape change represents aggregated sediment transport gradients from spatially and temporally variable marine and aeolian forces. Numerous tools exist that independently simulate subaqueous and subaerial coastal profile change in response to these physical forces on a range of time scales. In this capacity, coastal foredunes have been treated primarily as wind-driven features. However, there are several marine controls on coastal foredune growth, such as sediment supply and moisture effects on aeolian processes. To improve understanding of interactions across the land-sea interface, here the development of the new Windsurf numerical modeling framework is presented. Windsurf couples stand-alone subaqueous and subaerial coastal change models to simulate the co-evolution of the coastal zone in response to both marine and aeolian processes. Windsurf is applied to a progradational, dissipative coastal system in Washington, USA, demonstrating the ability of the model framework to simulate sediment exchanges between the nearshore, beach, and dune for a one year period. Windsurf simulations generally reproduce seasonal cycles of beach progradation and retreat and dune growth with reasonable skill. Consistent with field datasets, Windsurf supports the hypothesis that there are direct marine contributions to dune growth during some high total water level events that exceed the dune toe.

5.1 Introduction

Coastal landscape evolution reflects the aggregation of the combined effects of oceanographic, meteorological, geological, ecological, and anthropogenic influences (Cowell & Thom, 1995). Because of the broad range of physical processes driving temporal variabil-

ity of morphology in the coastal zone (e.g., Short & Hesp, 1982; Komar, 1998; Wright & Thom, 1977; Cowell et al., 2003), the coastal profile has often been compartmentalized into discrete morphologic units (e.g. nearshore, beach, dune; Gallop et al., 2015; Ruggiero et al., 2016) based on dominant transport processes (e.g., waves, currents, winds). Although dunes backing sandy beaches have largely been treated as a wind-controlled features, marine-driven processes play an active role in the accretional and erosional development of these landforms (e.g., Sherman and Bauer, 2003; Sallenger, 2000). In part reflecting these complex interactions, quantitative predictions of coastal dune evolution at scales beyond individual storm events are lacking (e.g., Elko et al., 2016; Walker et al., 2017) despite the important suite of ecosystem services they provide (e.g., coastal protection, habitat, recreation; Arkema et al., 2013; Martínez & Psuty, 2004; Miller et al., 2010; Sutton-Grier et al., 2015).

Much of our current understanding of coastal dune evolution remains largely conceptual (e.g., Short & Hesp, 1982; Sherman & Bauer, 1993; Psuty, 2004; Hesp, 2013; Walker et al., 2017; Zinnert et al., 2016) with attempts at quantifying dune growth and recovery from storms coming primarily from scaling up small-scale wind-driven sediment dynamics (e.g., de M. Luna et al., 2011; van Dijk et al., 1999) and exploration of ecomorphodynamics (e.g., Zarnetske et al., 2012; Durán & Moore, 2013; Keijsers et al., 2015). Although aeolian transport is the primary driver of coastal foredune growth, in many real-world systems wind climatology is not well correlated with dune growth rates (Davidson-Arnott & Law, 1996; de Vries et al., 2012; Houser, 2009; Ollerhead et al., 2012), making empirical prediction of dune evolution difficult.

The marine environment poses numerous constraints on instantaneous aeolian transport rates in sandy coastal systems, contributing to the nonlinear relationships between dune growth and climatic variables. As examples, swash-induced moisture (e.g., Davidson-Arnott et al., 2005), salt cementation (e.g., Nickling & Ecclestone, 1981), and tidally modulated groundwater tables (Jackson & Cooper, 1999) each have been found to reduce or prevent local aeolian transport. These supply limiters contribute to the widely observed fetch effect (e.g., Bauer & Davidson-Arnott, 2003; Delgado-Fernandez, 2010; Hoonhout & de Vries, 2016) whereby there is a minimum length scale required for aeolian sand trans-

port on beaches to reach saturation. Obliquely oriented wind results in larger effective fetch distances between the water line and the dune toe (e.g., Bauer et al., 2009; Bauer & Davidson-Arnott, 2003). Oblique winds therefore have the potential to transport more sediment to the dune as compared to cross-shore oriented winds of equal magnitude in supply limited circumstances (Davidson-Arnott et al., 2018). Conversely, the cross-shore component of aeolian transport is highest under shore-normal winds and reduces with increasing obliquity, leading to a potential decrease in sediment delivery to the dune under oblique wind conditions due to the cosine effect (e.g., Bauer & Davidson-Arnott, 2003).

In part due to a lack of fetch limitations (Jackson & Cooper, 1999), larger beach widths associated with low gradient, dissipative beaches promote higher rates of aeolian transport, leading to larger dune growth relative to narrower, steeper beaches (Short & Hesp, 1982; Sherman & Bauer, 1993; Durán & Moore, 2013). The relationship between grain size and beach slope (e.g., Bascom, 1951; Bagnold, 1937) also generally encourages higher transport rates on low sloping beaches.

Since fine grained sediment is preferentially transported by wind over coarse grained sediment, sediment sorting and armoring may subsequently occur on mixed-grain beaches (e.g., Carter & Rihan, 1978; Neuman et al., 2012; Hoonhout & de Vries, 2016) – leading to complex spatial patterns in instantaneous aeolian transport. In part due to armoring effects on the upper beach, it has been found that the intertidal zone is a primary sediment source area for backshore aeolian transport (de Vries et al., 2014, 2017; Hoonhout & de Vries, 2017a,b). The onshore propagation of sandbars into the intertidal zone has been recognized as a particularly important source of sediment for dune growth (e.g., Aagaard et al., 2004; Houser, 2009). In fact, it has been hypothesized (Houser, 2009) that dune growth is limited by the temporal co-occurrence of intertidal sandbar welding events with the capacity to mobilize sediment by wind. However, field data from a dissipative beach have demonstrated that dune growth can occur regardless of in-phase synchronization of maximum beach sediment supply and maximum dune growth (Cohn et al., 2018).

Energetic wave conditions and high water levels in the collision regime of Sallenger's (2000) Storm Impact Scaling Model have often been related to the erosion of coastal foredunes (e.g., Stockdon et al., 2007; Splinter et al., 2018). The exposure of coastal dunes to

erosion is related to a variety of morphologic and environmental controls (e.g., Saye et al., 2005; Burroughs & Tebbens, 2008), although low sloping, wide beaches are generally less vulnerable to dune erosion than steep, narrow beaches. It has been recently demonstrated that infragravity swash energy on dissipative beaches contributes directly to lower dune growth using both field data (Cohn et al., 2018) and numerical models (Cohn et al., in prep). These results give further evidence of the direct and indirect roles of the marine system in governing both accretive and erosive dune processes.

Despite a qualitative understanding of the dominant marine and aeolian processes controlling coastal foredune evolution, quantitative models able to simulate coastal dune recovery from storms and subsequent growth are lacking (e.g., Elko et al., 2016; Walker et al., 2017). Recognizing that major gaps in knowledge of sediment transport and morphological change across the land-sea interface still exist, here we introduce the coupled coastal profile modeling framework Windsurf. Windsurf couples three state-of-the-art open source models that independently account for subaqueous (XBeach; Roelvink et al., 2009) and subaerial (Aeolis; Hoonhout & de Vries, 2016; Coastal Dune Model; Durán & Moore, 2013) processes to explore the evolution of the coastal profile in response to both marine and aeolian forcing (Figure 5.1). The numerical models within Windsurf are capable of simulating complex coastal behaviors such as beach growth (Pender & Karunarathna, 2013), swash dynamics (Stockdon et al., 2014), wave-driven dune growth (Cohn et al., in prep), storm-induced dune erosion (de Winter et al., 2015), overwashing (McCall et al., 2010), aeolian sediment sorting (Hoonhout & de Vries, 2016), and ecological controls on dune growth (Durán & Moore, 2013). To discern the relative controls of marine and aeolian processes on coastal foredune evolution, we apply Windsurf to a prograding, dissipative field site in the U.S. Pacific Northwest (PNW) for a one year period.

The structure of the manuscript is as follows. Details of the new Windsurf modeling framework and its sub-models are described in Section 5.2. Morphologic and environmental field datasets from used to validate Windsurf are presented in Section 5.3. Model details of hindcast simulations of morphology change are described in Section 5.4. Discussion of the results and conclusions are given in Sections 5.5 and 5.6, respectively.
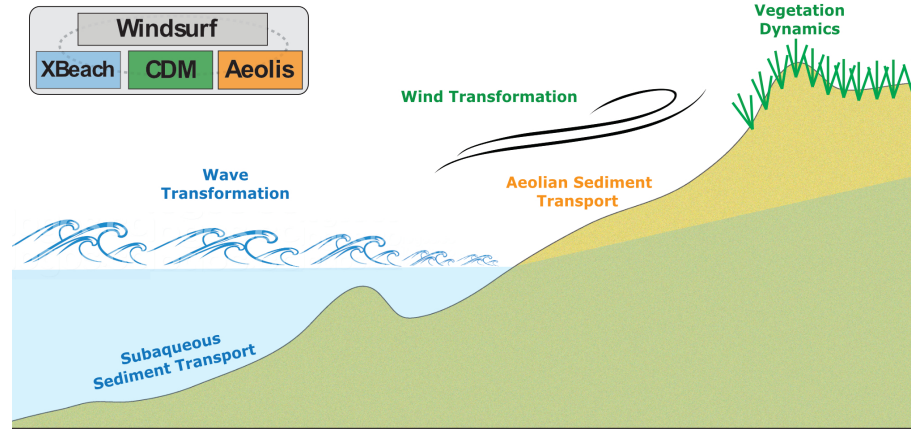
Figure 5.1: Cross-shore schematic of the Windsurf framework showing the general processes resolved by the model cores.

5.2 Windsurf Model Framework

The following section describes the details of the Windsurf model coupler, followed by details of the process capabilities of the individual numerical models within Windsurf.

5.2.1 Model Coupler

Windsurf couples three separate open-source numerical models [henceforth, model cores] which simulate subtidal morphodynamics related to waves and currents (XBeach), subaerial morphodynamics related to wind shear and vegetation (CDM), and multi-fraction aeolian sediment transport that includes the effects of supply limiters (Aeolis) (Figures 5.1 and 5.2). Together, these model cores simulate coastal profile evolution in response to both marine and aeolian forcing.

Windsurf serves as the backend coupler to these three model cores, with functionality to generate input files, execute model simulations, exchange information between model cores, and save model output. The Windsurf framework runs the individual model cores in series, with morphological, environmental, and ecological information exchanged between the models at user defined time steps (Figure 5.2). By using a loosely-coupled approach in
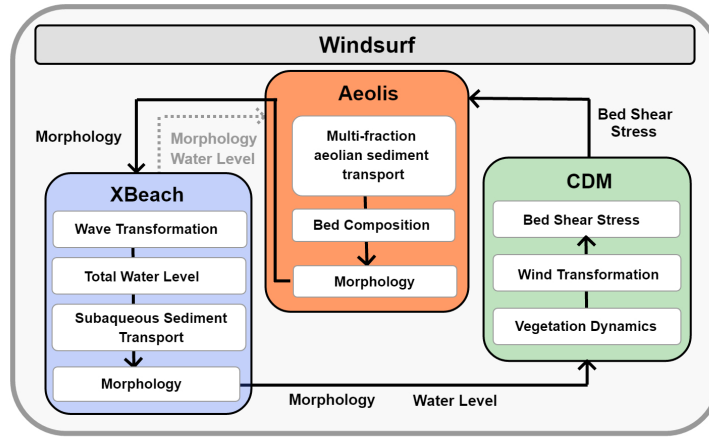
Figure 5.2: Schematic representing the general Windsurf model framework which includes three standalone numerical models (XBeach, Coastal Dune Model, Aeolis) that are coupled offline through a back-end Matlab interface. Major processes resolved within each model core and the outputs exchanged by the coupler are shown.

which the model cores are separate from the coupler, the individual models can continue to be developed independently and new model components can easily be captured by Windsurf. This approach allows for continued scientific exploration related to a wide array of research questions and across a broad range of time scales. New capabilities can be added as long as the additional model core can run on or be interpolated to a central model grid. Currently, Windsurf model grids are limited to 1D, cross-shore only applications, however, extension to 2D is planned for future work.

The work presented in this manuscript utilizes a version of the Windsurf framework coded in Matlab which runs the process-based model cores in an offline mode. That is, the model cores are initialized and fully executed before moving on to the next model core. As schematized in Figure 5.2, Windsurf first runs XBeach to simulate marine-related processes and resulting morphology change. XBeach runs are followed by CDM which simulates spatio-temporal vegetation dynamics and the cross-shore wind field. Finally, Aeolis simulates aeolian sediment transport and aeolian-driven morphology change.

5.2.2 XBeach

XBeach is an open-source process-based numerical model which simulates nearshore wave transformation, subaqueous sediment transport, and morphology change (Roelvink et al., 2009). XBeach has been used in numerous studies investigating wave transformation (van Dongeren et al., 2009; Buckley et al., 2014), swash processes (Stockdon et al., 2014; Cohn et al., 2018; Roelvink et al., 2018), and morphology change (McCall et al., 2010; de Winter et al., 2015; Harley et al., 2011a; Splinter & Palmsten, 2012; Splinter et al., 2014). Originally developed for assessing impacts from discrete storm events, the model has more recently been applied to simulate marine-driven morphologic changes on time scales of weeks to years (Pender & Karunarathna, 2013; Verheyen et al., 2014; Ramakrishnan et al., 2018). An overview of relevant processes and model parameters for XBeach are described below, while a full description of the model and its formulations can be found in Roelvink et al. (2009) and Roelvink et al. (2015).

When utilizing XBeach in hydrostatic (surfbeat) mode, the time dependent, short wave action balance equation solves for the wave group envelope (Holthuijsen et al., 1989; Roelvink et al., 2009). The short wave action balance equation is also coupled with the nonlinear shallow water equations to account for infragravity waves and mean currents. XBeach, which is a depth-averaged model, solves these spatially varying hydrodynamic processes in either 1DV (cross-shore profile model) or 2DH (area model).

Sediment transport is solved by an advection-diffusion equation (Galappatti & Vreugdenhil, 1985). In hydrostatic mode, as XBeach is presently applied in the Windsurf framework, wave groups are resolved but individual incident (short) waves are not modelled. As the wave shape is not directly simulated, the effect of wave nonlinearity on sediment transport is parameterized via the short wave related velocity asymmetry (*facAs*) and skewness (*facSk*) coefficients. Many studies provide guidance on the effects of *facAs* and *facSk* on simulating erosional and accretional processes with XBeach (e.g., Vousdoukas et al., 2012; Simmons et al., 2017; Dissanayake et al., 2015). Mean currents and long waves also contribute to sediment transport. Spatial gradients in the short wave and current related sediment transport rates simulated by XBeach are used to calculate the resulting bed level changes using a form of the Exner equation. McCall et al. (2010) found that morphology

change associated with overwash and other high-flow currents are often overpredicted. To address this issue, the *dilatancy* option accounts for the influence of pore water on bed stability, effectively increasing the local critical Shields parameter and thereby reducing transport rates during high flow conditions following the methods of van Rhee (2010). A morphologic acceleration factor (*morfac*) can also be implemented in XBeach according to the methods of Reniers (2004). *Morfac* allows morphology change to be scaled, enabling shorter duration numerical simulations without significant loss in process resolution (e.g., Reyns et al., 2014; Vousdoukas et al., 2012)

5.2.3   Coastal Dune Model

The Coastal Dune Model (CDM) is capable of simulating the evolution of vegetated coastal foredunes by solving a suite of differential equations describing ecomorphodynamic processes (Durán & Moore, 2013). The model originated as a 1D dry-environment saltation model (Sauermann et al., 2001) to simulate the formation and migration of desert dunes. Later work extended the model to a 2D area model and added the role of vegetation in stabilizing the dune form (Durán & Herrmann, 2006). The model has been utilized to explore the formation mechanisms and time scales of linear (Parteli et al., 2009), parabolic (Durán & Herrmann, 2006), and barchan (Schwämmle & Herrmann, 2005) dunes. The model has also been applied to simulate controls on coastal foredune ridge development (Moore et al., 2016), post-storm dune recovery on barrier islands (Durán & Moore, 2015), and controls on foredune hummockiness (Goldstein et al., 2017). A key driver of these different morphological forms is resolving the feedback of the topographic field on the local wind field. The efficient spectral wind model of Weng et al. (1991) that is implemented in CDM builds upon Hunt et al. (1988), an analytical solution for turbulent shear flow over a low sloping hump, to solve for the spatially variable bed shear perturbation field ($\delta\tau$) on the beach and dune.

In addition to resolving wind and aeolian transport dynamics, CDM tracks the spatial and temporal growth of dune vegetation by assuming a linear growth rate of the vegetation cover fraction (ρ_{veg}; Durán & Moore, 2013). The effective bed shear stress (τ_s) in the presence of vegetation, which is calculated by CDM, becomes:

$$\tau_s = \frac{\tau_o + \tau_o \delta\tau}{1 + \frac{m\,\beta}{\sigma}\,\rho_{veg}} \tag{EQ 5.1}$$

Where τ_o is the bed shear stress in the absence of variable topography or vegetation, m is the vegetation friction coefficient, σ is the ratio of the plant basal to frontal area, and β is the ratio of the plant drag coefficient to bare sand (Raupach et al., 1993).

CDM has the capability to simulate aeolian sediment transport utilizing the derived bed shear stress field. The model assumes a single (spatially constant) grain size and has shown success in simulating coastal dune dynamics in a variety of morphodynamic settings (e.g., Durán & Moore, 2013; Moore et al., 2016; Goldstein et al., 2017). When forced with cross-shore directed winds, CDM model results have suggested that *LVeg*, defined as the distance between the shoreline and the perennial vegetation line, can exert a primary control on the maximum height which dunes can grow (Durán & Moore, 2013). Since the shoreline position is typically non-stationary in real world settings, in Windsurf *LVeg* is modified to allow for vegetation growth that follows a fixed vertical contour position rather than a fixed beach width. That is, as beaches and dunes erode or prograde, the seaward-most location of vegetation in the model is assumed to follow the seaward most location of a fixed vertical contour rather than remain at a fixed horizontal position. Furthermore, to allow for obliquely oriented winds in Windsurf, the cross-shore oriented CDM grid is rotated at each coupling time step based on the wind direction to properly resolve the $\delta\tau$ field over the foredune. Within Windsurf, CDM is used to compute the spatially varying shear stress and vegetation fields. CDM is not used directly for these aeolian transport calculations within Windsurf in part because only a single grain size can be implemented in the model. Instead, using the CDM calculated spatially-variable bed shear stress field, multi-fraction aeolian sediment transport is simulated using Aeolis within the Windsurf framework. For additional information on CDM and its formulations see Durán & Moore (2013).

5.2.4 Aeolis

Aeolis is a multi-fraction aeolian sediment transport model specifically designed to simulate supply limiting processes (Hoonhout & de Vries, 2016). As wind processes entrain and transport sediment via saltation, the model accounts for the temporal and spatial evolution of the grain size distribution at the bed surface, and with depth, on either a 1D (cross-shore) or 2D domain. Within each model grid cell, local wind properties (bed shear stress and wind velocity) are used to calculate sediment transport rates for each grain size bin (d_n). The saturated sediment mass-flux transport rate (q_{sat}) is calculated for each d_n based on the formulation of Bagnold (1937):

$$q_{sat} = C_b \frac{\rho_a}{g} \sqrt{\frac{d_n}{D_n}} \ (u_* - u_{*th})^3 \qquad \text{(EQ 5.2)}$$

Where ρ_a is the air density, D_n is a reference grain size of 0.25 mm, u_* is the shear velocity, u_{*th} is the threshold shear velocity below which transport does not occur, and C_b is an empirical coefficient. The shear velocity threshold for transport is calculated via Bagnold (1937) and modified incorporating the effect of moisture following Belly (1964) (f_m):

$$u_{*th} = f_m A \sqrt{\frac{\rho_s - \rho_a}{\rho_a} \ g \ d_n} \qquad \text{(EQ 5.3)}$$

where ρ_s is the sediment density and A is an empirical coefficient. For the present application moisture related effects (f_m) are only utilized in the swash zone to limit aeolian transport in the presence of high TWLs; precipitation and groundwater–related moisture are not yet accounted for in Windsurf. A weighted saturated sediment concentration is calculated using the local bed grain size distribution. Sediment transport gradients, resulting from local sediment characteristics, supply limiting effects (e.g., moisture, salt content), and/or the spatially variable wind field, produce local bed elevation changes.

The Aeolis model has shown skill at simulating complex sediment sorting and beach armoring processes (Hoonhout & de Vries, 2016). Because of the added capability of simulating multi-fraction aeolian sediment transport and the inclusion of other supply limiting

effects, Aeolis is utilized as the subaerial transport model within Windsurf. Windsurf provides Aeolis with spatially varying wind and bed shear stress fields from CDM and the total water level from XBeach at each time step. Aeolis is run using the full bed shear stress derived from CDM to calculate aeolian sediment concentrations which are advected using only the cross-shore component of wind field for the 1D Windsurf simulations described in this manuscript. For additional information on the details of Aeolis, see Hoonhout & de Vries (2016).

5.3   Field Observations at a Prograding Coastal System

To test the ability of the new modeling framework to simulate realistic behavior, Windsurf is applied to a prograding coastal field site in the PNW. The following sections briefly describe the field site and the relevant datasets for model implementation.

5.3.1   Field Setting

The Long Beach Peninsula, WA (LBP; Figure 5.3) is a modally dissipative coastal system in the PNW characterized by wide, sandy beaches, and linear foredune ridges with dense *Ammophila breviligulata* (American beach grass; Ruggiero et al., 2005; Zarnetske et al., 2012; Figure 5.3b,c). In the Oysterville section of LBP, the beach is rapidly prograding (> 4 m/yr) in response to gradients in longshore sediment transport and cross-shore sediment feeding from the shoreface (Ruggiero et al., 2016). The dune complex is also prograding, with approximately 10-15 m^3/m/yr of dune growth (Cohn et al., 2018) which contributed to the generation of a new foredune since the late 1990s (Moore et al., 2016). High total water levels (TWLs) regularly impact the dune toe at Oysterville, WA. Previous observational (Cohn et al., 2018) and modeling (Cohn et al., in prep) studies have estimated that these elevated TWLs directly contribute approximately 1 to 15 m^3/m/yr to average annual dune growth.

High TWLs at Oysterville are primarily a result of large wave runup associated with an energetic wave climate in the PNW. The average deepwater winter significant wave height (H_s) offshore of the PNW is about 2.3 m, with numerous storms each year exceeding 8

Figure 5.3: (a) Map of the Oysterville field site on the Long Beach Peninsula, WA, USA.The locations of nearby wave (CDIP 036), tide (Toke Point, WA), and wind measurements (Toke Point, WA) and the SWAN wave model domain used to transform offshore waves locally to Oysterville are also shown. (b/c) Aerial photos of nearshore, beach, and dune at Oysterville, WA taken on 9 August 2016 during low energy wave conditions (H_s $\sim$ 1.5 m). Photo (c) is taken from directly above the foredune crest where a camera mast system (shown) and meteorological station (not shown) were located during SEDEX[2].

m (Ruggiero et al., 2005). These high energy conditions seasonally erode the foreshore, leading to oscillations of the mean high water (MHW, 2.1 m NAVD88) shoreline of over 30 m despite a net annual progradation of the system (Barnard et al., 2017; Ruggiero et al., 2005). Beach recovery occurs predominantly in the low energy summer period (H_s ~1.5 m on average) in response to the onshore propagation and welding of intertidal sandbars (Cohn et al., 2017, 2018).

The surf zone at the study site is typically characterized by numerous (2-4) subtidal sandbars which vary significantly on interannual time scales (Cohn & Ruggiero, 2016) as captured by a coastal monitoring program that has been ongoing since the late 1990s (Ruggiero et al., 2005). Recent work has focused on characterizing sub-annual coastal evolution at Oysterville (Cohn et al., 2017, 2018). The existence of morphology data at a wide range of time scales at a site with large morphology change signals makes Oysterville an ideal location to test the new Windsurf modeling framework

5.3.2   Morphology Data

5.3.2.1   Annual Scale

Topographic and bathymetric measurements have been made at Oysterville using real time kinematic GPS surveying techniques (Ruggiero et al., 2005). A single cross-shore transect that extends from at least -9 m water depth to landward of the foredune crest is utilized here. The measured cross-shore transect data are utilized for input to the numerical model and for comparison to model output. From these data, volumetric changes were calculated between morphological units, where the nearshore is defined here as the region from -9 to 1 m NAVD88 [all vertical references henceforth are relative to NAVD88]. The upper limit of the nearshore zone corresponds approximately to local mean sea level at the field site. The beach is defined here to be between the 1 m and 4 m contours and the dune region includes all areas above the 4 m contour, where 4 m is the approximate dune toe position. Measurements between 4 August 2016 and 9 August 2017 show nearshore ($\Delta V_{nearshore}$), beach (ΔV_{beach}), and dune (ΔV_{dune}) volume changes of -166 m^3/m (~ $\pm$ 300 m^3/m), -5.4 m^3/m (~ $\pm$ 13 m^3/m), and 16.7 m^3/m (~ $\pm$ 5 m^3/m), respectively (Figures 5.4 and 5.5). Note that
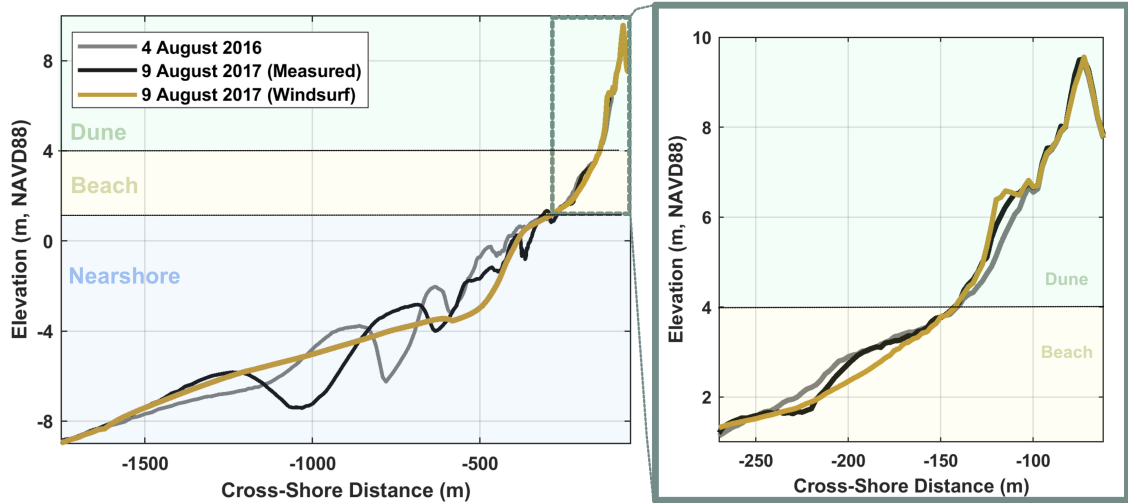
Figure 5.4: Measurements of coastal profile change of the nearshore, beach, and dune over a 1 year period between August 2016 (grey line) to August 2017 (black line). The calibrated Windsurf model prediction after one year is shown in yellow.

the listed volumetric change uncertainties are calculated using quadrature of the random vertical uncertainties associated with topographic ($\sim$ 8 cm; e.g., Ruggiero et al., 2005) and bathymetric ($\sim$ 13 cm; e.g., Gelfenbaum et al., 2015) field measurements, respectively.

The data shows that on annual scale there is significant variability in the subtidal sandbar configuration (Figure 5.4). The net sediment loss from the nearshore that was not gained by the beach reflects either longshore gradients in transport or large errors associated with volumetric estimation from bathymetric data. Between the two profile measurements, there was also a net 10 m retreat of the MHW shoreline (ΔX_{MHW}), with this apparent shoreline change occurring in part because of configurations of intertidal sandbar troughs at the time of the surveys (Figure 5.4). This indicates that despite measured dune growth at the site, there was effectively no net beach change over this particular year (within the error of the instrumentation).
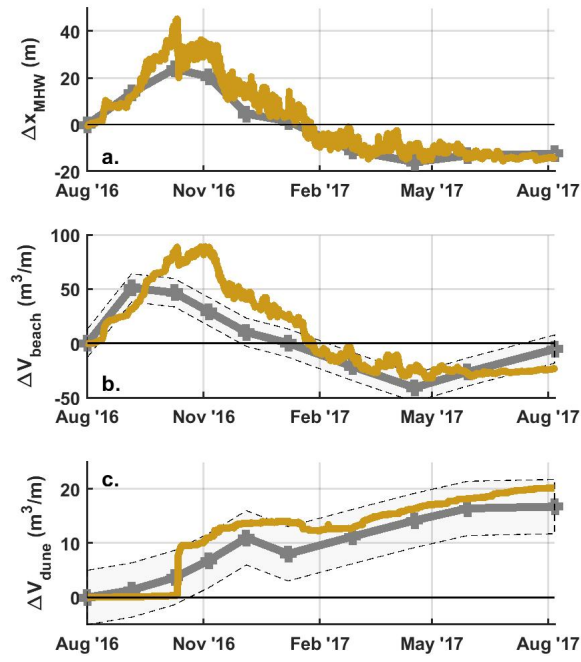
Figure 5.5: Measured (grey lines) versus calibrated model simulations (yellow lines) of (a) MHW shoreline change, (b) beach volume change, and (c) dune volume change. Error bars are added for the volumetric measurements assuming a ± 0.08 m vertical error for the topographic measurements.

5.3.2.2   Sub-Annual Scale

An additional 9 topographic surveys were completed between the August 2016 and August 2017 survey dates which are also utilized to inform the timing and magnitude of beach and dune morphology changes at sub-annual scale. Details of the morphology change on these time scales, utilizing data from the same field site, are described in Cohn et al. (2018). As MHW shoreline change is often used as a metric for coastal change (e.g., Hapke et al., 2011), temporal changes in the MHW shoreline are also extracted from the data (Figure 5.5a). These data show that between the August 2016 and August 2017 profile there is seasonality in the beach behavior. The beach was widest in summer (July – September)

and fall (October – December) and narrowest in winter (January – March) and spring (April – May), with about 40 m variability in ΔX_{MHW} over the full year. Volume changes in the beach and dune are also calculated at this monthly time scale (Figure 5.5b,c). ΔV_{beach} has the same seasonal behavior as ΔX_{MHW}. Conversely, the dune shows gradual dune growth throughout the year. The dune volume increases or remains constant between each survey (within the observational uncertainty), with the lowest rates of dune growth occurring in summer.

5.3.3   Environmental Data

5.3.3.1   Water Levels

Offshore waves and still water levels (SWL) are the primary drivers of marine-driven morphology change and therefore serve as important model boundary conditions. A Nortek Acoustic Wave and Current Profiler (AWAC) was deployed on a bottom mounted mooring at -9 m providing wave and SWL measurements for a 42 day period during summer 2016 as part of the Sandbar Aeolian Dune Exchange Experiment (SEDEX[2]) (Cohn et al., 2017). To temporally extend the record of oceanographic forcings at the study site beyond the SEDEX[2] period, additional nearby measurements from the U.S. National Oceanic and Atmospheric Administration (NOAA) Tides and Currents database, the U.S. National Data Buoy Center (NDBC), and the Coastal Data Information Program (CDIP) are utilized.

The AWAC-derived SWLs show similar tidal amplitudes (Figure 5.6a) as compared to measurements from the NOAA Toke Point, WA tide gauge located 20 km to the northeast of Oysterville in Willapa Bay (Figure 5.3a). Slight ($\leq$ 1 hr) tidal phase offsets between the sites contribute to a root mean square error (RMSE) of 0.29 m between the AWAC and Toke Point SWLs for the SEDEX[2] period. For modeling purposes, hourly tidal measurements from Toke Point, WA are used directly.
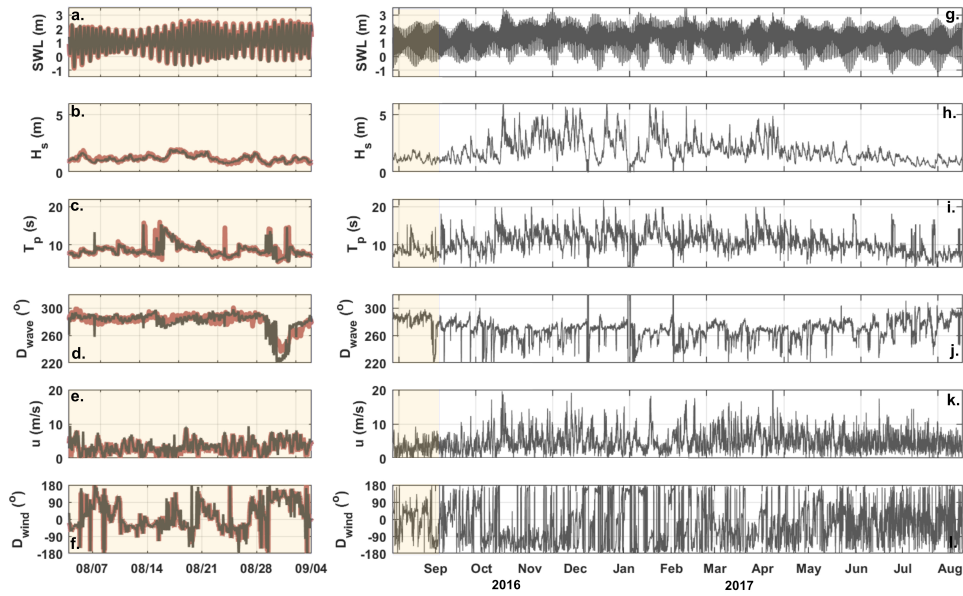
Figure 5.6: Locally measured (red) and transformed (grey) still water levels (a), significant wave heights (b), peak wave periods (c), wave direction (d), wind speed (e), and wind direction (f) for a 1 month period in summer 2016. The continuous, year long time series of environmental parameters between summer 2016 and summer 2017, which includes the one month period (shaded), for input to Windsurf is shown in panels (g-l) using the transformed variables, where applicable. Note that, as per model core conventions, 270° is shore-normal for D_{wave} (nautical convention) and 0° is shore-normal (onshore directed) for D_{wind}.

Table 5.1: RMSE and bias of transformed oceanographic and meteorological measurements, used to drive Windsurf boundary conditions, compared to local measurements. The local marine measurements used for comparison are 42 days and are 291 days for the wind measurements.

Environmental Parameter	Local Measurement	Locally Transformed Dataset	RMSE	$\Delta\mu$
SWL		Toke Point	0.29 m	0.04 m
H_s	AWAC		0.12 m	<0.01 m
T_p		CDIP 46211	1.7 s	0.03 s
D_{wave}			8 °	0.3 °
u	Dyacon	Toke Point	1.13 m/2	-0.37 m/s
D_{wind}			25.5 °	0.2 °

5.3.3.2 Waves

Offshore wave information, including significant wave height (H_s), peak wave period (T_p), and wave direction (D_{wave}), are acquired from CDIP buoy 036, located 35 km to the northwest of the study site in 40 m water depth (Figure 5.3a). The Simulating Waves Nearshore (SWAN) model (Booij et al., 1999) is utilized to transform waves from the CDIP buoy to the AWAC location. A 2D SWAN grid (dx = 100 m, dy = 100 m) that encompasses the northern half of LBP (Figure 5.3a) is set up using a regional, high resolution NOAA (Carignan et al., 2009) bathymetric digital elevation model to define the offshore water depths. Standard PNW model configurations (e.g., Allan et al., 2015) are utilized for this application. Local wind wave generation is neglected.

SWAN was used to transform waves to the AWAC location for each hour between August 2016 and August 2017 using the CDIP 036 measured H_s, T_p, D_{wave} and the tide gauge measured SWL (Figure 5.6b,c,d,h,i,j). SWAN performs well at modeling wave transformation to Oysterville, with minimal bias ($\Delta\mu$) and RMSEs of 0.12 m, 1.7 s, and 8.0° for H_s, T_p, and D_{wave}, respectively, relative to the AWAC data (Table 5.1; Figure 5.6b,c,d).

5.3.3.3   Wind

For the period between 3 August 2016 and 21 May 2017 a Dyacon MS-140 weather station was deployed on the foredune crest at the Oysterville site and provided bulk wind speed (u) and direction (D_{wind}) measurements. To extend the meteorological measurements beyond this local measurement period, available wind data from the NOAA Toke Point wind gauge were utilized. First, both datasets are transformed to their 10 m equivalent wind speeds. Then a linear transformation function was developed to relate u and D_{wind} from Toke Point, WA to Oysterville, WA using the overlapping time series. The transformation generally agrees well with local wind speed data (Figure 5.6e), with a RMSE for the locally predicted wind speed of 1.13 m/s with a small $\Delta\mu$ (-0.37 m/s). However, there are periods when wind direction is poorly resolved, likely because of the local topography within Willapa Bay. Therefore, while 77% of the locally transformed D_{wind} are within ± 5° of the measurements, there is a fairly high overall RMSE value of 25.5° for the wind direction transformation (Table 5.1). Because local wind measurements were made for 78% of the full year simulation period, the transformed data was utilized only when local measurements were not available.

5.4   Windsurf Simulations

Windsurf is applied to the Oysterville, WA field site. The following sections describe the procedure for model parameter calibration for a one year simulation period and present the results of the calibrated case.

5.4.1   Windsurf Calibration

5.4.1.1   Model Setup

To calibrate Windsurf to Oysterville, a set of model simulations were initialized with the measured topographic and bathymetric profile from 4 August 2016 and run for a one year period (until 9 August 2016) using the locally transformed SWLs, waves, and winds de-

scribed above. A one hour model coupling time step between the model cores was used, commensurate with the availability of oceanographic and meteorological forcing data and in order to adequately resolve processes on the intra-tide time scale. Within CDM the lower vertical limit of perennial vegetation is set to be 5.5 m based on local field observations (Figure 5.3b,c). CDM is initialized with spatially uniform vegetation above this elevation.

A locally measured grab sample was used to inform the grain size (D50 = 0.25 mm, D90 = 0.335 mm) input to Windsurf. In the absence of detailed spatio-temporal grain size data at the field site, the grain size distribution is assumed to be spatially constant in both XBeach and Aeolis.

The 1D cross-shore model grid has variable grid spacing between 20 m (offshore) and 2.5 m and encompasses the region from –9 m to landward of the foredune crest. It is important to note that during energetic wave conditions wave breaking occurs deeper than the –9 m depth, inducing sediment transport near the offshore boundary and also imposing implications on the incoming infragravity wave field. It was not practical to extend the model grid to significantly deeper water depths for this application. Therefore, consistent with the bathymetry observations (Figure 5.4) it was assumed that at the cells near the offshore model boundary (-9 m) that there is no net bed level change on the time scales of interest. Any XBeach simulated sediment losses in this region are assumed to be replenished by either cross-shore feeding from the shoreface and/or longshore transport gradients. No modifications are made to modify the incoming bound long wave field, but it is assumed that infragravity generation within the inner surf zone from active wave breaking is of first order importance over far-field infragravity generation mechanisms for this model application.

5.4.1.2   Calibration Procedure

Process-based numerical models, including each Windsurf model core, have a number of tuneable, site-specific parameters representing unknown model physics or site specific transport properties (e.g., Berard et al., 2017; Vousdoukas et al., 2012). Following preliminary model cores sensitivity testing, four specific model parameters were identified for fur-

ther exploration: the short wave related asymmetry (*facAs*, XBeach) and skewness (*facSk*, XBeach), the aeolian sediment transport coefficient (*Cb*, Aeolis), and the vegetation friction coefficient ((*m*, CDM). A choice of one year for model calibration is specifically chosen to ensure that the model is not biased towards simulating only accretional or erosional processes, as Oysterville has significant seasonal morphological variability (Figure 5.5).

As has been previously noted, XBeach is particularly sensitive to choices of *facAs* and *facSk* (e.g., Vousdoukas et al., 2012; Simmons et al., 2017; Dissanayake et al., 2015) – often requiring separate parameter combinations for accretional and erosional conditions (e.g., Pender & Karunarathna, 2013). Preliminary model core testing (not shown) did not yield realistic behaviors when utilizing constant *facAs* and *facSk* for the full year period. Therefore, following the general methods of Pender & Karunarathna (2013), different model parameter combinations for these two variables are calibrated for low energy (assumed to be when $H_s \leq 2$ m for our purposes) and high energy ($H_s > 2$ m) conditions. This wave height threshold is based on field observations for when intertidal sandbars are generally eroded at Oysterville (Cohn et al., 2018). When H_s is below this threshold, intertidal sandbars are typically observed to move onshore (Cohn et al., 2017).

To calibrate Windsurf to the field site, a set of one hundred year-long Windsurf simulations were first completed using random combinations of *m*, *Cb*, *facAs* (low energy), *facAs* (high energy), *facSk* (low energy), and *facSk* (high energy) (see Table 5.2 for range of values). Each of the 100 simulations is identical other than these random parameter settings. As XBeach, CDM, and Aeolis all have other configurable parameter settings, typical model parameter settings are utilized for all three model cores. Note that for XBeach a *morfac* of 2 was utilized and the *dilatancy* option was turned on.

Differences between the measured and modelled $\Delta V_{subaerial}$ ($\Delta V_{beach} + \Delta V_{dune}$) were calculated at 10 time intervals (9 monthly surveys and the final August 2017 survey) from all 100 Windsurf simulations. The locally calibrated (best-fit) simulation was defined as the model simulation with the lowest RMSE $\Delta V_{subaerial}$ as calculated from all 10 $\Delta V_{subaerial}$ error estimates. This calibration approach was designed with the overall aim of discerning the relative controls of marine and aeolian processes on coastal foredune evolution. While calibrating the model to the monthly volumetric change data ensures that the model adequately

resolves processes relevant for Oysterville, this exercise does not imply that Windsurf is validated to explore all coastal behaviors or for other sites (e.g., Oreskes & Belitz, 2001; Thieler et al., 2000).

Table 5.2: Listing of range of values tested and optimum parameter settings based on the calibration routine.

Model Parameter	Mode Core	Min Value Tested	Max Value Test	Calibrated Value
m	CDM	0.005	0.200	0.015
Cb	Aeolis	0.50	1.50	0.71
facSk (low energy)	XBeach	0	0.80	0.17
facSk (high energy)		0	0.20	0.14
facAs (low energy)		0	0.80	0.46
facAs (high energy)		0	0.2	0.03

5.4.2   Calibrated Model Results

The best fit calibrated simulation for Oysterville, WA between August 2016 and August 2017 is shown in Figure 5.4. Qualitatively, the simulated profile matches the field measurements, with growth of the dune and modest net changes to the beach modelled after one year. However, the model does not accurately reproduce the changes to the subtidal sandbars (Figure 5.4). Both subtidal and intertidal sandbars are smoothed during the simulations by XBeach (and potentially the other model cores).

In response to low wave energy conditions in summer, Windsurf simulates beach progradation by up to 45 m at the MHW shoreline (Figure 5.5). The widest beach state is modeled to occur in early October. Thereafter, the simulation shows gradual retreat of the MHW shoreline until April. The shoreline remains relatively stable (± 5 m) from April until the end of the simulation in August 2017. The beach volume changes track the same general temporal behavior as ΔX_{MHW}. A total of 20.8 m³/m/yr of dune growth is simulated compared to the field measured ΔV_{dune} of 16.7 ± 5 m³/m over the year. The majority of

simulated growth occurs above the vegetation line (5.5 m) but below 7 m (Figure 5.4). Inconsistent with the field measurements, Windsurf simulates erosion near the dune crest.

Outputs from each model time step are used to investigate the relative contributions of marine and aeolian processes to coastal profile change and to explore the timing of depositional and erosional processes. The outputs are binned into 0.5 m vertical increments as shown in Figure 5.7. In vertical cross-section, the numerical model results show reasonable agreement with the measured data over the annual scale (Figure 5.7a). Volumetric changes in the inner nearshore, between the 0 m and 1 m contours, are erosional in both the model and the observations. The location of accumulation above the 5 m contour also qualitatively matches between the model results and field observations. The model performance deviates the most from field measurements around the 3 m contour, where the model simulates more erosion than revealed in the observations.

Windsurf simulates that beach growth is largest in spring and summer, in agreement with the observations (Figure 5.7b). Similarly, the largest beach losses occur in fall and winter. Although there is relatively little (ΔV_{beach} <25 m^3/m) net change to the beach compartment over the year, the seasonal fluctuations in beach volume growth are significantly larger than volumetric variability within the dune region. The largest volume gains to the dune occur in the fall (10.7 m^3/m), followed by winter (4.6 m^3/m), spring (4.3 m^3/m), and summer (1.1 m^3/m).

As Windsurf saves the dz values related to marine transport by XBeach and aeolian transport by Aeolis at each coupling time step, volumetric changes across the profile can be attributed to either marine or aeolian processes, as shown in Figure 5.7c. The Windsurf simulations suggest that there are marine contributions to dune growth above the dune toe (6.6 m^3/m/yr), although dune growth in Oysterville is primarily driven by aeolian processes (14.2 m^3/m/yr).

These results suggest that marine-driven dune accumulation occurs primarily during high SWL events and/or during periods of large wave energy (elevated H$_s$ and/or T$_p$; Figure 5.8a,b,c,f,g,h). Although most environmental conditions show positive ΔV_{dune}, negative ΔV_{dune} for H$_s$ of 5.5 m (Figure 5.8b) and T$_p$ of 17.5 s (Figure 5.8c) indicate that marine processes can drive dune erosion at this site under some forcing conditions. There are fewer
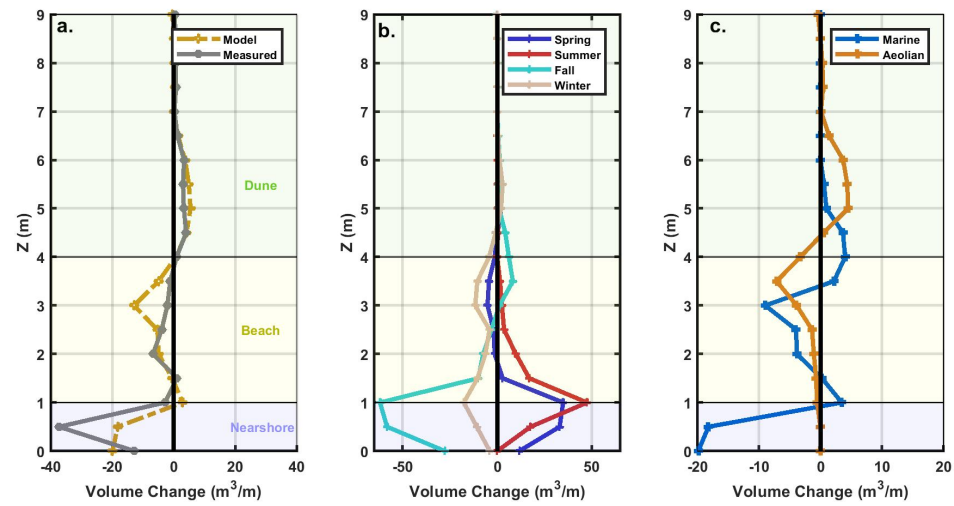
Figure 5.7: (a) Comparison of volume changes (binned vertically in 0.5 m increments) between the field measurements (dashed grey line) and model predictions (dashed yellow line) at annual scale for the calibrated simulation. (b) Windsurf output with vertically binned volume changes broken down by the seasonal cycles of deposition. (c) Windsurf simulated volume changes are distinguished between marine (solid blue line) and aeolian (solid orange line) contributions. Note that the x-axis limits change on each panel.
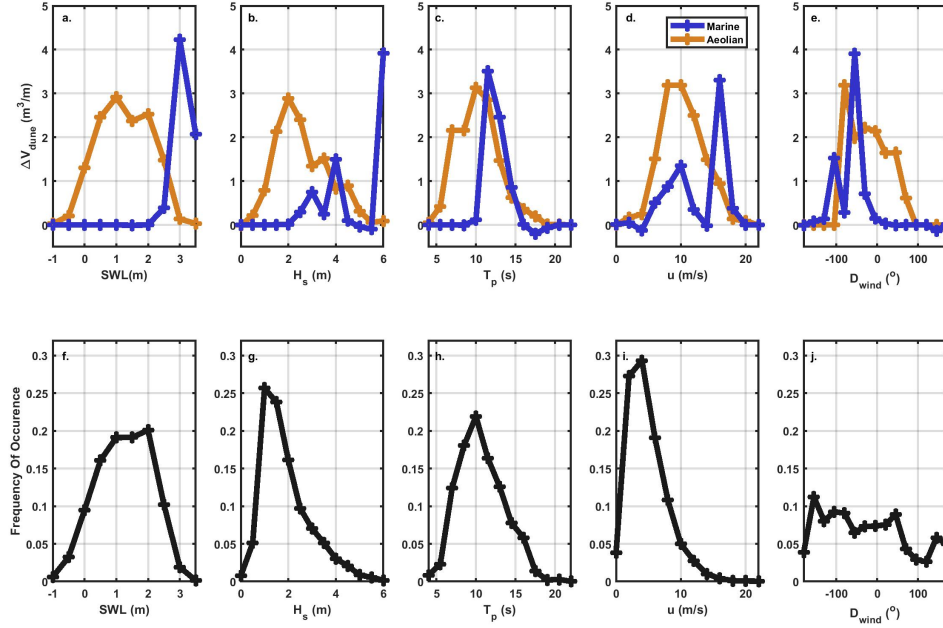
Figure 5.8: Marine (blue line) and aeolian (orange line) contributions to dune volume change binned based on (a) SWL, (b) H_s, (c) T_p, (d) u, and (e) D_{wind} for the one year calibrated Windsurf simulation. The frequency of occurrence of each (f) SWL, (g) H_s, (h) T_p, (i) u, and (j) D_{wind} forcing condition are also shown for the one year record for comparison.

environmental limiters on aeolian-driven dune growth (Figure 5.8), although the largest contribution to dune growth occurs from oblique winds from the south (Figure 5.8e).

5.5 Discussion

5.5.1 Simulation of Coastal Profile Behavior

This is the first field application of the Windsurf modeling framework, demonstrating the ability for a coupled process-based numerical model to simulate exchanges between the nearshore, beach, and dune portions of the coastal profile. Windsurf predicts realistic

morphologic evolution across the land-water divide with relatively limited model tuning. Despite the model framework not resolving all the exact details of morphological evolution at the field site (e.g., sandbar dynamics), the ability to simulate beach accretion and erosion, wave-driven dune accretion, and wind-driven dune growth within a single model framework indicates that the model cores are resolving many of the dominant transport processes relevant for Oysterville. Therefore, the model results are used to gain insights into the mechanisms contributing to beach and dune growth on sub-annual scale.

5.5.2   Insights Into Physical Processes Controlling Dune Evolution

5.5.2.1   Aeolian Controls on Dune Growth

Although high wind velocities have the highest aeolian transport potential (e.g., Bagnold, 1937), many of the highest wind events co-occur with energetic waves and high SWLs (Figure 5.6). The combination of high H_s and high SWL results in total water levels (TWL) in the collision regime numerous times per year at Oysterville. During periods when the TWL is near the dune toe, there is effectively no source area for aeolian transport – limiting aeolian contributions to dune growth under these forcing conditions. Dune growth instead occurs predominantly from aggregated transport under moderate wind conditions (6 – 12 m/s) (Figure 5.8d,i). Intermittent dune growth occurs throughout the year under these frequent moderate wind conditions (Figure 5.5c) which are above the threshold velocity for saltation (3 – 4 m/s based on the local grain size). The largest total aeolian-driven dune growth is simulated in the winter (Figure 5.5c and 5.7b). This is consistent with observations of the timing of maximum dune growth at Oysterville, WA as noted by Cohn et al. (2018). The model results also agree with field observations that documented limited dune growth occurring during the summer period (Figure 5.5c and 5.7b) when the beach is wide (high sediment supply) (Figure 5.5ab) but wind velocities are typically low (Figure 5.5k).

The largest modelled source area for aeolian sediment transport is between the 3 and 4 m contours (Figure 5.7c), although some sediment is sourced from lower elevations during lower tidal stages (Figures 5.8c). While this primary source region is located on the upper portion of the beach compartment (defined between 1 m to 4 m), this maximum source

region coincides with the approximate mean model-predicted TWL elevation during the fall and winter seasons (not shown). Thus, this modelled region of active aeolian transport generally supports previous findings that the upper intertidal zone is likely an important source of sediment for dune growth (e.g., de Vries et al., 2014).

Wind direction plays a role in controlling the apparent fetch length, which is thought to be an important factor for aeolian transport to dunes (e.g., Davidson-Arnott et al., 2018). Windsurf simulations suggest that oblique winds from the south provide the largest contribution to total dune growth (Figure 5.8e), in part because these are among the most common wind directions at the field site (Figure 5.8j). In Figure 5.9a, it is shown that the largest dune growth rates in the simulation occur when the wind speeds are largest, mostly independent of the wind direction. That is, similar ΔV_{dune} are simulated in the case of shore-normal or oblique winds for a given wind speed. There is some scatter in the hourly ΔV_{dune} predictions (Figure 5.9a), reflecting in part the cosine effect (e.g., Bauer & Davidson-Arnott, 2003) and/or unsaturated transport resulting from sediment supply limitations. However, when considering higher portions of the dune, shore-normal winds provide a larger contribution to dune growth for a given wind speed (Figure 5.9b). In the case of shore-normal winds, saltation can extend further horizontally past the vegetation line as a result of a larger cross-shore component of the wind velocity and increased wind velocities associated with flow acceleration over the steeper apparent dune slope.

5.5.2.2   Marine Controls on Dune Growth

Although the lack of observed dune erosion on some dissipative beaches has been hypothesized to be from synchronization of nearshore-beach-dune exchanges (Houser, 2009), which were thought to mask signs of erosion, modelled dune erosion at Oysterville, WA is infrequent because TWLs in the collision regime are not always erosional (Cohn et al., in prep). Windsurf predicts that numerous wave-driven events contribute to dune accretion at Oysterville during the 2016-2017 time frame (Figure 5.5, 5.7, and 5.8), with these events typically occurring during high SWL cases and/or during energetic wave periods (Figure 5.8,a,b). The simulations show that there were 3 hours, all in October 2016, which resulted in at least 1 m^3/m of marine-driven dune growth. An additional 13 hours occur-
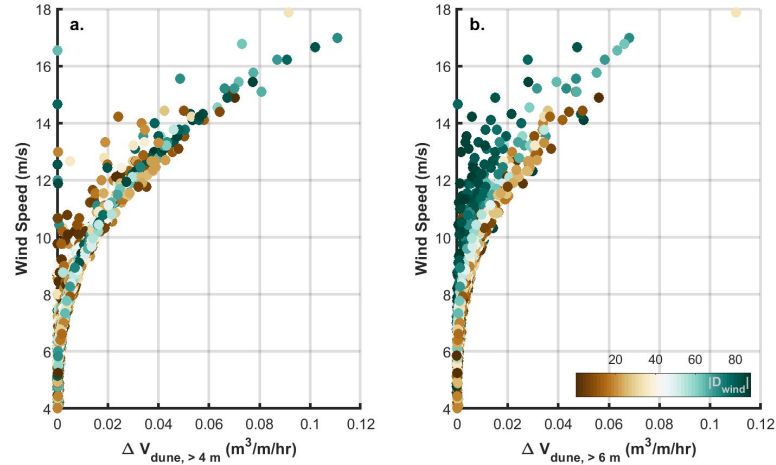
Figure 5.9: Hourly Windsurf simulated ΔV_{dune} above the 4 m contour (a) and 6 m contour (b) resulting from aeolian processes (marine related ΔV_{dune} are excluded) plotted against wind speed. Colors represent the absolute value of wind direction relative to shore normal.

ring in either fall or winter where marine derived dune growth of at least 0.1 m^3/m was simulated.

In Cohn et al. (2018), it was estimated that between ~1 and 5 m^3/m/yr of average annual dune growth at Oysterville, WA was driven by swash processes, in general agreement with the Windsurf estimates of 6.6 m^3/m/yr. The timing and vertical extent of this marine deposition also generally agrees with field observations of marine related dune accretion. Also consistent with the field measurements, the Windsurf results indicate that aeolian processes are a larger net contributor to dune growth (Figure 5.7c) – supplying 68% to total annual dune growth in these simulations.

While the model suggests that the majority of time when TWLs are in the collision regime a positive ΔV_{dune} is simulated, there are some oceanographic conditions which instead produce wave-driven dune erosion (Figure 5.5c and 5.8b,c). Therefore, Houser's (2009) assertion that marine related erosion can be masked by aeolian processes on dissipative coasts is supported by the model under some conditions. This finding complicates attempts to de-couple marine and aeolian contributions to dune sediment supply from field observations alone (e.g., Cohn et al., 2018).

5.5.3   Planned Windsurf Improvements and Future Applications

5.5.3.1   Model Processes and Parameterizations

Of the three model cores in Windsurf, XBeach has the largest number of configurable parameters and is also generally the most sensitive to those model parameter choices. Given that a separate high and low energy *facAs* and *facSk* were required for realistic model behavior, this implies that new formulations for these parameters that are more physically based may be necessary to make reliable forecasts of coastal progradation using XBeach in surfbeat mode. Recent improvements to XBeach add a non-hydrostatic correction term (McCall et al., 2015), which enables short waves to be modeled directly, and may provide a solution. In non-hydrostatic mode, the nonlinearity of the wave shape is calculated directly, avoiding the need for *facSk* and *facAs* as these parameters are inherently included within the flow field. Therefore, utilizing the wave resolving mode of XBeach could enable less site-specific model tuning. However, the non-hydrostatic model requires finer grid resolution which, for most applications, would substantially increase model run times. Further, new sediment transport algorithms relevant for the non-hydrostatic model first need to be developed in the open-source code.

Although not explored in detail in this study, the algorithms parameterizing spatio-temporal vegetation density are currently simplified (a single, spatially uniform maximum ρ_{veg} is currently implemented). However, the vegetation plays a major role in the sand trapping capacity of sediment and resulting geomorphic shapes (e.g., Hacker et al., 2012; Zarnetske et al., 2012). Simple formulations are suitable for understanding first order behavior, but the addition of more robust ecological algorithms will provide added capability for simulating these dune growth behaviors for more applied cases (e.g., Goldstein et al., 2017).

There are additional moisture-related limiters to aeolian sediment transport in the coastal zone that were not assessed for this study. Much of the functionality to incorporate both groundwater and precipitation related effects are already coded into XBeach and Aeolis. Including these additional supply limiting factors may be important for some locations,

particularly those characterized by high rainfall such as at Oysterville, WA. Linking the model cores to simulate these additional processes in Windsurf are forthcoming.

On coastal systems characterized by storm-induced scarping and sharp topographic changes, the presently incorporated Weng et al. (1991) solution for wind flow will have limitations in its applicability. For more complex settings a steady state wind solver may not be suitable. In these cases, a Navier-Stokes based numerical solver could be implemented, as computational fluid dynamics methods have been shown to be successful at modeling complex flow patterns over a range of dune shapes (e.g., Smyth et al., 2012; Smyth & Hesp, 2015). The framework of Windsurf is modular by nature which allows for new models to be implemented and tested with relative ease.

5.5.3.2 External Sediment Supply

While the assumption of local mass conservation for the time scales investigated for this study are appropriate, when extending simulations to longer time frames incorporating external sediment supply inputs is imperative (e.g., Anthony, 1995; Cowell et al., 2003). The definition of the offshore boundary in Windsurf currently allows for new sediment to be added to the local sediment budget via the replenishment of eroded near-boundary sediments. However, a more robust procedure for introducing both cross-shore shoreface feeding and longshore transport gradients would add value. A recent implementation of longshore gradients in transport into XBeach (*lsgrad*) provides one mechanism to do this for 1D applications based on an imposed length-scale for longshore transport gradients. Although not tested for this application, utilizing this feature in Windsurf requires no changes to the model framework. Including these 1D imposed longshore transport gradients, or extending Windsurf to 2D area applications, would better represent coastal systems, including Oysterville, WA, where longshore transport gradients are important.

5.5.3.3 Computational Efficiency

The present Windsurf application is run in an offline approach through Matlab. A python version of Windsurf is also in development which implements the basic model interface

(Peckham et al., 2013) and enables models to be run in an on-line approach, with boundary conditions updated on the fly. The latter approach significantly decreases model run times by eliminating computational overhead associated with frequent writing of model input and outputs to the disk. For the present application, completing one year simulations takes approximately 2.5 days utilizing 4 processors on a Dell C6100 Intel Xeon server running the CentOS 7 operating system. Reducing run-times, even fractionally, may make simulating longer term (> years, decades) simulations more practical.

5.5.3.4   Further Testing of Framework Limitations

These first proof of concept Windsurf simulations at Oysterville, WA suggest that a coupled approach for assessing the co-evolution of the nearshore-beach-dune system provides value over independent models for discrete morphological units. As this is the first field application of the modeling framework, the limits of Windsurf at simulating realistic behavior in other morphodynamic settings and for other environmental cases has not yet been demonstrated. Ideally, Windsurf is flexible enough to explore dune erosion, recovery, and growth across the continuum of reflective to dissipative beaches. However, to understand model limitations and extend model capabilities, the tool needs to first be applied in other data rich settings.

5.6   Conclusions

A new coupled numerical modeling framework is capable of simulating the co-evolution of the nearshore, beach, and dunes. Consistent with field measurements, the model simulates seasonal cycles of beach growth in summer, shoreline recession in winter, and net dune growth annually. Aeolian contributions to dune growth occur intermittently throughout the year, but are lowest in summer and highest in winter. Although cross-shore oriented winds are relatively infrequent at Oysterville, WA, Windsurf simulations suggest that cross-shore winds provide a proportionally larger contribution to upper dune growth than obliquely oriented winds. Consistent with field data, Windsurf demonstrates that both marine and aeolian processes directly contribute to the growth of coastal foredunes on a high energy,

dissipative coastline. While significant efforts are required to further test the model framework limitations for other morphodynamic settings and other environmental cases, Windsurf provides a new platform to explore complex interactions between the subaqueous and subaerial zones of the coastal profile for a variety of exploratory and applied applications.

Acknowledgements

Chapter 6: General Conclusion

This dissertation has explored the influence of coastal morphodynamic processes on flooding and erosion hazards along modally dissipative beaches in the Pacific Northwest (PNW).

In Chapter 2, field datasets that span time scales of days to decades were used to relate seasonal scale morphology changes to longer term coastal evolution (years to decades). Frequent observations from a one-year period at Oysterville, WA showed that the beach is characterized by a seasonal cycle of erosion and accretion, with the onshore migration and welding of intertidal sandbars being an important beach growth mechanism during the summer. The foredune at this field site was shown to accrete throughout the concentrated 2016-2017 measurement period, with the largest wind driven growth occurring in winter. Marine processes were also shown to contribute sediment directly to the lower dune in fall 2016. The newly developed morpho-stratigraphic method, applied to a twenty year record of seasonal topographic change, supported key findings regarding the timing, magnitude, and relative marine and aeolian contributions to coastal dune growth found from the shorter-term (daily to ~monthly) field measurements. The morpho-stratigraphic method indicates that marine processes contribute between 9% and 38% (~1 to 5 m^3/m/yr) to annual volumetric dune growth at the field site. These first observations of marine contributions of dune growth are in contrast the geomorphic responses expected in response to the collision regime of Sallenger's (2000) Storm Impact Scale model, requiring a paradigm shift away from considering collisional wave impacts as unconditionally erosional.

Chapter 3 was focused on the same Oysterville, WA field site, where the influence of variable subtidal and intertidal morphology on wave runup processes was explored. As shown in Chapter 3, the Oysterville, WA site is characterized by temporal variability of the subtidal profile via the formation and migration of subtidal sandbars. The numerical model results using XBeach indicate that interannual variability in sandbar configuration, associated with net offshore sandbar migration, has a larger influence on wave runup than does seasonal sandbar variability. However, the model simulations suggest that temporal

variability in beach morphology has a comparatively larger morphologic influence on wave runup than temporal variability in subtidal sandbars.

Over a regional scale throughout the Pacific Northwest (PNW) there is significant spatial variability in both subtidal and subaerial morphology. Chapter 4 aimed to isolate the role of variable shelf, nearshore, beach, and dune morphologies on influencing storm-induced dune response. Field datasets and numerical modeling both support the observation that marine processes can contribute positively to dune growth. The model results indicate that ~15 m^3/m/yr of average annual dune growth is potentially attributed to marine processes at Oysterville, WA. However, consistent with the typical expectation of dune response to the collision regime (e.g., Sallenger, 2000), dune erosion is observed by field measurements and predicted by XBeach for steeper sloped beaches. The field and model results suggest that marine driven dune growth is limited to end-member dissipative profiles and occurs only when the dynamic still water level (still water level combined with wave setup) does not exceed the dune toe.

As addressed in the previous chapters, marine and aeolian processes actively modify the coastal profile over a range of time scales. The application of Windsurf to the Oysterville, WA field site in Chapter 5 demonstrated that process-based numerical models can reproduce the growth and erosion of beach and dune systems with relatively little model tuning. The relative contributions of marine (~7 m^3/m/yr) and aeolian (~14 m^3/m/yr) processes to coastal foredune growth were similar to those found in Chapter 2. Although there is net accretion of the dune throughout the year modeled by Windsurf, the simulations indicate that there are also periods where marine processes are erosional to the dune. Additionally, the model results showed that while cross-shore oriented winds are relatively infrequent at Oysterville, WA, cross-shore winds provide a proportionally larger contribution to upper dune growth than obliquely oriented winds. The ability to simulate these complex coastal landscape change processes in Windsurf provides an exciting new research tool to further explore nearshore-beach-dune interactions. For example, the coupling of these numerical models potentially provides new insights on sediment exchanges across the land-sea interface which relatively sparse field data do not directly reveal.

Field data analyses and the application of numerical models presented within the chapters of this dissertation demonstrate that the beach and dune are both actively modified by marine and aeolian processes in low gradient, dissipative PNW systems. Furthermore, morphodynamic feedbacks from shelf, nearshore, and dune morphology were shown to have important controls on the erosion or accretion of coastal foredunes, providing new insights on the connectivity between the subaqueous and subaerial portions of the coastal profile. In addition to identifying coastal morphodynamic processes, Chapters 3, 4, and 5 showed that there is reasonable skill at simulating these hydrodynamic and morphology change processes using existing numerical models. Validation and testing of these models provides an incremental step forward towards being able to reliably simulate and predict coastal landscape changes across the full range of time scales relevant for coastal adaptation and planning efforts (days to centuries).

While this dissertation explored coastal morphodynamic processes contributing to flooding and erosion hazards, many of the most at-risk coastal systems are located in environments that are morphodynamically dissimilar to dissipative PNW beaches. Future work will be aimed at exploring coastal morphodynamic processes across the land-sea interface over a broader range (e.g., reflective to dissipative, eroding to prograding) of coastal environments using both field-based and numerical modeling methods.

Bibliography

Aagaard, T., Davidson-Arnott, R., Greenwood, B., & Nielsen, J. (2004). Sediment supply from shoreface to dunes: linking sediment transport measurements and long-term morphological evolution. *Geomorphology*, *60*(1-2), 205–224.

Alexander, P. S., & Holman, R. A. (2004). Quantification of nearshore morphology based on video imaging. *Marine Geology*, *208*(1), 101–111.

Allan, J., & Komar, P. (2002). Extreme storms on the Pacific Northwest coast during the 1997-98 El Niño and 1998-99 La Niña. *Journal of Coastal Research*, *18*(1), 174–193.

Allan, J., Ruggiero, P., Cohn, N., García-Medina, G., Brien, F. O., Serafin, K., Stimley, L., & Roberts, J. (2015). Coastal flood hazard study, Lincoln County, Oregon. Tech. Rep. O-15-06, Oregon Department of Geology and Mineral Industries, Newport, OR, USA.

Allan, J., Stimley, L., & McConnell, V. (2013). Oregon Beach Shoreline Mapping and Analysis Program: Quantifying Short-to Long-term Beach and Shoreline Changes in the Gold Beach, Nesika Beach, and Netarts Littoral Cells, Curry and Tillamook Counties, Oregon. Tech. Rep. O-13-07, Oregon Department of Geology and Mineral Industries, Newport, OR, USA.

Allan, J. C., Hart, R., & Tranquili, J. V. (2006). The use of passive integrated transponder (PIT) tags to trace cobble transport in a mixed sand-and-gravel beach on the high-energy Oregon coast, USA. *Marine Geology*, *232*(1-2), 63–86.

Allan, J. C., & Komar, P. D. (2006). Climate controls on US West Coast erosion processes. *Journal of Coastal Research*, *223*, 511–529.

Anderson, D., & Ruggiero, P. (2015). Modeling interannual to multi-decadal shoreline rotations of headland–bounded littoral cells. In P. Wang, J. Rosati, & J. Cheng (Eds.) *The Proceedings of the Coastal Sediments 2015*. San Diego, CA.

Anthony, E. J. (1995). Beach-ridge development and sediment supply: examples from West Africa. *Marine Geology*, *129*(1-2), 175–186.

Anthony, E. J., Vanhee, S., & Ruz, M.-H. (2006). Short-term beach–dune sand budgets on the north sea coast of France: Sand supply from shoreface to dunes, and the role of wind and fetch. *Geomorphology*, *81*(3-4), 316–329.

Arkema, K. K., Guannel, G., Verutes, G., Wood, S. A., Guerry, A., Ruckelshaus, M., Kareiva, P., Lacayo, M., & Silver, J. M. (2013). Coastal habitats shield people and property from sea-level rise and storms. *Nature Climate Change*, *3*(10), 913–918.

Austin, M. J., Scott, T. M., Russell, P. E., & Masselink, G. (2013). Rip current prediction: Development, validation, and evaluation of an operational tool. *Journal of Coastal Research*, *287*, 283–300.

Bagnold, R. A. (1937). The transport of sand by wind. *The Geographical Journal*, *89*(5), 409.

Bailard, J. A. (1981). An energetics total load sediment transport model for a plane sloping beach. *Journal of Geophysical Research*, *86*(C11), 10938.

Baldock, T. (2012). Dissipation of incident forced long waves in the surf zone—implications for the concept of "bound" wave release at short wave breaking. *Coastal Engineering*, *60*, 276–285.

Baldock, T., Manoonvoravong, P., & Pham, K. S. (2010). Sediment transport and beach morphodynamics induced by free long waves, bound long waves and wave groups. *Coastal Engineering*, *57*(10), 898–916.

Barnard, P. L., Allan, J., Hansen, J. E., Kaminsky, G. M., Ruggiero, P., & Doria, A. (2011). The impact of the 2009-10 El Niño Modoki on U.S. West Coast beaches. *Geophysical Research Letters*, *38*(13).

Barnard, P. L., Hoover, D., Hubbard, D. M., Snyder, A., Ludka, B. C., Allan, J., Kaminsky, G. M., Ruggiero, P., Gallien, T. W., Gabel, L., McCandless, D., Weiner, H. M., Cohn, N., Anderson, D. L., & Serafin, K. A. (2017). Extreme oceanographic forcing and coastal response due to the 2015–2016 El Niño. *Nature Communications*, *8*, 14365.

Barnard, P. L., Short, A. D., Harley, M. D., Splinter, K. D., Vitousek, S., Turner, I. L., Allan, J., Banno, M., Bryan, K. R., Doria, A., Hansen, J. E., Kato, S., Kuriyama, Y., Randall-Goodwin, E., Ruggiero, P., Walker, I. J., & Heathfield, D. K. (2015). Coastal vulnerability across the Pacific dominated by El Niño/Southern Oscillation. *Nature Geoscience*, *8*(10), 801–807.

Barnard, P. L., van Ormondt, M., Erikson, L. H., Eshleman, J., Hapke, C., Ruggiero, P., Adams, P. N., & Foxgrover, A. C. (2014). Development of the coastal storm modeling system (CoSMoS) for predicting the impact of storms on high-energy, active-margin coasts. *Natural Hazards*, *74*(2), 1095–1125.

Bascom, W. N. (1951). The relationship between sand size and beach-face slope. *Transactions, American Geophysical Union*, *32*(6), 866.

Battjes, J. (1974). Surf similarity. In *The Proceedings of Conference on Coastal Engineering 1974*. Copenhagen, Denmark: American Society of Civil Engineers.

Bauer, B., Davidson-Arnott, R., Hesp, P., Namikas, S., Ollerhead, J., & Walker, I. (2009). Aeolian sediment transport on a beach: Surface moisture, wind fetch, and mean transport. *Geomorphology*, *105*(1-2), 106–116.

Bauer, B. O., & Davidson-Arnott, R. G. (2003). A general framework for modeling sediment supply to coastal dunes including wind angle, beach geometry, and fetch effects. *Geomorphology*, *49*(1-2), 89–108.

Belly, P. (1964). Sand movement by wind. Tech. Rep. CERC Memorandum 1, U.S. Army Corps of Engineers, Vicksburg, MS.

Benimoff, A. I., Fritz, W. J., & Kress, M. (2015). Superstorm Sandy and Staten Island: Learning from the past, preparing for the future. In *Learning from the Impacts of Superstorm Sandy*, (pp. 21–40). Elsevier.

Berard, N. A., Mulligan, R. P., da Silva, A. M. F., & Dibajnia, M. (2017). Evaluation of XBeach performance for the erosion of a laboratory sand dune. *Coastal Engineering*, *125*, 70–80.

Bertin, X., de Bakker, A., van Dongeren, A., Coco, G., André, G., Ardhuin, F., Bonneton, P., Bouchette, F., Castelle, B., Crawford, W. C., Davidson, M., Deen, M., Dodet, G., Guérin, T., Inch, K., Leckler, F., McCall, R., Muller, H., Olabarrieta, M., Roelvink, D., Ruessink, G., Sous, D., Stutzmann, É., & Tissier, M. (2018). Infragravity waves: From driving mechanisms to impacts. *Earth-Science Reviews*, *177*, 774–799.

Biel, R. G., Hacker, S. D., Ruggiero, P., Cohn, N., & Seabloom, E. W. (2017). Coastal protection and conservation on sandy beaches and dunes: context-dependent tradeoffs in ecosystem service supply. *Ecosphere*, *8*(4).

Birchler, J. J., Stockdon, H. F., Doran, K. S., & Thompson, D. M. (2014). National assessment of hurricane-induced coastal erosion hazards: Northeast Atlantic Coast. Tech. Rep. 20141243, US Geological Survey.

Booij, N., Ris, R. C., & Holthuijsen, L. H. (1999). A third-generation wave model for coastal regions: 1. model description and validation. *Journal of Geophysical Research: Oceans*, *104*(C4), 7649–7666.

Bosboom, J., Aarninkhof, S., Reniers, A., Roelvink, J., & Walstra, D. (2000). Unibest-tc 2.0 overview of model formulations. Tech. rep., WL Delft Hydraulics, Delft, the Netherlands.

Brinkkemper, J., Torres-Freyermuth, A., Mendoza, E., Salles, P., & Ruessink, G. (2013). Parameterization of wave run-up on beaches in Yucatan, Mexico: a numerical study. In *Proceedings of the Coastal Dynamics Conference 2013*, (pp. 225 – 233). Arcachon, France.

Brodie, K. L., Slocum, R. K., & McNinch, J. E. (2012). New insights into the physical drivers of wave runup from a continuously operating terrestrial laser scanner. In *Proceedings of the Oceans Conference 2012*. Hampton Roads, VA: IEEE.

Buckley, M., Lowe, R., & Hansen, J. (2014). Evaluation of nearshore wave models in steep reef environments. *Ocean Dynamics*, *64*(6), 847–862.

Burroughs, S. M., & Tebbens, S. F. (2008). Dune retreat and shoreline change on the Outer Banks of North Carolina. *Journal of Coastal Research*, *2*, 104–112.

Camus, P., Mendez, F. J., Medina, R., & Cofiño, A. S. (2011). Analysis of clustering and selection algorithms for the study of multivariate wave climate. *Coastal Engineering*, *58*(6), 453–462.

Carignan, K., Taylor, L., Eakins, B., & Warnken, R. (2009). Digital elevation model of astoria, oregon: Procedures, data sources and analysis. Tech. Rep. NESDIS NGDC-22, U.S. National Oceanic and Atmospheric Administration, U.S. Dept. of Commerce, Boulder, CO.

Carter, R., & Rihan, C. (1978). Shell and pebble pavements on beaches: Examples from the north coast of Ireland. *CATENA*, *5*(3-4), 365–374.

Carter, R. W. G., & Balsillie, J. H. (1983). A note on the amount of wave energy transmitted over nearshore sand bars. *Earth Surface Processes and Landforms*, *8*(3), 213–222.

Castelle, B., Marieu, V., Bujan, S., Splinter, K. D., Robinet, A., Sénéchal, N., & Ferreira, S. (2015). Impact of the winter 2013–2014 series of severe Western Europe storms on a double-barred sandy coast: Beach and dune erosion and megacusp embayments. *Geomorphology*, *238*, 135–148.

Castelle, B., Turner, I., Ruessink, G., & Tomlinson, R. (2007). Impact of storms on beach erosion: Broadbeach (Gold Coast, Australia). *Journal of Coastal Research*, (pp. 534–539).

Clemmensen, L. B., Pye, K., Murray, A., & Heinemeier, J. (2008). Sedimentology, stratigraphy and landscape evolution of a holocene coastal dune system, Lodbjerg, NW Jutland, Denmark. *Sedimentology*, *48*(1), 3–27.

Cohn, N., Anderson, D., & Ruggiero, P. (2015). Observations of intertidal bar welding along a high energy, dissipative coastline. In P. Wang, J. Rosati, & J. Cheng (Eds.) *The Proceedings of the Coastal Sediments 2015*. San Diego, CA: World Scientific.

Cohn, N., & Ruggiero, P. (2016). The influence of seasonal to interannual nearshore profile variability on extreme water levels: Modeling wave runup on dissipative beaches. *Coastal Engineering*, *115*, 79–92.

Cohn, N., & Ruggiero, P. (2018). SEDEX2 topographic and bathymetric data. `https://doi.org/10.6084/m9.figshare.5959945.v1`.

Cohn, N., Ruggiero, P., de Vries, S., & García-Medina, G. (2017). Beach growth driven by intertidal sandbar welding. In T. Aagaard, R. Deigaard, & D. Fuhrman (Eds.) *Proceedings of the Coastal Dynamics Conference 2017*, (pp. 1059 – 1069).

Cohn, N., Ruggiero, P., de Vries, S., & Kaminsky, G. (2018). New insights on the relative contributions of marine and aeolian processes to coastal foredune growth. *Geophysical Research Letters*.

Cohn, N., Ruggiero, P., García-Medina, G., Anderson, D., Serafin, K., & Biel, R. (in prep). Environmental and morphologic control on wave induced dune response. *prepared for submission to Geomorphology*.

Cohn, N., Ruggiero, P., Ortiz, J., & Walstra, D. (2014). Investigating the role of complex sandbar morphology on nearshore hydrodynamics. *Journal of Coastal Research*, *70*, 53–58.

Cooper, J., Jackson, D., Navas, F., McKenna, J., & Malvarez, G. (2004). Identifying storm impacts on an embayed, high-energy coastline: examples from western Ireland. *Marine Geology*, *210*(1-4), 261–280.

Cooper, W. (1958). *Coastal sand dunes of Oregon and Washington*, vol. 72. Geological Society of America.

Costas, S., Alejo, I., Vila-Concejo, A., & Nombela, M. A. (2005). Persistence of storm-induced morphology on a modal low-energy beach: A case study from NW-Iberian Peninsula. *Marine Geology*, *224*(1-4), 43–56.

Cowell, P., Stive, M., Niedoroda, A., de Vriend, H., Swift, D., Kaminsky, G., & Capobianco, M. (2003). The coastal-tract (part 1): a conceptual approach to aggregated modeling of low-order coastal change. *Journal of Coastal Research*, (pp. 812–827).

Cowell, P., & Thom, B. G. (1995). Morphodynamics of coastal evolution. In R. W. G. Carter, & C. D. Woodroffe (Eds.) *Coastal Evolution*, (pp. 33–86). Cambridge University Press.

Cox, N., Dunkin, L. M., & Irish, J. L. (2013). An empirical model for infragravity swash on barred beaches. *Coastal Engineering*, *81*, 44–50.

Davidson-Arnott, R., Hesp, P., Ollerhead, J., Walker, I., Bauer, B., Delgado-Fernandez, I., & Smyth, T. (2018). Sediment budget controls on foredune height: Comparing simulation model results with field data. *Earth Surface Processes and Landforms*.

Davidson-Arnott, R., & Law, M. (1996). Measurement and prediction of long-term sediment supply to coastal foredunes. *Journal of Coastal Research*, (pp. 654–663).

Davidson-Arnott, R. G., MacQuarrie, K., & Aagaard, T. (2005). The effect of wind gusts, moisture content and fetch length on sand transport on a beach. *Geomorphology*, *68*(1-2), 115–129.

de M. Luna, M. C., Parteli, E. J., Durán, O., & Herrmann, H. J. (2011). Model for the genesis of coastal dune fields with vegetation. *Geomorphology*, *129*(3-4), 215–224.

De Vet, P., McCAll, R., Biemen, J. D., Stive, M., & van Ormondt, M. (2015). Modelling dune erosion, overwash, and breaching at Fire Island, NY during Hurricane Sandy. In P. Wang, J. Rosati, & J. Cheng (Eds.) *The Proceedings of the Coastal Sediments 2015*. San Diego, CA: World Scientific.

de Vries, S., Arens, S., de Schipper, M., & Ranasinghe, R. (2014). Aeolian sediment transport on a beach with a varying sediment supply. *Aeolian Research*, *15*, 235–244.

de Vries, S., Southgate, H., Kanning, W., & Ranasinghe, R. (2012). Dune behavior and aeolian transport on decadal timescales. *Coastal Engineering*, *67*, 41–53.

de Vries, S., Verheijen, A., Hoonhout, B., Vos, S., Cohn, N., & Ruggiero, P. (2017). Measured spatial variability of beach erosion due to aeolian processes. In T. Aagaard, R. Deigaard, & D. Fuhrman (Eds.) *Proceedings of the Coastal Dynamics Conference 2017*. Helsignor, Denmark.

de Winter, R., Gongriep, F., & Ruessink, B. (2015). Observations and modeling of alongshore variability in dune erosion at Egmond aan Zee, the Netherlands. *Coastal Engineering*, *99*, 167–175.

Dean, R. (1991). Equilibrium beach profiles: characteristics and applications. *Journal of Coastal Research*, *7*(1), 53–84.

Delgado-Fernandez, I. (2010). A review of the application of the fetch effect to modelling sand supply to coastal foredunes. *Aeolian Research*, *2*(2-3), 61–70.

Di Leonardo, D., & Ruggiero, P. (2015). Regional scale sandbar variability: Observations from the U.S. Pacific Northwest. *Continental Shelf Research*, *95*, 74–88.

Diez, J., Cohn, N., Kaminsky, G., Medina, R., & Ruggiero, P. (2018). Spatial and temporal variability of dissipative dry beach profiles in the Pacific Northwest, U.S.A. *Journal of Coastal Research*.

Dissanayake, P., Brown, J., & Karunarathna, H. (2015). Impacts of storm chronology on the morphological changes of the Formby beach and dune system, UK. *Natural Hazards and Earth System Science*, *15*(7), 1533–1543.

Durán, O., & Herrmann, H. J. (2006). Vegetation against dune mobility. *Physical Review Letters*, *97*(18).

Durán, O., & Moore, L. J. (2013). Vegetation controls on the maximum size of coastal dunes. *Proceedings of the National Academy of Sciences*, *110*(43), 17217–17222.

Durán, O., & Moore, L. J. (2015). Barrier island bistability induced by biophysical interactions. *Nature Climate Change*, *5*(2), 158–162.

Elko, N., Brodie, K., Stockdon, H., Nordstrom, K., Houser, C., McKenna, K., Moore, L., Rosati, J., Ruggiero, R., Thuman, R., & Walker, I. (2016). Dune management challenges on developed coasts. *Shore and Beach*, *84*(1), 15–28.

Elko, N., Feddersen, F., Foster, D., Hapke, C., McNinch, J., Mulligan, R., Özkan-Haller, H., Plant, N., & Raubenheimer, B. (2015). The future of nearshore processes research. *Shore and Beach*, *83*(1).

Figlus, J., Kobayashi, N., Gralher, C., & Iranzo, V. (2011). Wave overtopping and overwash of dunes. *Journal of Waterway, Port, Coastal, and Ocean Engineering*, *137*(1), 26–33.

Galappatti, G., & Vreugdenhil, C. B. (1985). A depth-integrated model for suspended sediment transport. *Journal of Hydraulic Research*, *23*(4), 359–377.

Gallop, S. L., Collins, M., Pattiaratchi, C. B., Eliot, M. J., Bosserelle, C., Ghisalberti, M., Collins, L. B., Eliot, I., Erftemeijer, P. L. A., Larcombe, P., Marigómez, I., Stul, T., & White, D. J. (2015). Challenges in transferring knowledge between scales in coastal sediment dynamics. *Frontiers in Marine Science*, *2*.

García-Medina, G., Özkan-Haller, H. T., & Ruggiero, P. (2014). Wave resource assessment in Oregon and southwest Washington, USA. *Renewable Energy*, *64*, 203–214.

Geer, P. V., Vries, B. D., Dongeren, A. V., & Van Thiel de Vries, J. (2012). Dune erosion near sea walls: model-data comparison. *Coastal Engineering Proceedings*, *1*(33), 102.

Gelfenbaum, G., & Kaminsky, G. M. (2010). Large-scale coastal change in the Columbia River littoral cell: An overview. *Marine Geology*, *273*(1-4), 1–10.

Gelfenbaum, G., Stevens, A. W., Miller, I., Warrick, J. A., Ogston, A. S., & Eidam, E. (2015). Large-scale dam removal on the Elwha River, Washington, USA: Coastal geomorphic change. *Geomorphology*, *246*, 649–668.

Goldstein, E. B., Moore, L. J., & Vinent, O. D. (2017). Lateral vegetation growth rates exert control on coastal foredune hummockiness and coalescing time. *Earth Surface Dynamics*, *5*(3), 417–427.

Guedes, R., Bryan, K. R., & Coco, G. (2012). Observations of alongshore variability of swash motions on an intermediate beach. *Continental Shelf Research*, *48*, 61–74.

Guedes, R., Bryan, K. R., Coco, G., & Holman, R. A. (2011). The effects of tides on swash statistics on an intermediate beach. *Journal of Geophysical Research*, *116*(C4).

Guza, R. T., & Feddersen, F. (2012). Effect of wave frequency and directional spread on shoreline runup. *Geophysical Research Letters*, *39*(11).

Hacker, S. D., Zarnetske, P., Seabloom, E., Ruggiero, P., Mull, J., Gerrity, S., & Jones, C. (2012). Subtle differences in two non-native congeneric beach grasses significantly affect their colonization, spread, and impact. *Oikos*, *121*(1), 138–148.

Hapke, C., Himmelstoss, E., Kratzmann, M., List, J., & Thieler, E. (2011). National assessment of shoreline change: Historical shoreline change along the New England and Mid-Atlantic coasts. Tech. Rep. Open-File Report 2010-1118, U.S. Geological Survey.

Harley, M., Armaroli, C., & Ciavola, P. (2011a). Evaluation of xbeach predictions for a real-time warning system in Emilia-Romagna, Northern Italy. In *Proceedings of the 11th International Coastal Symposium*, vol. 64, (pp. 1861 – 1863).

Harley, M. D., Turner, I. L., Short, A. D., & Ranasinghe, R. (2011b). A reevaluation of coastal embayment rotation: The dominance of cross-shore versus alongshore sediment transport processes, Collaroy-Narrabeen Beach, southeast Australia. *Journal of Geophysical Research*, *116*(F4).

Haxel, J. H., & Holman, R. A. (2004). The sediment response of a dissipative beach to variations in wave climate. *Marine Geology*, *206*(1-4), 73–99.

Hein, C. J., FitzGerald, D. M., Carruthers, E. A., Stone, B. D., Barnhardt, W. A., & Gontz, A. M. (2012). Refining the model of barrier island formation along a paraglacial coast in the Gulf of Maine. *Marine Geology*, *307-310*, 40–57.

Herbers, T. H. C., Elgar, S., & Guza, R. T. (1995). Generation and propagation of infragravity waves. *Journal of Geophysical Research*, *100*(C12), 24863.

Hesp, P. (2006). Sand beach ridges: definitions and re-definition. *Journal of Coastal Research*, (pp. 72–75).

Hesp, P. A. (1981). The formation of shadow dunes. *SEPM Journal of Sedimentary Research*, *Vol. 51*.

Hesp, P. A. (2013). Conceptual models of the evolution of transgressive dune field systems. *Geomorphology*, *199*, 138–149.

Hoefel, F. (2003). Wave-induced sediment transport and sandbar migration. *Science*, *299*(5614), 1885–1887.

Holman, R. (1986). Extreme value statistics for wave run-up on a natural beach. *Coastal Engineering*, *9*(6), 527–544.

Holman, R., & Stanley, J. (2007). The history and technical capabilities of Argus. *Coastal Engineering*, *54*(6-7), 477–491.

Holman, R. A., Lalejini, D. M., Edwards, K., & Veeramony, J. (2014). A parametric model for barred equilibrium beach profiles. *Coastal Engineering*, *90*, 85–94.

Holman, R. A., & Sallenger, A. H. (1985). Setup and swash on a natural beach. *Journal of Geophysical Research*, *90*(C1), 945.

Holthuijsen, L., Booij, N., & Herbers, T. (1989). A prediction model for stationary, short-crested waves in shallow water with ambient currents. *Coastal Engineering*, *13*(1), 23–54.

Hoonhout, B., & de Vries, S. (2017a). Aeolian sediment supply at a mega nourishment. *Coastal Engineering*, *123*, 11–20.

Hoonhout, B., & de Vries, S. (2017b). Field measurements on spatial variations in aeolian sediment availability at the Sand Motor mega nourishment. *Aeolian Research*, *24*, 93–104.

Hoonhout, B. M., & de Vries, S. (2016). A process-based model for aeolian sediment transport and spatiotemporal varying sediment availability. *Journal of Geophysical Research: Earth Surface*, *121*(8), 1555–1575.

Houser, C. (2009). Synchronization of transport and supply in beach-dune interaction. *Progress in Physical Geography*, *33*(6), 733–746.

Houser, C. (2013). Alongshore variation in the morphology of coastal dunes: Implications for storm response. *Geomorphology*, *199*, 48–61.

Houser, C., & Hamilton, S. (2009). Sensitivity of post-hurricane beach and dune recovery to event frequency. *Earth Surface Processes and Landforms*, *34*(5), 613–628.

Houston, J. R. (1995). The economic value of beaches. Tech. Rep. The CERCular, U.S. Army Corps of Engineers Coastal Engineering Research Center.

Hunt, J. C. R., Leibovich, S., & Richards, K. J. (1988). Turbulent shear flows over low hills. *Quarterly Journal of the Royal Meteorological Society*, *114*(484), 1435–1470.

Irish, J. L., Lynett, P. J., Weiss, R., Smallegan, S. M., & Cheng, W. (2013). Buried relic seawall mitigates Hurricane Sandys impacts. *Coastal Engineering*, *80*, 79–82.

Jackson, & Cooper (1999). Beach fetch distance and aeolian sediment transport. *Sedimentology*, *46*(3), 517–522.

Johnson, B., Kobayashi, N., & Gravens, M. (2012). Cross-shore numerical model cshore for waves, currents, sediment transport and beach profile evolution. Tech. Rep. Report ERDC/CHL-TR-12-22, U.S. Army Corps of Engineers Coastal Engineering Research Center, Vicksburg, MS, USA.

Kaminsky, G. M., Ruggiero, P., Buijsman, M. C., McCandless, D., & Gelfenbaum, G. (2010). Historical evolution of the Columbia River littoral cell. *Marine Geology*, *273*(1-4), 96–126.

Karanci, A., Kurum, O. M., & Overton, M. (2014). Land cover effect on dune erosion and overwash. In P. Lynett (Ed.) *The Proceedings of the Coastal Engineering Conference 2014*, (p. 53). Seoul, South Korea: Coastal Engineering Research Council.

Keijsers, J., Groot, A. D., & Riksen, M. (2015). Vegetation and sedimentation on coastal foredunes. *Geomorphology*, *228*, 723–734.

Klemas, V. (2011). Beach profiling and LIDAR bathymetry: An overview with case studies. *Journal of Coastal Research*, *277*, 1019–1028.

Komar, P. (1998). *Beach processes and sedimentation*. Upper Saddle River, NJ: Prentice Hall.

Komar, P., McDougal, W., Marra, J., & Ruggiero, P. (1999). The rational analysis of setback distances: Applications to the Oregon coast. *Shore and Beach*, *67*(1), 41–49.

Komar, P. D., Allan, J., Días-Méndez, G. M., Marra, J. J., & Ruggiero, P. (2001). El Niño and La Niña: Erosion processes and impacts. In B. Edge (Ed.) *The Proceedings of the Coastal Engineering Conference 2000*. Sydney, Australia: American Society of Civil Engineers.

Komar, P. D., Allan, J. C., & Ruggiero, P. (2011). Sea level variations along the U.S. Pacific Northwest Coast: Tectonic and climate controls. *Journal of Coastal Research*, *276*, 808–823.

Kriebel, D. L., & Dean, R. G. (1993). Convolution method for time-dependent beach-profile response. *Journal of Waterway, Port, Coastal, and Ocean Engineering*, *119*(2), 204–226.

Larson, M., Erikson, L., & Hanson, H. (2004). An analytical model to predict dune erosion due to wave impact. *Coastal Engineering*, *51*(8-9), 675–696.

Larson, M., & Kraus, N. (1989). SBEACH: numerical model for simulating storm-induced beach change. report 1. empirical foundation and model development. Tech. Rep. CERC-TR-89-9, U.S. Army Corps of Engineers, Vicksurg, MS, USA.

Lindemer, C., Plant, N., Puleo, J., Thompson, D., & Wamsley, T. (2010). Numerical simulation of a low-lying barrier islands morphological response to Hurricane Katrina. *Coastal Engineering*, *57*(11-12), 985–995.

Luger, M. I. (1991). The economic value of the coastal zone. *Journal of Environmental Systems*, *21*(4), 279–301.

Luijendijk, A., Hagenaars, G., Ranasinghe, R., Baart, F., Donchyts, G., & Aarninkhof, S. (2018). The state of the world's beaches. *Scientific Reports*, *8*(1).

Martínez, M., & Psuty, N. (2004). *Coastal dunes*. Berlin, Germany: Springer.

Masselink, G., & Puleo, J. A. (2006). Swash-zone morphodynamics. *Continental Shelf Research*, *26*(5), 661–680.

McCall, R., Masselink, G., Poate, T., Roelvink, J., & Almeida, L. (2015). Modelling the morphodynamics of gravel beaches during storms with XBeach-G. *Coastal Engineering*, *103*, 52–66.

McCall, R., Van Thiel de Vries, J., Plant, N., Dongeren, A. V., Roelvink, J., Thompson, D., & Reniers, A. (2010). Two-dimensional time dependent hurricane overwash and erosion modeling at Santa Rosa Island. *Coastal Engineering*, *57*(7), 668–683.

McGranahan, G., Balk, D., & Anderson, B. (2007). The rising tide: assessing the risks of climate change and human settlements in low elevation coastal zones. *Environment and Urbanization*, *19*(1), 17–37.

Miller, T. E., Gornish, E. S., & Buckley, H. L. (2010). Climate and coastal dune vegetation: disturbance, recovery, and succession. *Plant Ecology*, *206*(1), 97–104.

Moore, L. J., Vinent, O. D., & Ruggiero, P. (2016). Vegetation control allows autocyclic formation of multiple dunes on prograding coasts. *Geology*, *44*(7), 559–562.

Mull, J., & Ruggiero, P. (2014). Estimating storm-induced dune erosion and overtopping along U.S. West Coast beaches. *Journal of Coastal Research*, *298*, 1173–1187.

Nelson, D. (1991). Factors effecting beach morphology changes caused by Hurricane Hugo, northern South Carolina. *Journal of Coastal Research*, *8*, 163–179.

Neuman, C. M., Li, B., & Nash, D. (2012). Micro-topographic analysis of shell pavements formed by aeolian transport in a wind tunnel simulation. *Journal of Geophysical Research: Earth Surface*, *117*(F4).

Neumann, B., Vafeidis, A., Zimmermann, J., & Nicholls, R. (2015). Correction: Future coastal population growth and exposure to sea-level rise and coastal flooding - a global assessment. *PLOS ONE*, *10*(6), e0131375.

Nickling, W. G., & Ecclestone, M. (1981). The effects of soluble salts on the threshold shear velocity of fine sand. *Sedimentology*, *28*(4), 505–510.

NOAA NCEI (2018). U.S. billion-dollar weather and climate disasters. `https://www.ncdc.noaa.gov/billions`. Accessed 2018-04-14.

Ollerhead, J., Davidson-Arnott, R., Walker, I. J., & Mathew, S. (2012). Annual to decadal morphodynamics of the foredune system at Greenwich Dunes, Prince Edward Island, Canada. *Earth Surface Processes and Landforms*, *38*(3), 284–298.

Oreskes, N., & Belitz, K. (2001). Philosophical issues in model assessment. In M. Anderson, & P. Bates (Eds.) *Model validation: Perspectives in hydrological science*, (pp. 23–41). Hoboken, NJ: John Wiley and Sons.

Pachauri, R., Allen, M., Barros, V., Broome, J., Cramer, W., Christ, R., Church, J., Clarke, L., Dahe, Q., et al. (2014). Climate change 2014: Synthesis report. contribution of working groups i, ii and iii to the fifth assessment report of the intergovernmental panel on climate change. Tech. rep., Intergovernmental Panel on Climate Change, Geneva, Switzerland.

Palmsten, M. L., & Holman, R. A. (2012). Laboratory investigation of dune erosion using stereo video. *Coastal Engineering*, *60*, 123–135.

Palmsten, M. L., & Splinter, K. D. (2016). Observations and simulations of wave runup during a laboratory dune erosion experiment. *Coastal Engineering*, *115*, 58–66.

Pape, L., Kuriyama, Y., & Ruessink, B. G. (2010). Models and scales for cross-shore sandbar migration. *Journal of Geophysical Research*, *115*(F3).

Parteli, E. J. R., Durán, O., Tsoar, H., Schwämmle, V., & Herrmann, H. J. (2009). Dune formation under bimodal winds. *Proceedings of the National Academy of Sciences*, *106*(52), 22085–22089.

Peckham, S. D., Hutton, E. W., & Norris, B. (2013). A component-based approach to integrated modeling in the geosciences: The design of CSDMS. *Computers & Geosciences*, *53*, 3–12.

Pender, D., & Karunarathna, H. (2013). A statistical-process based approach for modelling beach profile variability. *Coastal Engineering*, *81*, 19–29.

Peterson, C., Darienzo, M., Pettit, J., Jackson, P., & Rosenfeld, C. (1991). Littoral-cell development in the convergent Cascadia Margin of the Pacific Northwest, USA. *Society for Sedimentary Geology*, *SI 46*.

Plant, N. G., Holman, R. A., Freilich, M. H., & Birkemeier, W. A. (1999). A simple model for interannual sandbar behavior. *Journal of Geophysical Research: Oceans*, *104*(C7), 15755–15776.

Psuty, N. (2004). The coastal foredune: a morphological basis for regional coastal dune development. In M. Martínez, & N. Psuty (Eds.) *Coastal dunes*, (pp. 11–27). Berlin: Springer.

Ramakrishnan, R., Agrawal, R., Remya, P., NagaKumar, K., Demudu, G., Rajawat, A., Nair, B., & Rao, K. N. (2018). Modelling coastal erosion: A case study of Yarada beach near Visakhapatnam, east coast of India. *Ocean & Coastal Management*, *156*, 239–248.

Raupach, M. R., Gillette, D. A., & Leys, J. F. (1993). The effect of roughness elements on wind erosion threshold. *Journal of Geophysical Research: Atmospheres*, *98*(D2), 3023–3029.

Reniers, A., MacMahan, J., Thornton, E., & Stanton, T. (2006). Modelling infragravity motions on a rip-channel beach. *Coastal Engineering*, *53*(2-3), 209–222.

Reniers, A. J. H. M. (2004). Morphodynamic modeling of an embayed beach under wave group forcing. *Journal of Geophysical Research*, *109*(C1).

Revell, D., Komar, P., & Sallenger, A. (2002). An application of lidar to analyses of El Niño erosion in the Netarts Littoral Cell, Oregon. *Journal of Coastal Research*, *18*(4), 792–801.

Reyns, J., Dastgheib, A., Ranasinghe, R., Luijendijk, A., Walstra, D.-J., & Roelvink, D. (2014). Morphodynamic upscaling with the morfac approach in tidal conditions: the critical morfac. In P. Lynett (Ed.) *The Proceedings of the Coastal Engineering Conference 2014*, (p. 27). Seoul, South Korea: Coastal Engineering Research Council.

Roelvink, D., McCall, R., Mehvar, S., Nederhoff, K., & Dastgheib, A. (2018). Improving predictions of swash dynamics in XBeach: The role of groupiness and incident-band runup. *Coastal Engineering*, *134*, 103–123.

Roelvink, D., Reniers, A., van Dongeren, A., van Thiel de Vries, J., McCall, R., & Lescinski, J. (2009). Modelling storm impacts on beaches, dunes and barrier islands. *Coastal Engineering*, *56*(11-12), 1133–1152.

Roelvink, D., van Dongeren, A., McCall, R., Hoonhout, B., van Rooijen, A., van Geer, P., de Vet, L., Nederhoff, K., & Quataert, E. (2015). Xbeach technical reference: Kingsday release. Tech. rep., Deltares, Delft, the Netherlands.

Roelvink, J., Meijer, T., Houwman, K., Bakker, R., & Spanhoff, R. (1995). Field validation and application of a coastal profile model. In *Proceedings of the Coastal Dynamics Conference 1995*, (pp. 818 – 828).

Roelvink, J. A., & Stive, M. J. F. (1989). Bar-generating cross-shore flow mechanisms on a beach. *Journal of Geophysical Research*, *94*(C4), 4785.

Ruessink, B., & Kroon, A. (1994). The behaviour of a multiple bar system in the nearshore zone of Terschelling, the Netherlands: 1965–1993. *Marine Geology*, *121*(3-4), 187–197.

Ruessink, B. G., Kleinhans, M. G., & van den Beukel, P. G. L. (1998). Observations of swash under highly dissipative conditions. *Journal of Geophysical Research: Oceans*, *103*(C2), 3111–3118.

Ruessink, B. G., & Kuriyama, Y. (2008). Numerical predictability experiments of cross-shore sandbar migration. *Geophysical Research Letters*, *35*(1).

Ruessink, B. G., Kuriyama, Y., Reniers, A. J. H. M., Roelvink, J. A., & Walstra, D. J. R. (2007). Modeling cross-shore sandbar behavior on the timescale of weeks. *Journal of Geophysical Research*, *112*(F3).

Ruggiero, P., Holman, R., & Beach, R. (2004). Wave run-up on a high-energy dissipative beach. *Journal of Geophysical Research*, *109*(C6).

Ruggiero, P., Kaminsky, G. M., Gelfenbaum, G., & Cohn, N. (2016). Morphodynamics of prograding beaches: A synthesis of seasonal- to century-scale observations of the Columbia River littoral cell. *Marine Geology*, *376*, 51–68.

Ruggiero, P., Kaminsky, G. M., Gelfenbaum, G., & Voigt, B. (2005). Seasonal to interannual morphodynamics along a high-energy dissipative littoral cell. *Journal of Coastal Research*, *213*, 553–578.

Ruggiero, P., Komar, P., McDougal, W., Marra, J., & Beach, R. (2001). Wave runup, extreme water levels and the erosion of properties backing beaches. *Journal of Coastal Research*, (pp. 402–419).

Ruggiero, P., Komar, P. D., & Allan, J. C. (2010). Increasing wave heights and extreme value projections: The wave climate of the U.S. Pacific Northwest. *Coastal Engineering*, *57*(5), 539–552.

Ruggiero, P., Kratzmann, M. G., Himmelstoss, E. A., Reid, D., Allan, J., & Kaminsky, G. (2013). National assessment of shoreline change: historical shoreline change along the Pacific Northwest coast. Tech. Rep. 2012-1007, US Geological Survey.

Russell, P. E. (1993). Mechanisms for beach erosion during storms. *Continental Shelf Research*, *13*(11), 1243–1265.

Sallenger, A. (2000). Storm impact scale for barrier islands. *Journal of Coastal Research*, *16*(3), 890–895.

Sauermann, G., Kroy, K., & Herrmann, H. J. (2001). Continuum saltation model for sand dunes. *Physical Review E*, *64*(3).

Saye, S., van der Wal, D., Pye, K., & Blott, S. (2005). Beach–dune morphological relationships and erosion/accretion: An investigation at five sites in England and Wales using LIDAR data. *Geomorphology*, *72*(1-4), 128–155.

Schwämmle, V., & Herrmann, H. J. (2005). A model of barchan dunes including lateral shear stress. *The European Physical Journal E*, *16*(1), 57–65.

Sénéchal, N., Coco, G., Bryan, K., MacMahan, J., Brown, J., & Holman, R. (2013). Tidal effects on runup in presence of complex 3d morphologies under dissipative surf zone

conditions. In *Proceedings of the Coastal Dynamics Conference 2013*. Arcachon, France.

Serafin, K. A., & Ruggiero, P. (2014). Simulating extreme total water levels using a time-dependent, extreme value approach. *Journal of Geophysical Research: Oceans*, *119*(9), 6305–6329.

Serafin, K. A., Ruggiero, P., & Stockdon, H. F. (2017). The relative contribution of waves, tides, and non-tidal residuals to extreme total water levels on US west coast sandy beaches. *Geophysical Research Letters*.

Shand, R., Hesp, P., & Shepard, M. (2006). Beach cut in relation to net offshore bar migration. In *Proceedings of the 8th International Coastal Symposium (Brazil)*, vol. 39, (pp. 334 – 340).

Shand, R., Shand, T., McComb, P., & Johnson, D. (2011). Evaluation of empirical predictors of extreme run-up using field data. In *Proceedings of 20th Australasian Coastal and Ocean Engineering Conference. Perth, Australia.*.

Sherman, D. J., & Bauer, B. O. (1993). Dynamics of beach-dune systems. *Progress in Physical Geography*, *17*(4), 413–447.

Short, A., & Hesp, P. (1982). Wave, beach and dune interactions in southeastern Australia. *Marine Geology*, *48*(3-4), 259–284.

Sigren, J., Figlus, J., & Armitage, A. (2014). Coastal sand dunes and dune vegetation: restoration, erosion, and storm protection. *Shore and Beach*, *82*(4), 5–12.

Simmons, J. A., Harley, M. D., Marshall, L. A., Turner, I. L., Splinter, K. D., & Cox, R. J. (2017). Calibrating and assessing uncertainty in coastal numerical models. *Coastal Engineering*, *125*, 28–41.

Smallegan, S. M., Irish, J. L., Dongeren, A. R. V., & Bieman, J. P. D. (2016). Morphological response of a sandy barrier island with a buried seawall during Hurricane Sandy. *Coastal Engineering*, *110*, 102–110.

Smyth, T. A., & Hesp, P. A. (2015). Aeolian dynamics of beach scraped ridge and dyke structures. *Coastal Engineering*, *99*, 38–45.

Smyth, T. A., Jackson, D. W., & Cooper, J. A. G. (2012). High resolution measured and modelled three-dimensional airflow over a coastal bowl blowout. *Geomorphology*, *177-178*, 62–73.

Soldini, L., Antuono, M., & Brocchini, M. (2013). Numerical modeling of the influence of the beach profile on wave run-up. *Journal of Waterway, Port, Coastal, and Ocean Engineering*, *139*(1), 61–71.

Splinter, K. D., Carley, J. T., Golshani, A., & Tomlinson, R. (2014). A relationship to describe the cumulative impact of storm clusters on beach erosion. *Coastal Engineering*, *83*, 49–55.

Splinter, K. D., Kearney, E. T., & Turner, I. L. (2018). Drivers of alongshore variable dune erosion during a storm event: Observations and modelling. *Coastal Engineering*, *131*, 31–41.

Splinter, K. D., & Palmsten, M. L. (2012). Modeling dune response to an East Coast Low. *Marine Geology*, *329-331*, 46–57.

Stephens, S. A., Coco, G., & Bryan, K. R. (2011). Numerical simulations of wave setup over barred beach profiles: Implications for predictability. *Journal of Waterway, Port, Coastal, and Ocean Engineering*, *137*(4), 175–181.

Stockdon, H., & Holman, R. (2011). Observations of wave runup, setup, and swash on natural beaches. Tech. Rep. USGS Data Series 602, U.S. Geological Survey.

Stockdon, H., Thompson, D., Plant, N., & Long, J. (2014). Evaluation of wave runup predictions from numerical and parametric models. *Coastal Engineering*, *92*, 1–11.

Stockdon, H. F., Doran, K. S., & Sallenger, A. H. (2009). Extraction of lidar-based dune-crest elevations for use in examining the vulnerability of beaches to inundation during hurricanes. *Journal of Coastal Research*, *10053*, 59–65.

Stockdon, H. F., Holman, R. A., Howd, P. A., & Sallenger, A. H. (2006). Empirical parameterization of setup, swash, and runup. *Coastal Engineering*, *53*(7), 573–588.

Stockdon, H. F., Sallenger, A. H., Holman, R. A., & Howd, P. A. (2007). A simple model for the spatially-variable coastal response to hurricanes. *Marine Geology*, *238*(1-4), 1–20.

Storms, J. E. (2003). Event-based stratigraphic simulation of wave-dominated shallow-marine environments. *Marine Geology*, *199*(1-2), 83–100.

Suanez, S., Cancouët, R., Floc'h, F., Blaise, E., Ardhuin, F., Filipot, J.-F., Cariolet, J.-M., & Delacourt, C. (2015). Observations and predictions of wave runup, extreme water

levels, and medium-term dune erosion during storm conditions. *Journal of Marine Science and Engineering*, *3*(3), 674–698.

Susa, T., Ruggiero, P., Anderson, D., & Cohn, N. (2014). Morphological change and sand transport mechanisms in the dynamic dune complex of South Beach State Park, Oregon. *Shore and Beach*, *82*(4), 24–34.

Sutton-Grier, A. E., Wowk, K., & Bamford, H. (2015). Future of our coasts: The potential for natural and hybrid infrastructure to enhance the resilience of our coastal communities, economies and ecosystems. *Environmental Science & Policy*, *51*, 137–148.

Taylor, M., & Stone, G. (1996). Beach-ridges: a review. *Journal of Coastal Research*, *12*(3), 612–621.

Theuerkauf, E. J., Rodriguez, A. B., Fegley, S. R., & Luettich, R. A. (2014). Sea level anomalies exacerbate beach erosion. *Geophysical Research Letters*, *41*(14), 5139–5147.

Thieler, E., Pilkey, H., Young, R., Bush, D., & Chai, F. (2000). The use of mathematical models to predict beach behavior for US coastal engineering : a critical review. *Journal of Coastal Research*, (pp. 48–70).

Thornton, E., MacMahan, J., & Sallenger, A. (2007). Rip currents, mega-cusps, and eroding dunes. *Marine Geology*, *240*(1-4), 151–167.

Thornton, E. B., & Guza, R. T. (1983). Transformation of wave height distribution. *Journal of Geophysical Research*, *88*(C10), 5925.

van de Graaff, J. (1977). Dune erosion during a storm surge. *Coastal Engineering*, *1*, 99–134.

van Dijk, P. M., Arens, S. M., & van Boxel, J. H. (1999). Aeolian processes across transverse dunes. II: modelling the sediment transport and profile development. *Earth Surface Processes and Landforms*, *24*(4), 319–333.

van Dongeren, A., Bolle, A., Vousdoukas, M. I., Plomaritis, T., Eftimova, P., Williams, J., Armaroli, C., Idier, D., Geer, P. V., Van Thiel de Vries, J., Haerens, P., Taborda, R., Benavente, J., Trifonova, E., Ciavola, P., Balouin, Y., & Roelvink, D. (2009). Micore: Dune erosion and overwash model validation with data from nine European field sites. In M. Mizuguchi, & S. Sato (Eds.) *Proceedings of Coastal Dynamics Conference 2009*. Tokyo, Japan: World Scientific.

van Gent, M., van Thiel de Vries, J., Coeveld, E., de Vroeg, J., & van de Graaff, J. (2008). Large-scale dune erosion tests to study the influence of wave periods. *Coastal Engineering*, *55*(12), 1041–1051.

van Rhee, C. (2010). Sediment entrainment at high flow velocity. *Journal of Hydraulic Engineering*, *136*(9), 572–582.

van Rijn, L. C. (2009). Prediction of dune erosion due to storms. *Coastal Engineering*, *56*(4), 441–457.

Van Thiel de Vries, J., Dongeren, A. V., McCall, R., & Reniers, A. (2011). The effect of the longshore dimension on dune erosion. In J. Smith, & P. Lynett (Eds.) *The Proceedings of the Coastal Engineering Conference 2010*, (p. 49). Shanghai, China: Coastal Engineering Research Council.

Vellinga, P. (1986). *Beach and dune erosion during storm surges*. Ph.D. thesis, Technical University of Delft, Delft, the Netherlands.

Verheyen, B., Gruwez, V., Zimmermann, N., Wauters, P., & Bolle, A. (2014). Medium term time-dependent morphodynamic modelling of beach profile evolution in Ada, Ghana. In *Proceedings of the 11th International Conference on Hydroscience and Engineering*. Hamburg, Germany.

Vigdor, J. (2008). The economic aftermath of Hurricane Katrina. *Journal of Economic Perspectives*, *22*(4), 135–154.

Villarroel-Lamb, D. A., Hammeken, A., & Simons, R. (2014). Quantifying the effect of bed permeability on maximum wave runup. *Coastal Engineering Proceedings*, *1*(34), 45.

Vousdoukas, M. I., Ferreira, Ó., Almeida, L. P., & Pacheco, A. (2012). Toward reliable storm-hazard forecasts: XBeach calibration and its potential application in an operational early-warning system. *Ocean Dynamics*, *62*(7), 1001–1015.

Vousdoukas, M. I., Wziatek, D., & Almeida, L. P. (2011). Coastal vulnerability assessment based on video wave run-up observations at a mesotidal, steep-sloped beach. *Ocean Dynamics*, *62*(1), 123–137.

Wahl, T., Plant, N. G., & Long, J. W. (2016). Probabilistic assessment of erosion and flooding risk in the northern Gulf of Mexico. *Journal of Geophysical Research: Oceans*, *121*(5), 3029–3043.

Walker, I. J., Davidson-Arnott, R. G., Bauer, B. O., Hesp, P. A., Delgado-Fernandez, I., Ollerhead, J., & Smyth, T. A. (2017). Scale-dependent perspectives on the geomorphology and evolution of beach-dune systems. *Earth-Science Reviews*, *171*, 220–253.

Walstra, D., Reniers, A., Ranasinghe, R., Roelvink, J., & Ruessink, B. (2012). On bar growth and decay during interannual net offshore migration. *Coastal Engineering*, *60*, 190–200.

Weng, W. S., Hunt, J. C. R., Carruthers, D. J., Warren, A., Wiggs, G. F. S., Livingstone, I., & Castro, I. (1991). Air flow and sand transport over sand-dunes. In *Aeolian Grain Transport*, (pp. 1–22). Springer Vienna.

Wijnberg, K. M., & Terwindt, J. H. (1995). Extracting decadal morphological behaviour from high-resolution, long-term bathymetric surveys along the Holland coast using eigenfunction analysis. *Marine Geology*, *126*(1-4), 301–330.

Wright, L., & Short, A. (1984). Morphodynamic variability of surf zones and beaches: A synthesis. *Marine Geology*, *56*(1-4), 93–118.

Wright, L., & Thom, B. (1977). Coastal depositional landforms. *Progress in Physical Geography: Earth and Environment*, *1*(3), 412–459.

Xu, J., Meyers, E., & White, S. (2010). Datum for the coastal waters of north/central California, Oregon, and Western Washington: Tidal datums and sea surface topography. Tech. Rep. NOS-CS-22, U.S. National Oceanic and Atmospheric Administration, U.S. Dept. of Commerce, Silver Spring, MD.

Zarnetske, P. L., Hacker, S. D., Seabloom, E. W., Ruggiero, P., Killian, J. R., Maddux, T. B., & Cox, D. (2012). Biophysical feedback mediates effects of invasive grasses on coastal dune shape. *Ecology*, *93*(6), 1439–1450.

Zinnert, J. C., Stallins, J. A., Brantley, S. T., & Young, D. R. (2016). Crossing scales: The complexity of barrier-island processes for predicting future change. *BioScience*, *67*(1), 39–52.